Biomechanical analysis and simulation of backward falls with head impact in older adults

by

Karam Elabd

B.Sc. (Electrical Engineering), University of Manitoba, 2017

Thesis Submitted in Partial Fulfillment of the
Requirements for the Degree of
Master of Applied Science

in the
School of Engineering Science
Faculty of Applied Sciences

© Karam Elabd 2020
SIMON FRASER UNIVERSITY
Summer 2020

Copyright in this work rests with the author. Please ensure that any reproduction or re-use is done in accordance with the relevant national copyright legislation.

Approval

Name:	**Karam Elabd**
Degree:	**Master of Applied Science**
Title:	**Biomechanical analysis and simulation of backward falls with head impact in older adults**
Examining Committee:	**Chair:** Jie Liang Professor
	Stephen Robinovitch Senior Supervisor Professor Department of Biomedical Physiology and Kinesiology
	Carolyn Sparrey Supervisor Associate Professor School of Mechatronic Systems Engineering
	Andrew Rawicz Supervisor Professor School of Engineering Science
	Edward Park External Examiner Professor School of Mechatronic Systems Engineering
Date Defended/Approved:	August 5, 2020

Ethics Statement

The author, whose name appears on the title page of this work, has obtained, for the research described in this work, either:

a. human research ethics approval from the Simon Fraser University Office of Research Ethics

or

b. advance approval of the animal care protocol from the University Animal Care Committee of Simon Fraser University

or has conducted the research

c. as a co-investigator, collaborator, or research assistant in a research project approved in advance.

A copy of the approval letter has been filed with the Theses Office of the University Library at the time of submission of this thesis or project.

The original application for approval and letter of approval are filed with the relevant offices. Inquiries may be directed to those authorities.

Simon Fraser University Library
Burnaby, British Columbia, Canada

Update Spring 2016

Abstract

This thesis examined the dynamics of backward falls in older adults involving head impact. Time-varying kinematics were extracted from digitizing videos of 11 real-life falls by residents of long-term care. The pelvis always impacted the ground before the head. On average, the head descended 1.2 m, and had a vertical velocity of 1.7 m/s just before it struck the ground. A novel dummy was used to examine how fall mechanics and compliant flooring affect head acceleration. Landing with a curved versus flat torso decreased peak rotational acceleration by 27% (4633 versus 5901 rad/s^2). Landing with fixed versus freely rotating hips lowered peak translational accelerations by 36% (101.5 versus 158.7 g) and peak rotational accelerations by 38% (4168 versus 6366 rad/s^2). The protective benefit of compliant flooring depended on torso curvature and hip stiffness. These results show that unexplored aspects of fall mechanics strongly influence head impact severity.

Keywords: Falls; traumatic brain injury; head injury; older adults; kinematics; anthropomorphic test device; protective technology

To my parents, whose encouragement, support, and faith in us means everything. To my little brother, for being my role model. I love and miss you guys beyond comprehension.

To Rassin and Karim, my dearest and closest friends, for being utterly useless throughout. Mabrook el Shattaf.

Acknowledgements

I would like to acknowledge and offer gratitude to my friends and lab mates who have been so helpful, kind, and patient with me. First, to Dr. Vicki Komisar for your indefatigable and inspirational willingness to see me succeed. To Natalie Shishov for personifying tenacity, capability and strong will. To Helen Chong and Brigitte Potvin for your valuable technical skills and efforts at maintaining my sanity throughout. And of course, to Olivia Aguiar for taking the time to peek over her monitor every fraction of a minute and make sure everything is fine. To the lovely and inspiring family, I have made during my time at SFU as a member of the Injury Prevention and Mobility Lab, and as an adopted BPK child.

I would also like to acknowledge my supervisory committee members, Dr. Carolyn Sparrey and Dr. Andrew Rawicz for all their guidance and support throughout this process. Learning from your insight and feedback has been a very valuable experience.

Finally, and most importantly, I would like to humbly thank and acknowledge Dr. Stephen Robinovitch, without whom I would not have been able to accomplish this work. Steve, learning under your distinguished guidance and exquisite mentorship has been such a great honor. Thank you for putting-in so much time and careful thought into tailoring such a rich and formative graduate school experience for me to carry forward in my career. I will always be grateful, and I hope that we continue working together as friends and colleagues. Thank you.

Table of Contents

List of Tables

List of Figures

List of Acronyms and Abbreviations

ANOVA	Analysis of Variance
ASTM	American Society for Testing and Materials
ATD	Anthropomorphic Test Device
BP	Back Profile Marker
BSIP	Body Segment Inertia Parameters
CA	Christina Applegate
CDC	Centers for Disease Control
CF	Compliant Flooring
CG	Center of Gravity
COM	Center of Mass
COP	Center of Pressure
CT	Computed Tomography
CTFH	Curved Torso, Fixed Hips
CTRH	Curved Torso, Rotating Hips
DAI	Diffuse Axonal Injury
DAQ	Data Acquisition
DAS	Data Acquisition System
DOF	Degrees of Freedom
ED	Emergency Department
FPS	Frames Per Second
FTFH	Flat Torso, Fixed Hips
FTRH	Flat Torso, Rotating Hips
GCS	Glasgow Coma Scale
GT	Greater Trochanter
HD80	80 Durometer High Density Stiff Foam
HIC	Head Injury Criteria
ICC	Intraclass Correlation Coefficient
JC	Joint Center of Rotation
LAC	Library and Archives Canada
LAC	Library and Archives Canada
LTC	Long Term Care
MADYMO	MAthematical DYnamic MOdels

MMOI	Mass Moment of Inertia
MoCap	Motion Capture
MOI	Moment of Inertia
mTBI	mild Traumatic Brain Injury
OR	Odds Ratio
PHAC	Public Health Agency of Canada
RMSE	Root Mean Square Error
SAR	Successive Approximation Register
SD	Standard Deviation
SDH	Subdural Hematoma
SE	Standard Error
SFU	Simon Fraser University
SFU	Simon Fraser University
TBI	Traumatic Brain Injury
TTP	Time-To-Peak
WHO	World Health Organization

Chapter 1.

Introduction

1.1. Falls and fall-related head injuries in older adults

1.1.1. Epidemiology of falls in older adults

The World Health Organization defines a fall as an event in which a person inadvertently comes to rest on the ground, floor or other lower level (Kalache, Alexandre. Ku et al., 2007). Falls are the leading cause of injury-related deaths in adults over age 70 worldwide (World Health Organization, 2014). In Canada, falls in individuals over age 65 caused 73,000 hospitalizations between 2008-2009 (Billette & Janz, 2011; CIHI, 2010, 2011).

About 30% of adults over age 65 report experiencing one or more falls in the past year (Blake et al., 1988; Campbell, Reinken, Allan, & Martinez, 1981; Exton-Smith, 1977; Lord et al., 1994; O'loughlin, Robitaille, Boivin, & Suissa, 1993; Prudham & Evans, 1981) Based on 2014 data, the Centers for Disease Control in the United States (US), estimated that there were 29 million falls among community-dwelling older adults in the US alone, 38% of which necessitated some form of clinical treatment (Bergen, Stevens, & Burns, 2016).

When compared to community-dwelling older adults, the prevalence of falls in older adults living in long term care (LTC) is up to three times higher (Luukinen, Koski, Hiltunen, & Kivelä, 1994; Rubenstein, 2006). Based on the findings from five published and two unpublished studies on falls in long-term care, Rubenstein et al. calculated a mean annual fall incidence rate of 1.7 falls per person in LTC (Rubenstein et al., 1988). According to the Public Health Agency of Canada (PHAC), approximately half of all LTC residents will experience at least one fall each year, and 40% will experience two or more falls (Stinchcombe, Kuran, & Powell, 2014).

1.1.2. Epidemiology of fall-related head injuries in older adults

Falls are a frequent cause of head impact and injury in older adults. Among individuals aged 75- 80, the head was the most common site of injury from falls (representing 32% of all cases), and more common than upper limb or hip injuries (Saari, Heikkinen, Sakari-Rantala, & Rantanen, 2007). In the LTC setting, 33% of falls were observed to cause head impact, with the back of the head being the most common site of impact (44% of cases) (Yang et al., 2017).

Fall-related traumatic brain injuries (TBI) represent the number one cause of fall-related deaths among older individuals (Taylor, Bell, Breiding, & Xu, 2017). Every year in the US, fall-related TBIs account for 142,000 emergency department visits, 81,500 hospitalizations, and nearly 14,000 deaths (Filer & Harris, 2015). Increased age is associated with worse outcomes after a TBI, with the odds for death increasing 1.47-fold per 10 year increase in age (Hukkelhoven, Steyerberg, Rampen, & Farace, 2003). Up to 88% of TBIs in older adults are caused by falls (Utomo, Gabbe, Simpson, & Cameron, 2009), and the age-adjusted rate among older adults for hospitalization due to TBI has doubled over the past decade (Harvey & Close, 2012).

Older adults who report to the emergency department (ED) with a fall-related head trauma are 2.6-fold more likely to experience a repeated fall-related head trauma in the following year (Southerland et al., 2016).

Traumatic brain injury (TBI) can been defined as a disruption to normal brain function caused by an external force applied to the head (Taylor et al., 2017). TBI encompasses a range of brain injuries, including intracerebral hemorrhage (at the level of the subdural, epidural or subarachnoid space), contusions and diffuse axonal injury. The severity of TBI is assessed using a combination of neuroimaging, biomarker and metabolic testing, and clinical tools such as the Glasgow Coma Scale (GCS), which scores TBIs as mild, moderate or severe according to a standardized component-based functional assessment of visual, verbal and motor responses (Teasdale et al., 2014). Concussion, a milder form of TBI (or mTBI) is the most common form of TBI from falls in older adults (CDC, 2012). Moreover, the frequency of fall-related concussions in older adults may be underestimated considerably, given that pre-existing cognitive impairment, combined with the lack of imaging abnormalities in concussion, makes

diagnosis of fall-related concussion challenging in the older adult population (Filer & Harris, 2015).

1.1.3. Mechanisms and biomechanics of fall-related head injuries

Nearly two-thirds of fall-related TBIs in older adults are due to falls from standing height onto a level surface (Harvey & Close, 2012). For older adults who visited hospital emergency rooms after hitting their head in a fall, the likelihood for acute brain lesions from computed tomography (CT) scanning was 4-fold higher for those who fell backward than forward (Hwang, Cheng, Chien, Yu, & Lin, 2015), and 2-fold higher for falls causing impact to the occipital (posterior) region of the skull, when compared to falls with an unknown impact location (Pöyry et al., 2013).

The risk for TBI in a fall depends on the strains applied to brain tissues during the impact event, which in turn depends on the magnitude and duration of translational and rotational head acceleration. The pattern of head acceleration during a fall will depend, in turn, on the inertia of the head, the impact velocity, the location of impact, and the stiffness of the interface between the head and the contact surface (Post & Hoshizaki, 2012). While researchers agree that a given head impact will tend to induce both translational and rotational acceleration to the head, the relative importance of each in the etiology of TBI remains unknown. Translational acceleration has traditionally been regarded as the dominant determinant of risk for TBI (King, Yang, Zhang, & Hardy, 2003) and continues to serve as the basis for mechanical testing systems for evaluating helmets and ground surfaces (E. Gurdjian, Lissner, Evans, Patrick, & Hardy, 1961; E. S. Gurdjian, Webster, & Lissner, 1955; Hodgson et al., 1969). Support for this perspective is based on primate research in the 1950's by Gurdjian and colleagues, who found that the magnitude of translational acceleration associated with risk for skull fracture, brain deformation and changes in intracranial pressure (E. Gurdjian et al., 1961; E. S. Gurdjian et al., 1955). Later experiments by Ommaya et al. showed that unrealistically high magnitudes of rotational acceleration were required to produce the same levels of injury. Furthermore, Ono et al., found no correlation in primates between rotational acceleration and the occurrence of mTBI (Ono, Kikuchi, Nakamura, Kobayashi, & Nakamura, 1980).

However, others have presented growing evidence of the importance of rotational acceleration as a mechanism of TBI (Holbourn, 1943). Gennarelli et al. demonstrated through primate experiments that translational acceleration of the head tended to produce focal brain injuries (cerebral contusions and intracerebral hematomas), while rotational acceleration produced diffuse axonal injury, which is thought to be an important cause of concussion (Gennarelli, Adamns, & I., 1981; Gennarelli, Thibault, & Ommaya, 1972a, 1972b). Unterharnscheidt suggested that purely translational loading results in a transcranial pressure gradient, while purely rotational acceleration imposes differential motion between the skull and brain resulting in shear stress and strain (Unterharnscheidt, 1971). Hoshizaki and Brien stated that, while approaches to reduce translational acceleration (e.g., through helmet design) have reduced the incidence of focal brain injuries and skull fracture in sport, the prevalence of diffuse injury has yet to be resolved (Hoshizaki & Brien, 2004). In a more recent review of the literature, Post and Hoshizaki described that the primary mechanisms of brain injury are: (a) contusions resulting from skull deformation and brain motion; (b) intracranial pressure gradients produced from impacts; (c) rotation causing skull/brain relative motion; and (d) combined linear and rotational acceleration from impact (Hardy, Khalil, & King, 1994; King et al., 2003; Post & Hoshizaki, 2012; Viano, King, Melvin, & Weber, 1989)

1.2. Injury thresholds

Emerging evidence on the role of head acceleration in brain injury has led researchers to propose various head injury tolerance thresholds (Table 1 and Table 2) to predict injury outcomes from the kinematics of a given head impact event (Post & Hoshizaki, 2012).

Ommaya proposed that peak head translational and rotational accelerations above 90 g and 1800 rad/s^s, respectively, led to concussion and 16,000 rad/s^2 resulted in DAI (Ommaya, Hirsch, Yarnell, & Harris, 1967). Through laboratory reconstructions of video-captured National Football League (NFL) impacts, Zhang et al. reported that values of 66, 82, and 106 g for peak translational acceleration and 4600, 5900, and 7900 rad/s^2 for rotational acceleration resulted in a 25%, 50%, and 80% probability for mTBI (L. Zhang, Yang, & King, 2004).

Others have reported that peak translational accelerations of 82 g are a lower bound for mTBI (Duma et al., 2005; Schnebel, Gwin, Anderson, & Gatlin, 2007; L. Zhang et al., 2004), and 130 g results in subdural hematoma (Willinger & Baumgartner, 2003). Willinger and Baumgartner found that mTBI occurred from rotational accelerations of 3000 to 4000 rad/s^2. Data from human volunteer impact experiments has shown conflicting results, with one study showing no reported injuries resulting from rotational head accelerations of 2700 rad/s^2 (Ewing, Thomas, Patrick, Beeler, & Smith, 1969), and another showing 16,000 rad/s^2 (Pincemaille et al., 1989).

Table 1. Summary of translational acceleration-based head injury thresholds

Lesion type	Threshold (g)	Measurement method	Reference
mTBI	82 for 50% chance	Laboratory reconstruction	Zhang et al. (2004)
mTBI	81	Instrumented helmets	Duma et al. (2005)
mTBI	103	Instrumented helmets	Brolinson et al. (2006)
mTBI	82 - 146	Instrumented helmets	Schnebel et al. (2007)
mTBI	103	Dynamic modeling	Fréchède and McIntosh (2009)
mTBI	90	Primate impacts	Gurdjian et al. (1966)
SDH	130	Laboratory reconstruction	Willinger and Baumgartner (2003)

mTBI = mild traumatic brain injury, SDH = subdural hematoma. Reprinted from the 2012 Post & Hoshizaki review.

Table 2. Summary of rotational acceleration-based head injury thresholds

Lesion type	Threshold (rad/s^2)	Measurement method	Reference
mTBI	5900 rad/s^2 for 50% chance	Laboratory reconstruction	Zhang et al. (2004)
mTBI	3000 - 4000	Laboratory reconstruction	Willinger and Baumgartner (2003)
mTBI	8020	Dynamic modeling	Fréchède and McIntosh (2009)
No lesion	2700	Human volunteers	Ewing (1975)
No lesion	16,000	Human volunteers	Pincemaille et al. (1989)
SDH	4500	Cadaver impacts	Lowenhielm (1974)
mTBI	1800	Primate impacts	Ommaya et al. (1967)
DAI	16,000	Primate, physical and numerical model impacts	Ommaya et al. (1967)

mTBI = mild traumatic brain injury, SDH = subdural hematoma, DAI = diffuse axonal injury. Reprinted from the 2012 Post & Hoshizaki review.

1.3. Kinematics and dynamics of falls and head injuries

Given the safety and ethical challenges of experiments with living human participants involving head impact, the dynamics of fall-related head impacts have most often been studied using anthropomorphic test devices (ATDs), consisting of physical systems that replicate key aspects of the human body, and inertial sensors that measure

body segment accelerations (Caccese et al., 2016; Fanta, Kubový, Lopot, Pánková, & Jelen, n.d.; Hajiaghamemar, Seidi, Ferguson, & Caccese, 2015; Ivancic, 2014; Nagata & Ohno, 2007; Schulz, Lee, Lloyd, Lee Iii, & Lloyd, 2008; Seidi, Hajiaghamemar, & Caccese, 2015). A second important approach for analyzing the dynamics of head impact in falls is through mathematical models (Doorly, Phillips, & Gilchrist, 2005; Kim & Ashton-Miller, 2009; Sandler & Robinovitch, 2001; Wach & Unarski, 2014; J. Zhang, Yoganandan, & Pintar, 2009).

The external validity of these approaches depends on the accuracy of the models in recreating the initial conditions of the head impact event, including the configuration and velocity of the head at the instant of impact (Music, Kamnik, & Munih, 2008; Nguyen & Reynolds, 2014; Oeur, Gilchrist, & Hoshizaki, 2018; Sen & Vinh, 2016; Zhi-Chao, Lu, Yao-Xin, & Dan, 2008). Furthermore, the ability of the models to predict how the mechanics of the fall influence the initial conditions for head impact, will depend on the realism of the model in simulating the initiation, descent and impact stages of the fall, including initial or simultaneous impacts to body parts other than the head (e.g., pelvis, torso, hands and shoulder).

1.3.1. Cadaveric experiments

Hardy et al. used high-speed biplane x-rays to study brain displacement and deformation in human cadaveric heads to impacts delivered using a pneumatic piston device (Hardy et al., 2007). The peak translational acceleration for the unprotected tests ranged from 153 to 408 g (average = 280 g) and the peak rotational acceleration results ranged from 7.40 to 39.43 krad/s^2 (average = 20.11 krad/s^2).

(J. Zhang et al., 2009) conducted free fall experiments at varying heights leading to lateral impacts to 10 unembalmed cadaver head specimens. The impact velocity ranged from 2.44 to 7.70 m/s or until skull fracture was identified biomechanically. Skull fractures occurred at translational and rotational accelerations of 263 – 376 g, and 20 – 34 krad/s^2, respectively. The authors also observed strong correlation between translational head acceleration and impact velocity (R^2 = 0.92).

1.3.2. Numerical models and simulations

Doorly (Doorly et al., 2005) used the Mathematical Dynamic Models (MADYMO) numerical simulation package to simulate head impacts in 10 real-life pedestrian falls. The models incorporated a mean impact velocity of 6.54 m/s, and translational and rotational head accelerations averaged 313 g (range = 189 to 456 g) and 30.1 krad/s^2 (range = 7.4 to 49.2 krad/s^2), respectively. Of note, the authors reported that results were highly dependent on the model's initial and boundary conditions.

(O'Riordain, Thomas, Phillips, & Gilchrist, 2003) used MADYMO to simulate four real-life falls (persons aged 11, 24, 37, and 76 years) with reported head injury. Head injuries varied from small frontal lobe contusions to skull fractures. One fall was initiated from standing height, and the remaining three falls involved heights ranging from 13-138 cm above ground level. Reported peak translational and rotational acceleration outcomes ranged from 311 to 1015 g and 17.6 to 43.5 krad/s^2.

1.3.3. Mechanical models and simulations

1.3.3.1. Drop towers and mechanical testing standards

A drop tower is a mechanical apparatus that is commonly used to simulate head impact following a period of free fall. Drop towers are incorporated into a variety of existing testing standards for evaluating the protective value of helmets for bicycle, motorcycle, hockey, skiing, riot police and equestrian use (ASTM F1045-07, 2007; ASTM F1447-18, 2018; CSA Z262.1-15, 2015; CSA Z611-02, 2012; ISO 8894-2, 2006). Drop towers are also used in standards for sport surfaces and flooring(ASTM F1292-18, 2004), and hip protectors to prevent fall-related hip fractures (CSA EXP08, 2017; CSA Z325:20, 2020).

Drop towers can be categorized based on whether the descent of the head towards the impact surface is guided or unguided. Guided drop towers conventionally use a filar apparatus where the headform or payload is attached via low-friction bearings to vertical guide wires or rails, and subsequently released onto the impact surface. Unguided drop towers typically use an elevated clutch or electromagnetic to drop the unconstrained headform onto the impact surface. In contrast to an unguided drop tower, a guided drop tower does not allow for free rotation of the headform during impact.

Furthermore, drop towers involve one dimensional translational energy exchanges, that may not accurately simulate the rotational velocity of the head and impact, as well as the rotational accelerations occurring during impact from a fall.

Caccese et al. conducted simulated fall-related head impacts with a guided drop tower (Caccese et al., 2016). The system was designed to meet the specifications described in ASTM F1446 (ASTM F1446-15, 2011), and incorporated a Hybrid-III (Humanetics; Plymouth, MO, US) head and neck assembly. Tests were conducted for front, rear and side head orientations, and two neck stiffnesses (a standard 70-80 Shore A durometer, and a 35 Shore A durometer having 25-27% of the stiffness of the standard neck in extension and flexion). Drop heights ranged from 20 to 65 cm, and corresponding impact velocities ranged from 1.94 m/s to 3.58 m/s. Translational accelerations were minimally affected by the orientation of the head or neck stiffness, whereas rotational acceleration outcomes were highly sensitive to impact orientation and neck stiffness. Peak accelerations for rear impact conditions ranged from 136-422.2 g, and 5.92 to 16.14 krad/s^2.

1.3.3.2. Anthropomorphic test devices

Nagata conducted simulated backward falls (Nagata & Ohno, 2007) with a customized dummy having total body height of 167 cm and mass of 61 kg. Tests were conducted to simulate backward falls from standing height with different segment linkage properties, achieved by either fixing or unfixing the lower limb joints (hips, knees and ankles). The aim of the study was to examine the influence of lower limb joints on impact velocity and descent duration. The dummy was suspended using an electromagnet-activated tether, that was configured to trigger in synchrony with a motorized platform that suddenly translated the feet. Fall dynamics were characterized using video analysis at a 30Hz capture rate. The highest reported average impact velocity of the head (6.75 m/s) was observed when the knee and hip joints were unfixed, and the ankles were fixed. The lowest average head impact velocity of 4.78 m/s was observed when both ankle and hip joints were unfixed, resulting in the longest fall duration of 940 ms. When all three joints were fixed, impact velocities ranged between 6.11-6.39 m/s and descent durations averaged 830 ms. While head accelerations were not reported, the study results suggest that falling with the ankles and hips in a relaxed state lowers head

impact velocity, by allowing the torso to remain relatively upright during the initial stage of descent (i.e. up to pelvis impact).

In a similar study, Hajiaghamemar et al., (Hajiaghamemar et al., 2015) conducted fall simulations with full-body Hybrid III ATDs (50th percentile male and 5th percentile female), including backward falls with and without hip flexion (similarly achieved by either fixing or unfixing the hip joints). The fixed hip ATD experienced head impact almost instantaneous after pelvis impact (interval between pelvis and head impacts = 25-45 ms), while in the unfixed hips, the interval between pelvis and head impact ranged from 350-450 ms. Head accelerations were substantially higher in the fixed hip condition (451 +/- 38 (range: 390-524) g and 29.2 +/- 5.8 (range: 19.6-41.0) krad/s^2) than in the unfixed hip condition (295 +/- 89 (range: 198-447) g and 19.3 +/- 9.6 (range: 10.7-38.2) krad/s^2). The average peak translational impact velocity was 6.75 +/- 0.27 (range: 6.31-7.11) m/s and 4.85 +/- 1.33 (range: 3.29-6.80) m/s, for the fixed and unfixed hip conditions respectively. Additional tests simulated falls from standing with a Hybrid III 5% female, 50% male, and 95% male. Falls by the 50% male and 5% female ATDs resulted in average peak translational accelerations of 302g (recorded maximum = 243 g) and 202g (recorded maximum = 518 g). The Hybrid III 95% male achieved remarkably high peak translational accelerations averaging 1153 g (recorded maximum = 1340 g).

While the Hybrid III dummy neck has been criticized in the past for its lack of biofidelity in terms of range of motion and directional stiffness, and more biofidelic options have since been developed (Nelson & Cripton, 2010), the 50th percentile hybrid III head and neck complex is the most widely-accepted and used surrogate in the impact biomechanics literature. The standard Hybrid III neck was designed to provide biofidelic flexion and extension response under high-speed rear-end and frontal impacts (Foster, Kortege, & Wolanin, 1977). Results from Mertz (Mertz, 1985), comparing the Hybrid III head to cadaver data support the claim that the Hybrid III is human-like for frontal impacts and viable for surrogate comparisons with post-mortem human subject data. Furthermore, a study by Caccese et al., (Caccese et al., 2016), using a Hybrid III head and neck assembly, examined the influence of neck stiffness on acceleration outcomes for rear and frontal impacts, and found no effect of neck stiffness on peak translational acceleration, with percent differences ranging from -4.3 to 8.8% varied by drop height. In terms of peak rotational acceleration magnitudes, the authors report 7.3% greater

average acceleration magnitudes for the lower stiffness neck compared to the standard durometer neck.

1.3.4. Lab-based falling experiments with humans

While obviously challenging due to safety precautions, at least two previous studies have examined the effect of neck muscle activation on head impact velocities in backward falls. Choi et al. conducted experiments with young adult participants (n=8; ages 19 – 35; five females) to test the effect of neck flexor muscle activation on the impact velocity of the head in backward falls from standing height (Choi, Robinovitch, Ross, Phan, & Cipriani, 2017). Participants wore helmets and landed on a 30 cm thick gymnasium mat, and were instructed before each trial to either “prevent their head from impacting the mat” (no head impact condition), “allow their head to impact the mat, but with minimal impact severity” (soft impact condition), or “allow their head to impact the mat, while inhibiting efforts to reduce impact severity” (hard impact condition). Head impact was estimated as the instant a helmet marker descended below its baseline resting height on the mat surface. When compared to soft impact trials, hard impact trials led 87% greater vertical impact velocity (3.23 versus 1.73 m/s) and 83% greater horizontal impact velocity (2.74 versus 1.50 m/s). For every 10% increase in sternocleidomastoid muscle activation, the vertical impact velocity decreased by 0.24 m/s and the horizontal impact velocity decreased 0.22 m/s.

Ito et al. investigated head-righting behaviors and the functional influence of neck muscle reflexes in response to isolated falls of the head (Ito, Corna, von Brevern, Bronstein, & Gresty, 1997). Participants (n = 10; ages 23-49 years; seven males) lay supine with a sling supporting the head at 30^{o} to the horizontal, over a cushioned bed. Peak head velocities were measured after sudden release of the sling via an electromagnet. Participants were instructed to either “relax as much as possible” (passive fall) or “relax between drops but to be ready to right their head as quickly as possible when released” (active fall). Descent durations averaged approximately 200 ms. Peak vertical velocities were significantly lower in active than passive falls (1.52+/-0.25 versus 0.96+/-0.18).

1.3.5. Video capture and analysis of falls in older adults

Video footage of real-life falls in older adults provides objective evidence on fall characteristics. The earliest study of this type (to my knowledge) was conducted by Holliday et al. who used surveillance cameras at entrances and common areas to record 25 falls by 17 people (of average age 81 years; eight females) in a long-term care facility in Toronto, Canada (Holliday, Fernie, Gryfe, & Griggs, 1990). The first impacting body part was most often noted to be the hip, buttock or knee. However, no mention was made of head impact or distribution of fall directions.

Since 2007, our research group has partnered with two long-term care (LTC) facilities in the Vancouver lower mainland (Delta View, a 312-bed facility in Delta, British Columbia, and New Vista, a 236-bed facility in Burnaby, British Columbia) to collect video footage of 2776 falls in 795 residents, through surveillance cameras in common areas (dining rooms, lounges, and corridors). Using a structured, validated questionnaire to classify key aspects of the initiation, descent and impact stages of the fall (Yang, Schonnop, Feldman, & Robinovitch, 2013), we found that head impact occurred in 37% of falls in LTC (Schonnop et al., 2013). While forward falls created a greater risk for head impact, backward falls were nearly four times more common, and represented the most common scenario leading to head impact.

The potential for extracting impact velocities from analysis of video-captured, real-life falls was demonstrated by Choi et al. (Choi, Wakeling, & Robinovitch, 2015), who digitized the time-varying positions of the head and pelvis in 21 backward and 4 forward falls experienced by older adults in LTC. In backward falls with head impact (n=8), peak vertical velocities averaged 2.67 (SD = 0.82) m/s for the head, and 1.98 (SD = 0.45) m/s for the pelvis. Peak horizontal velocities averaged 2.59 (SD=1.20) m/s for the head, and 0.65 (SD=0.35) m/s for the pelvis. The mean interval between onset of the fall and impact to the pelvis was 440 ms, and the interval between pelvis and head impact averaged 325 ms.

Recent analysis of the LTC falls video database has examined the factors that separate falls that result in head impact from falls where head impact is avoided. Kuo et al. examined the role of muscle activation in generating torques at the hips and neck to prevent head impact in backward falls (Kuo et al., 2020). Shishov and Robinovitch

analyzed 215 backward falls, including 85 falls that caused head impact, and found that the occurrence of leg raise after pelvis impact reduced the odds for head impact by 5-fold (Shishov & Robinovitch, 2018). The authors proposed that the underlying mechanisms may relate to conservation of angular momentum (Figure 1), with rotation of the lower limbs slowing downward rotation of the torso as the body pivots about the pelvis. However, no study to my knowledge has assessed the effect of leg raise on head impact velocity.

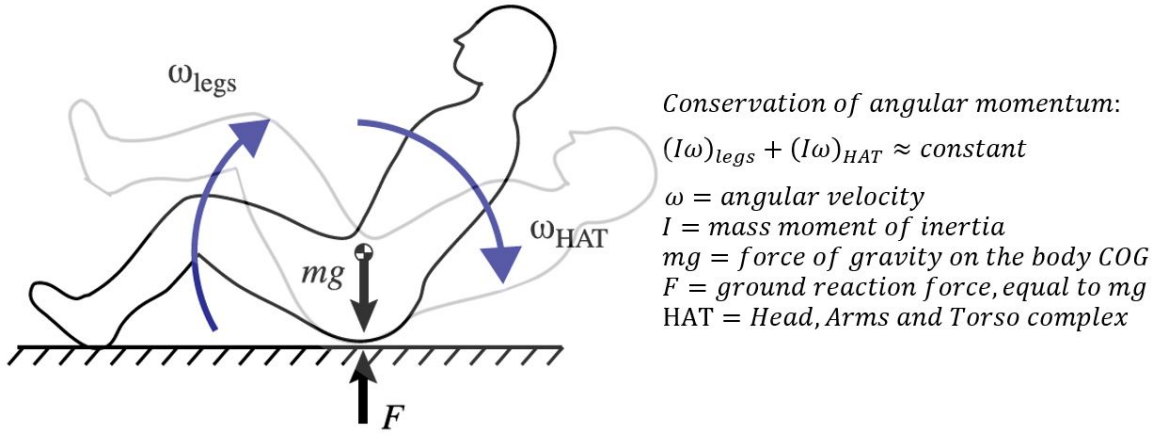

Figure 1. Angular momentum considerations in a backward fall
Adapted from (Shishov & Robinovitch, 2018)

1.4. Overview and evaluation of fall-injury protection equipment

With growing recognition of the problem of fall- related TBI in older adults, a wide range of compliant flooring and protective head gear has emerged (headbands, padded toques, soft-shell helmets) that is marketed to seniors and health care providers. However, unlike helmets for cycling or athletics (ASTM F1045-07, 2007; ASTM F1447-18, 2018; CSA Z262.1-15, 2015), standards do not exist for products marketed as head protection from falls in older adults. Furthermore, studies have not examined the impact velocities and loading conditions associated with head injuries from falls in older adults, to serve as the scientific basis for test systems. Current evidence is based on fall simulations with anthropometric dummies (Caccese et al., 2016; Hajiaghamemar et al., 2015; Seidi et al., 2015) (which may fall in a manner that differs greatly from older adults), and interviews of older patients in emergency rooms (Hwang et al., 2015).

Analysis of the dynamics of head injuries from falls in seniors is required to provide a scientific approach for improved product design and evaluation.

Wright & Laing showed that impact velocity affects the protective value of a compliant flooring that is commonly marketed for fall injury prevention in older adults (25 mm thick SmartCells; SATECH, Inc., Chehalis, Washington, US). Experiments were conducted with a monorail drop tower (Wright & Laing, 2011) and medium-sized headform meeting guidelines from the National Operating Committee for Standards on Athletic Equipment (NOCSAE), which impacted the samples at velocities of 1.5, 2.5, and 3.5 m/s. Floor type was found to affect peak impact force, peak translational acceleration, and Head Injury Criteria (HIC; which accounts for both magnitude and duration of translational acceleration (Greenwald, Gwin, Chu, & Crisco, 2008)). Reported peak accelerations ranged from 54 to 262 g for impacts on carpets and rubber, and from 27 to 157 g for impact on SmartCells. When compared to carpet, Smartcells provided between 25% and 70% attenuation in peak translational acceleration, depending on impact velocity.

Similar trends were shown by (Laing & Robinovitch, 2009) in measures of the impact force attenuation properties of low stiffness floors during simulated falls on the hip involving impact velocities of 2, 3, and 4 m/s. The two compliant flooring conditions (25 mm thick SmartCell and SoftTile) attenuated impact force by up to 47%. However, the test results depended strongly on impact velocity. While the force attenuation provided by compliant flooring increased as impact velocity increased, an opposite trend emerged for the foam floors, due to the foam tiles bottoming out at high impact energy. These trends highlight the challenge of designing products that work well over a range of impact velocities, and the importance of evaluating products under externally valid testing conditions.

1.5. Thesis statement and objectives

TBI is a common and often devastating consequence of falls in older adults. Protective headgear and compliant flooring are two promising solutions for preventing fall-related TBIs in high-risk populations or environments. Improved understanding is required of the nature of head trauma in falls, in order to develop externally valid approaches (i.e., mechanical testing systems and mathematical models) for evaluating

the protection provided by various types of headgear and compliant flooring. Of particular importance is the impact velocity and configuration of the head at impact. Current standards for helmet testing rely on mechanical test systems with guided monorails or wired drop assemblies that impart translational but not rotational acceleration to the head (ASTM F1292-18, 2004; ASTM F1446-15, 2011; Connor et al., 2016).

In Chapter 2 of this thesis, I examine the time-varying positions and velocities of the head (and other body parts), from analysis of video footage of real-life backward falls in older adults that resulted in head impact. My specific research questions were:

(1) For backward falls in older adults that involve head impact, what is the velocity of the head as it approaches impact with the ground? Is the peak velocity, as reported by (Choi et al., 2015), representative of the velocity of the head at impact?

(2) What is the temporal sequence of impacts to the pelvis, hands, shoulders and head, and what are the configurations of the body at these instants? Does the pelvis tend to impact the ground before the head?

In Chapter 3 of the thesis, I describe results from experiments with a falling dummy, that examined how the characteristics of backward falls affect the magnitude and duration of head accelerations during impact. In particular, I systematically altered the characteristics of the dummy and environment, to address the following research questions:

(1) How does head impact severity (as measured by the magnitude and duration of translational and rotational head acceleration at impact) depend on torso curvature during landing? I compared a “curved torso” condition simulating spinal flexion that produced a rolling contact of the torso against the ground, to a “flat back” condition where the torso impacted the ground near-simultaneous with the head. The rolling contact provided by a curved torso may more effectively distribute the impact energy of the fall and lower the impact velocity of the head. Based on this consideration, I hypothesized that head impact severity would be lower in falls with the dummy involving a curved torso than a flat torso configuration.

(2) How does head impact severity depend on lower limb dynamics after pelvis impact? We previously reported that raising of the legs after pelvis impact reduced the risk for head impact in backward falls in older adults (Shishov & Robinovitch, 2018), possibly due to rotation of the lower limbs reducing the downward angular momentum of the torso. Accordingly, I hypothesized that falls with the dummy having fixed hips, thereby allowing leg raise, would result in lower magnitudes of head impact severity, when compared to falls with freely rotating hips (that allow for minimal leg raise).

(3) How does head impact severity depend on modifications to the stiffness of the ground, and how does the effect of surface stiffness on head impact severity depend on the potentially interacting effects of torso curvature, lower limb dynamics, and impact velocity? Compliant flooring is a promising approach for reducing the risk for TBI in high-risk environments such as long term care (Mackey et al., 2019), but such floors must be designed to be soft enough to substantially reduce impact severity during falls, while stiff enough to allow for rolling of equipment and wheelchairs. The reduction in impact severity must be measured under conditions that realistically simulate falls in older adults. I used my falling dummy to evaluate the protective value of modifications in ground stiffness under different falling conditions. I hypothesized that the effect of reducing floor stiffness on head impact severity would depend on torso curvature, lower limb dynamics, and impact velocity.

Chapter 2.

Video-based kinematic analysis of backward falls with head impacts experienced by older adults in long-term care

2.1. Introduction

Falls are the cause of up to 80% of traumatic brain injuries (TBIs) in adults over age 65 (Fu, Fu, Jing, Mcfaull, & Cusimano, 2017). Furthermore, the problem is increasing, with several studies showing a doubling to tripling in the age-adjusted rate of TBI in older adults over the past decade (Harvey & Close, 2012; Kannus, Parkkari, & Poutala, 1999; Watson & Mitchell, 2011)

Older adults residing in long-term care (LTC) are at especially high risk for fall-related TBI. A study in New South Wales, Australia found that, while only 6% of older adults reside in LTC, over one-quarter of TBIs in older adults occur in the LTC setting (Harvey & Close, 2012). Through a unique partnership with two LTC homes in the Vancouver Lower Mainland involving video capture of real-life falls, my SFU lab group found that the average LTC resident falls three times per year (van Schooten et al., 2018) and over one-third of falls result in impact to the head (Schonnop et al., 2013; Yang et al., 2017).

In terms of frequency and severity, backward falls appear to be the most common cause of head impact and TBI in older adults. In a study of TBI in older adults in the emergency room setting, the risk for brain lesions detected through CT scanning (indicative of moderate to severe TBI, as opposed to mild TBI) was 4-fold higher for cases caused by backward falls than forward falls (Hwang et al., 2015). Analysis by my lab group of video-captured falls in LTC showed that forward falls created the highest risk for head impact, but backward falls were much more common, and 42% of head impacts were to the back of the head (Schonnop et al., 2013).

Protective headgear (e.g., helmets or padded hats) and compliant flooring represent promising approaches for reducing head accelerations and preventing fall-related TBIs in LTC (Lemoine, Tate, Lacombe, & Hood, 2017; McIntosh, McCrory, &

Finch, 2004; Post, Oeur, Hoshizaki, & Gilchrist, 2013). However, valid approaches are required to measure the protective value of these products. Impact velocity and configuration are strong determinants of product performance (Campolettano, Gellner, & Rowson, 2018; Denny-Brown & Russell, 1941; Oeur et al., 2018; Oeur, Gilchrist, & Hoshizaki, 2019), and existing testing standards for helmets (Dll3.2-M89, 2009; F1045-07, 2007; F1292-18, 2004; F1446-15, 2011; Z262.1-15, 2015; Z263.1-14, 2015) and ground surfaces (ASTM F1292-18, 2004; ASTM F2223-19a, 2019) in sport and recreation involve impact velocities between 4-6 m/s, which may poorly represent those occurring in falls in older adults. Improved understanding is required of the impact velocities and configurations accompanying real-life falls in older adults, to serve as the scientific basis for biomechanical test systems for evaluating the protective benefit of head gear and flooring in the context of fall-related head injuries in older adults.

The goal of this study was to address this need by analyzing video footage of real-life falls in older adults, collected through our on-going cohort study in long-term care (Robinovitch et al., 2013; Yang et al., 2017, 2013), to determine the kinematics of backward falls causing head impact. My results build on those reported by Choi et al. (Choi et al., 2015) who analyzed 21 backward falls, eight of which involved head impact, and reported peak velocities of the pelvis, head and hand that averaged 2.14 m/s (SD=0.63), 2.91 m/s (SD=0.86), and 2.87 m/s (SD=1.60), respectively. I also build on the findings of Shishov et al. (Shishov & Robinovitch, 2018) who reported a 5-fold lower risk for head impact in backward falls with substantial leg raise after the instant of pelvis impact ($p<0.0001$), when compared to falls without leg raise. My specific research questions were:

(1) For backward falls in older adults that involve head impact, what is the velocity of the head as it approaches impact with the ground? Is the peak velocity, as reported by Choi et al., (Choi et al., 2015) representative of the velocity of the head at impact?

(2) What are the relative timings and configurations of the body at the instant of impact to the pelvis, hands, shoulders, and head during backward falls that involve head impact in older adults? Does the pelvis tend to impact the ground before the head?

2.2. Methods

2.2.1. Fall video database

This study draws on a database of video footage of real-life falls (Robinovitch et al., 2013) experienced by older adult residents of two LTC facilities in the Vancouver region (Delta View, a 312-bed facility in Delta, BC, and New Vista, a 236-bed facility in Burnaby, BC). All falls occurred in common areas (dining rooms, lounges, and corridors). The baseline characteristics of each fall were classified by trained raters using a structured questionnaire, that has been validated for inter-rater reliability (Yang et al., 2013). The questionnaire examined the activity at the time of the fall, the height of the fall (standing height or greater and lower than standing), the use of mobility aids at the time of falling, the initial fall direction and the landing configuration, and the occurrence of impact to key body sites such as the hand(s), knee(s), pelvis, and head.

The study was approved by the Office of Research Ethics at Simon Fraser University and allows for sharing of the video with the research team [study number 2013s0200], with additional written consent obtained from individuals for use of their images for education.

2.2.2. Video selection

My video selection criteria (Figure 2) focused on identifying video footage of backward falls from standing height that involved the head impacting the ground. Starting from a subset of 654 fall videos that involved initial and final backward landing directions, I excluded cases that did not involve head impact (n = 419). From the remaining 235 cases, I excluded falls that occurred from above or below standing height (n = 66). I then excluded videos that resulted in head impact against surfaces other than the floor, such as walls or furniture (n=73).

Next, I excluded videos with an obstructed view of body segments during the fall (n=17), videos with a framerate lower than 30 fps (n=18), and videos where the angle between the plane of the fall and the camera's optical axis was less than 30 degrees (n=13). Previous studies of head impact in sport have shown that, while a significantly higher capture rate is required to estimate the peak accelerations of the head at impact

(L. C. Wu et al., 2017), a 30 Hz video capture rate should be adequate for determining body segment movements during descent, including the velocity of the head immediately prior to impact (Pellman, Viano, Tucker, Casson, & Waeckerle, 2003). I test the validity of this assumption, as described in Section 2.2.4. Finally, I excluded fall videos where I was unable to secure video footage of the calibration panel (n=37). The final analyzed dataset included 11 backward falls experienced by 10 older adults (2 male and 8 female).

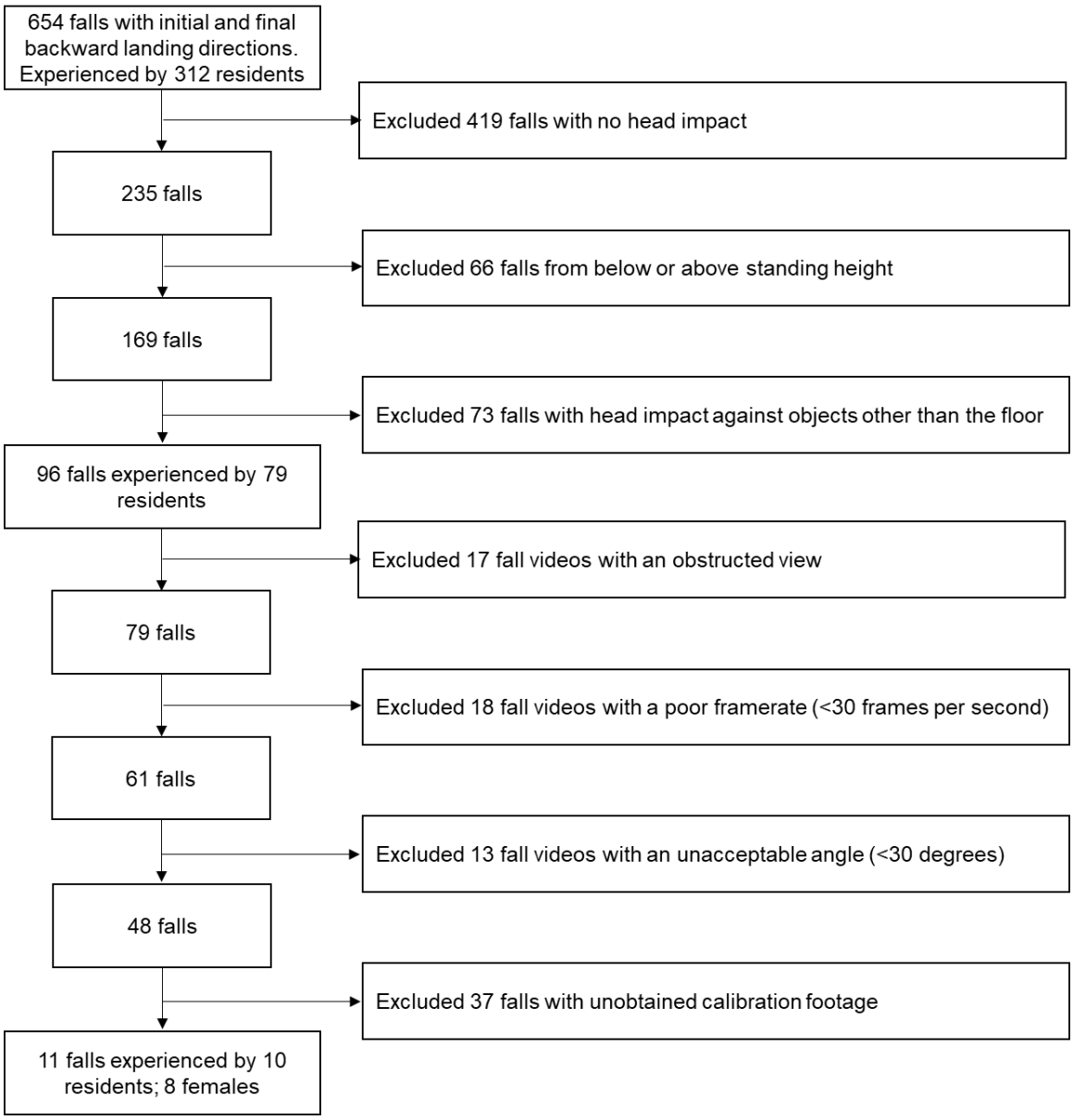

Figure 2. Fall video selection process.
This process summarizes the exclusion criteria for selecting video footage of 11 backward falls for analysis from an initial subset of 654 falls with backward initial fall directions and landing configurations.

2.2.3. Digitization of time-varying positions

Fall videos were analyzed with Kinovea, an open-source digitization and video analysis software (Kinovea – 0.8.27, www.kinovea.org/) to manually digitize the location of 13 key body sites (Table 3 and Figure 3) frame-by-frame, over an interval beginning

one frame before the perceived onset of descent of the head, and ending five frames after the perceived end of the fall, when the individual maintained a roughly stationary posture on the ground. In addition to the head and torso, I tracked sites on the upper and lower limb closest to the camera.

Table 3. Tracked body site definitions

Body site	Site definition
Head	Head center of gravity (CG)
Back profile 1 (BP1)	C7-T1
Back profile 2 (BP2)	T5
Back profile 3 (BP3)	T7
Back profile 4 (BP4)	T10
Back profile 5 (BP5)	T12-L1
Back profile 6 (BP6)	L5-S1
Shoulder	Shoulder joint center of rotation (JC)
Elbow	Elbow JC
Wrist	Wrist JC
Pelvis	Hip JC
Knee	Knee JC
Ankle	Ankle JC

CG = center of gravity, JC = joint center of rotation

Tracking was done at 600% zoom (Puig-Diví et al., 2019). The digitized coordinates were calibrated by capturing an image (from the same camera that captured the fall) of a calibration panel placed at the site of the fall in the LTC facility, oriented in the estimated plane of the fall (Figure 3).

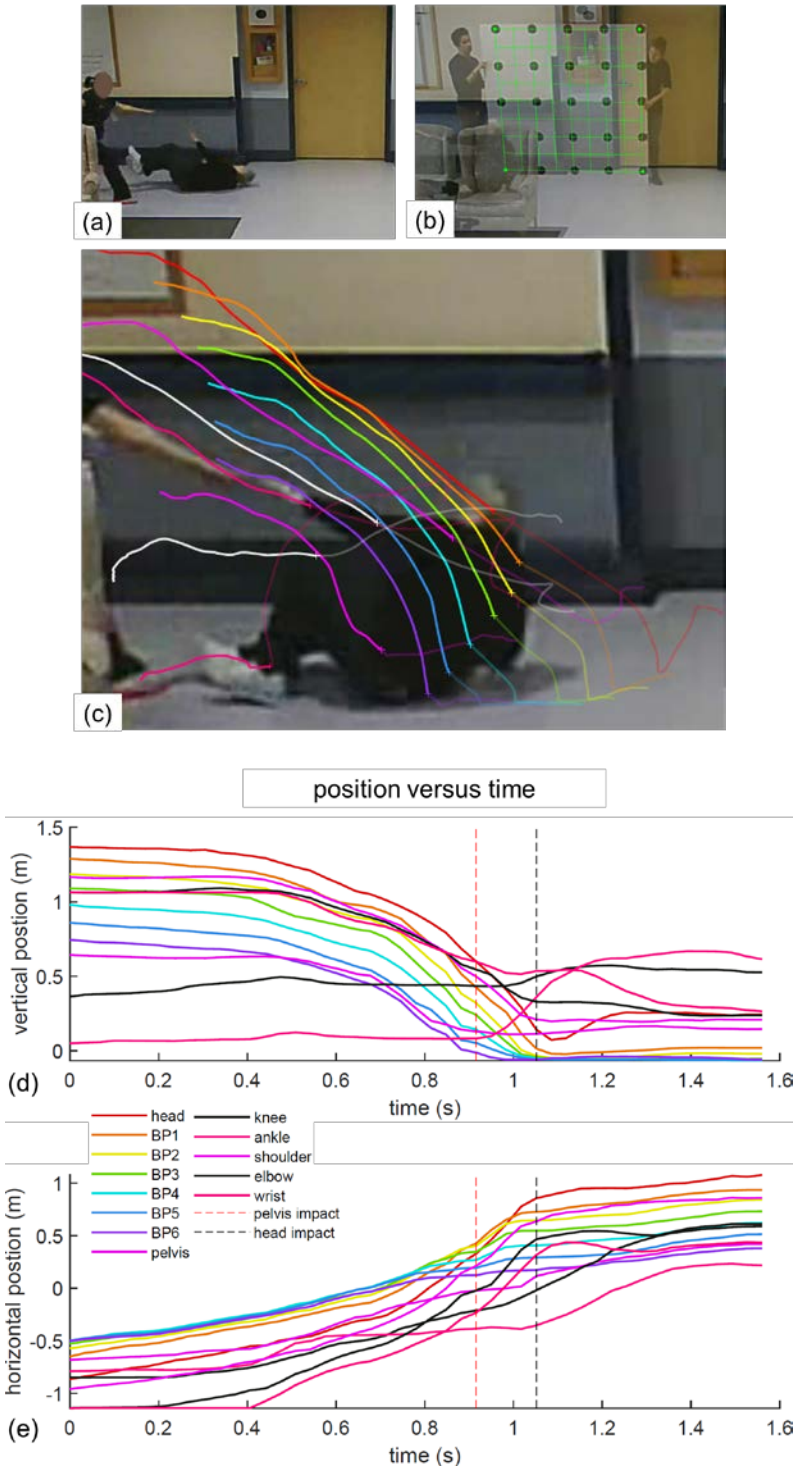

Figure 3. Digitization procedure for a sample fall.
(a) Snapshot from footage of a sample real-life fall (fall ID = 10) in long-term care. (b) Snapshot of calibration footage, where researchers positioned the calibration board (160x160 cm) at the estimated site and plane of the fall. (c) Sample digitized traces from Kinovea for 13 markers tracked manually. Calibrated (d) vertical and (e) horizontal position versus time data for the full duration of the fall, with red and black dotted lines indicating the perceived instants of pelvis and head impact, respectively.

2.2.4. Kinovea Validation

Previous studies have examined the reliability and accuracy of Kinovea in estimating body segment kinematics from planar video. (Post et al., 2018) used Kinovea to analyze video from typical broadcast cameras to measure skating speed during ice hockey exercises and compared Kinovea estimates to values measured by a high-speed camera (Photron Motion Tools) placed orthogonal to the plane of movement. They found no significant difference between speeds measured by the high-speed camera and those estimated by Kinovea from broadcast camera video ($p<0.05$). The lowest accuracy (R^2 =0.815; absolute percent error = 10.45%) resulted when the tracked athlete was moving directly toward the broadcast camera. Puig-Divi and colleagues (Puig-Diví et al., 2019) used Kinovea to derive data of the position of a physical model of the lower limb placed in different poses, from video footage acquired from cameras at four different perspectives (90, 75, 60, and 45 degrees). Kinovea position estimates were then compared to those derived from an AutoCAD model of the limb. They concluded that Kinovea was reliable in estimating 2D planar distances 5 m from the camera for all camera perspectives, and that optimal results were provided by an angle of 90 degrees. (El-Raheem, Kamel, & Ali, 2015) investigated the inter- and intra-rater reliability of Kinovea for measuring wrist joint range of motion, and reported Intraclass Correlation Coefficients (ICC) ranging from 0.877-0.987, depending on the type of movement. (Balsalobre-Fernández, Tejero-González, Campo-Vecino, & Bavaresco, 2014) used Kinovea to measure the jump height and flight time of 125 vertical jumps, and reported ICC=1 for both parameters between two observers.

I extended these efforts by examining the agreement between Kinovea and motion capture in describing the kinematics of backward falls acquired in the laboratory with two participants (one female and one male; aged 32 and 34 years). The participant was instructed to “fall naturally” in response to sudden forward translation of a 4.4x3.8 m padded, robotic platform, resulting in a backward fall (peak displacement = 0.8 m, peak velocity = 2.2 m/s, peak acceleration = 10 m/s^2). Whole-body movements were acquired with an 8-camera 3D motion capture system (MoCap) collecting data at 600Hz (Qualisys MIQUS), and a 30Hz 640x480 resolution surveillance video camera (Lorex LNZ44P4B) selected to closely match the specifications of cameras located in the LTC facilities. Reflective markers were placed on the participant’s head, shoulder, and greater trochanter (GT). The surveillance cameras were oriented perpendicular to the plane of

the fall (90 degrees), and at angles of 60 and 30 degrees to the plane of the fall. Marker positions were manually digitized frame-by-frame throughout the fall in Kinovea. Pixel values from the video were converted to distances using a custom 160x160 cm calibration panel, containing a 5x5 grid of circular markers spaced 40 cm apart, which was positioned in the plane of the fall. frequency of 5Hz was <0.24 m/s, or 5.69% of the peak amplitude of the velocity.

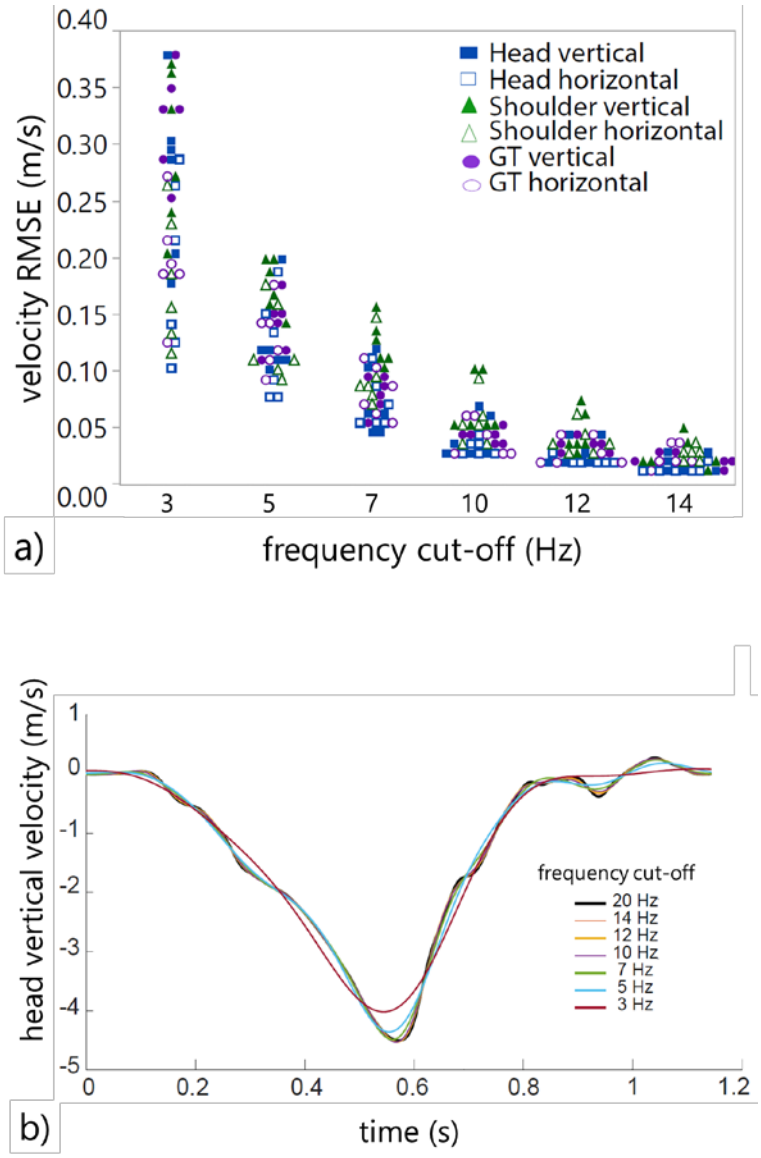

Figure 4. Results from MoCap frequency content analysis.
Analysis of the frequency content of velocities of different body sites from 600Hz motion capture (Qualisys). a) root mean square error (RMSE) for velocity data derived from Qualisys position data filtered with a range of cut-off frequencies, when compared to 'ground truth' velocity data from filtering at 20 Hz. b) head vertical velocity versus time, showing how the velocity profile changes with cut-off frequency.

A power analysis of time-varying velocities derived from differentiating unfiltered MoCap position data revealed that over 80% of the signal energy resided below 20Hz. The Root Mean Square Error (RMSE) between MoCap velocities low-pass filtered with a 20 Hz cut-off frequency (considered to be 'ground truth') and Kinovea data filtered with a cut-off

To assess the inter-rater reliability of Kinovea in digitizing backward falls, I compared the results from two raters who independently digitized one fall from three different camera angles (30, 60 and 90 degrees). For all camera views, the RMSE for head position data between the two raters was less than 0.9 cm, and the RMSE in peak head velocity was below 0.11 (SD = 0.07) m/s for vertical velocity and 0.19 (0.13) m/s for horizontal velocity. For a 90 degree camera angle, the RMSE in vertical velocity was 0.0913 (SD = 0.074) m/s, and the RMSE in horizontal velocity was 0.0825 (SD = 0.053) m/s.

2.3. Data Analysis

2.3.1. Fitting and differentiation

For each fall, I used Kinovea to digitize raw, calibrated position data. The raw data were linearly interpolated to 30 Hz to account for imperfections with the surveillance camera capture rates and ensure equal spacing between datapoints. The interpolated data were then smoothed using a 4^{th}-order zero-phase digital Butterworth filter at a 5Hz cut off (Figure 5). Vertical and horizontal velocity profiles were then estimated by applying central finite numerical differentiation to position data.

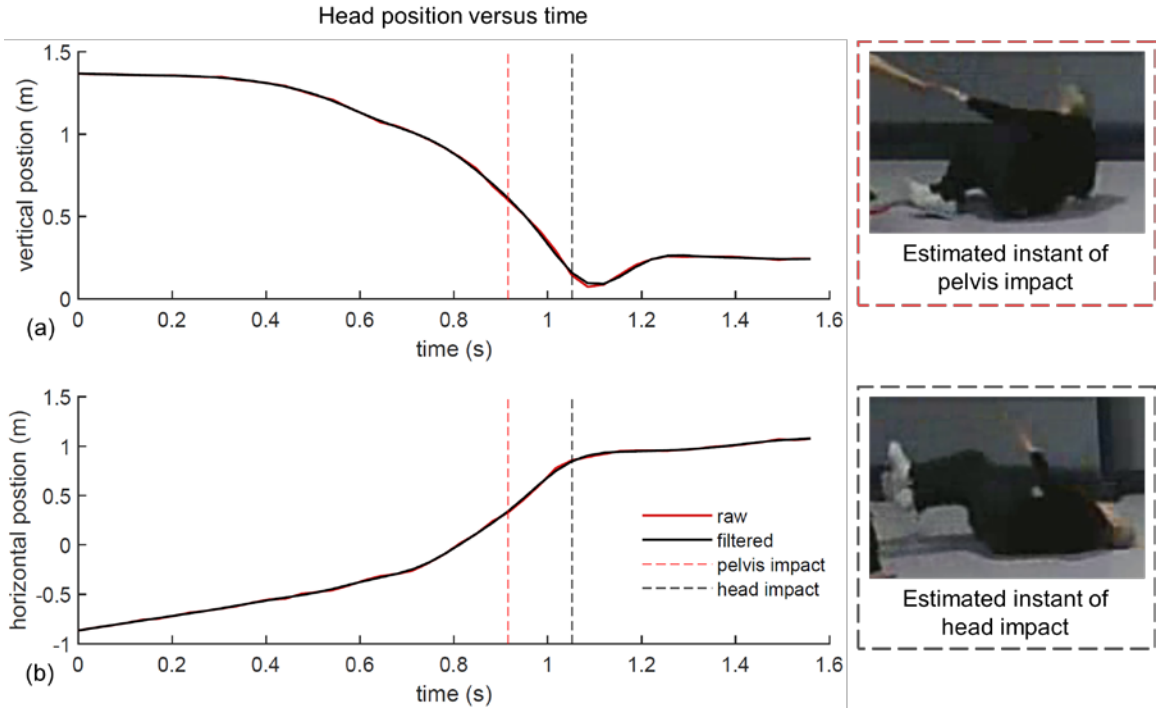

Figure 5. Effect of filtering in Kinovea.
Sample fall (video ID = 10) showing the effect of filtering on vertical and horizontal position versus time traces for the full fall duration. The red and black dashed vertical lines indicate the estimated instants of pelvis and head impact, respectively.

2.3.2. Impact Velocity

I report peak vertical velocities of the head, and corresponding magnitudes of horizontal head velocity. I also report values of head velocity when the head was 5, 7.5 and 10 cm above the ground (Figure 6). I regarded the latter as more accurate estimates of the impact velocity of the head at the instant it first contacts the ground, based on the observation that all falls involved pelvis and shoulder impact before head impact, and the likelihood that these earlier impacts may have slowed the downward velocity of the head, before the head experienced impact. For these reasons, I examined head velocities at specific heights (5, 7.5 and 10 cm) above the position of the head at impact, as representative of the impact velocity of the head just before it contacts the ground. The position of the head at impact was defined as the minimum vertical position within a 200 ms window centered about the head impact frame as identified by the team of three observers.

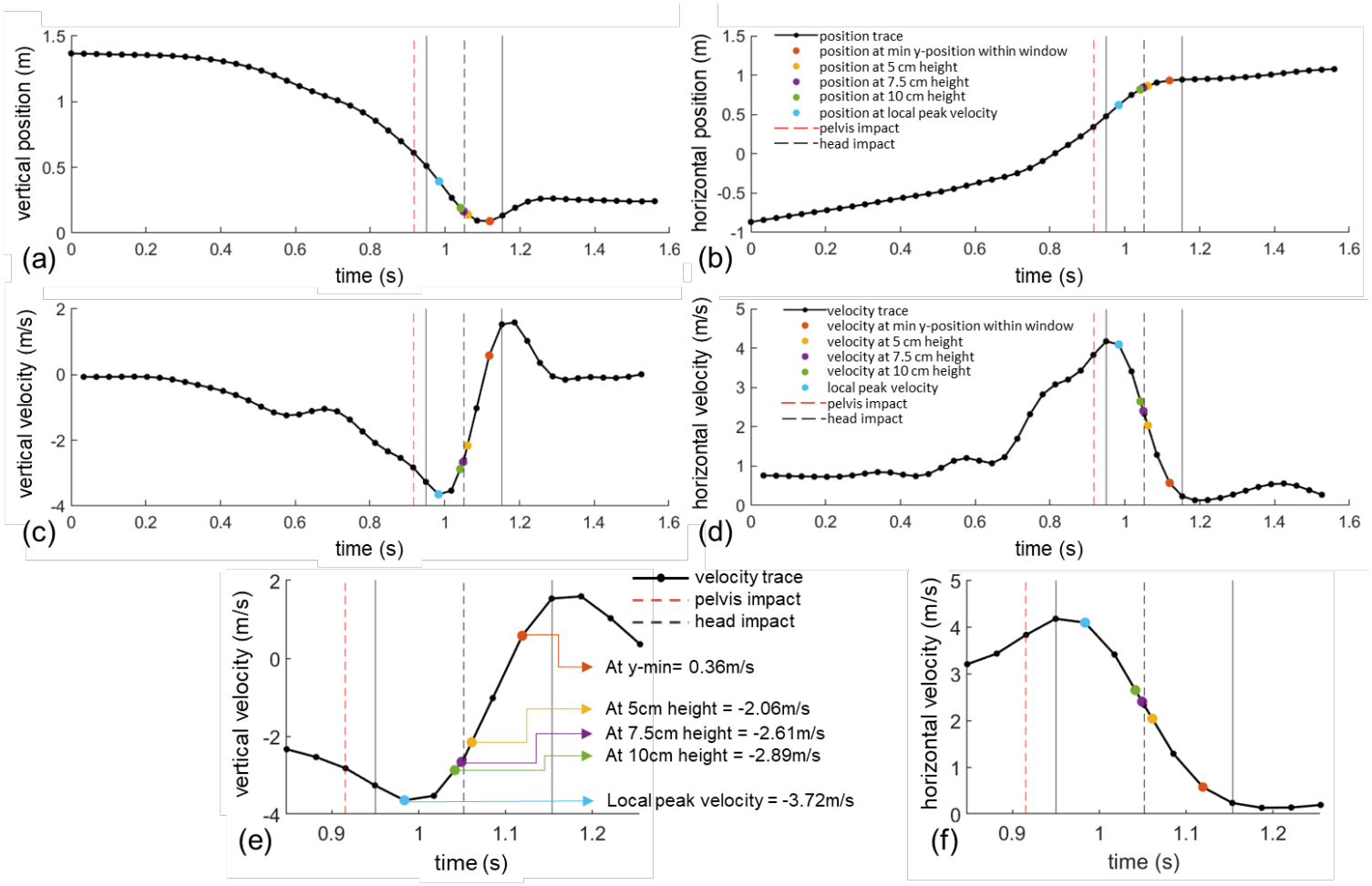

Figure 6. Technique for determining reported head velocities at different heights.
Top row (a & b): Time-varying vertical and horizontal positions of the head. Middle row (c & d): Head velocities based on differentiating the position data. Bottom row (e & d): 400ms window illustrating head velocity at peak downward position of the head (red circles: vertical velocity is close to zero), at heights of 5, 7.5 and 10 cm above the peak downward position (yellow, purple, and green circles), and at the instant of peak vertical velocity (blue circle).

2.3.3. Fall descent duration

Fall descent duration was defined as the interval between the onset of steady descent of the head and the instant of perceived impact for each marker of interest. Each of these two instants was estimated independently by three observers, and average values were used to determine reported fall descent durations.

2.3.4. Fall descent height

The descent height for each tracked body site was defined as the maximum vertical distance traversed by each marker between the start and the end of the fall. Fall descent heights were also calculated for the stage of descent occurring after pelvis impact.

2.3.5. Segment angles

I quantified absolute angles for the torso, head, and upper and lower limbs throughout the fall. Using the digitized body landmarks, segment endpoints were defined based on corresponding joint centers (JC) of rotation (Table 4). Angles were computed with respect to the horizontal axis, measured positive in a counterclockwise direction (Figure 7). Additionally, I calculated the curvature of the torso at different instances during the fall, where the main findings are briefly summarized in Section 2.4.5. A more detailed report of the approach used to characterize back curvature features is presented in the appendix (0).

Table 4. Body segment definitions for rotational kinematics

Body segment	proximal endpoint	distal endpoint
Head segment	shoulder JC	Head CG
Torso segment	pelvis JC	shoulder JC
Thigh segment	pelvis JC	knee JC
Shank segment	knee JC	ankle JC
Upperarm segment	shoulder JC	elbow JC
Forearm segment	elbow JC	wrist JC

CG = center of gravity, JC = joint center of rotation

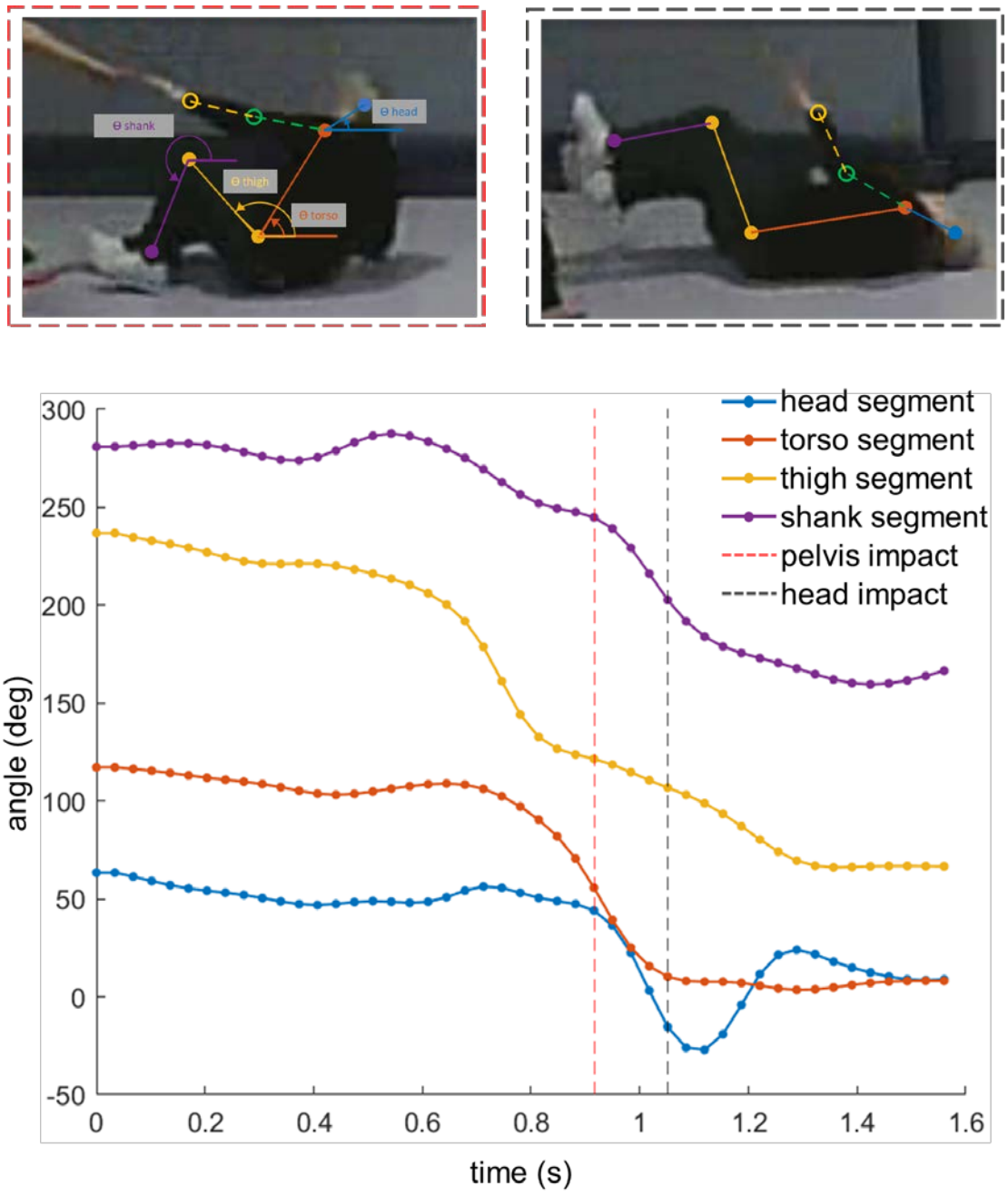

Figure 7. Sample body segment definitions and angle time histories
Sample fall (Video ID = 10) segment angle definitions for the head, torso, thigh, and shank segments. Segment angle time histories for this fall. The red and black dotted lines indicate the instant of pelvis and head impact respectively.

2.4. Results

2.4.1. Fall characteristics

The 11 backward falls from standing height included in this analysis (Table 5) were experienced by 10 older adults (2 males and 8 females) of average age 80.5 years (SD = 11.0), body height 158.8 cm (SD = 6.0) and body mass 60.0 kg (SD = 17.9). The activity at the time of the fall was standing for 6 of the 11 falls (55%), walking for 3 falls (27%), standing supported by a mobility aid (rollator) for 1 case (9%) and transferring from standing for 1 case (9%). The perceived biomechanical cause of the fall was incorrect weight shifting/transfer for 5 cases (46%), bump/hit for 3 cases (27%), trip/stumble for one case, loss of support for one case, and loss of consciousness for one. In 10 of the 11 falls, contact occurred to at least one hand/wrist, and contact to the elbow/forearm occurred in all falls. All falls involved pelvis impact before head impact.

Table 5. Summary of resident characteristics and fall data

Video ID	Resident ID	Standing height (cm)	Body mass (kg)	BMI (kg/m/m)	Age (yrs)	Sex; 8 females	Cause	Activity	Stepping response	hand / wrist impact	elbow / forearm impact
1	1	162	46.5	17.7	68	F	B	S	Yes	Yes	Yes
2	1	162	46.5	17.7	68	F	IT	S	Yes	Yes	Yes
3	2	156	59.0	24.2	78	F	B	S	Yes	Yes	Yes
4	3	161	89.7	34.6	83	M	LOS	SS	No	No	Yes
5	4	152	47.9	20.7	89	F	T	W	Yes	Yes	Yes
6	5	164	59.0	21.9	59	F	LOC	S	No	Yes	Yes
7	6	153	48.4	20.7	90	F	IT	Tx	No	Yes	Yes
8	7	152	46.7	20.2	89	F	B	W	Yes	Yes	Yes
9	8	168	97.8	34.7	83	M	IT	S	No	Yes	Yes
10	9	165	65.6	24.1	93	F	IT	W	Yes	Yes	Yes
11	10	152	53.3	23.1	86	F	IT	S	No	Yes	Yes
mean		158.8	60.0	23.6	80.5						
standard deviation		6.0	17.9	5.9	11.0						
minimum		152.0	46.5	17.7	59.0						
maximum		168.0	97.8	34.7	93.0						

Sex: F = female, M = male; Cause of fall: B = Bump, IT = incorrect transfer/shift of body weight, LOS = loss of support with external object, T = trip/stumble, LOC = loss of consciousness; Activity at time of fall: S = standing, Wh = wheeling a mobility aid, W = walking, Tx = transferring from standing to sitting.

2.4.2. Descent heights

The total descent heights for the head, shoulder, hand and pelvis averaged 122.2 (SD=13.4), 107.6 (10.9), 79.4 (15.0), and 63.5 (11.3) cm, respectively (Table 6). The descent heights after the instant of pelvis impact averaged 45.8 (SD=17.0), 32.4 (13.8), and 7.4 (10.2) cm for the head, shoulder and hand.

2.4.3. Descent durations

Descent durations for the head, shoulder, hand and pelvis averaged 1168 (SD=390), 1124 (389), 865 (345), and 902 (360) ms, respectively (Table 6). The average descent time of the head between pelvis and head impact was 265 (SD=120) ms, and the average time interval between shoulder and head impact was 44 (15) ms.

2.4.4. Impact velocities

The average values of vertical head velocity at heights of 5, 7.5, and 10 cm before impact were 1.67 (SD=0.42), 2.05 (0.54), and 2.30 (0.65) m/s, respectively (Table 6). The peak vertical velocity of the head averaged 2.79 (SD=1.21) m/s. On average, peak vertical velocity occurred 4.6 frames (~150 msec) before the perceived instant of head impact based on viewing the video (Figure 6). All falls displayed clearly identifiable vertical velocity peaks after pelvis impact except for one (Video ID = 8). On average, the head was found to reach peak velocity at a height of 20.83 cm higher than the head's minimum position, where the lowest recorded height at which the head acheived peak velocity was 7.7 cm (corresponding to Video ID = 1). The. Horizontal head velocities at 5, 7.5, and 10cm heights averaged 1.17(SD=0.73), 1.43(0.76) and 1.67 (0.81) m/s, and the horizontal velocity at peak vertical velocity averaged 2.44(1.49) m/s. The peak vertical velocity of the pelvis throughout the fall averaged 1.61(SD=1.24) m/s, and the corresponding horizontal velocity averaged 0.90(0.69) m/s (Table 6).

Table 6. Translational fall kinematics

		Head												Pelvis			
						vertical velocity (m/s)				horizontal velocity (m/s)						vertical velocity (m/s)	horizontal velocity (m/s)
Video ID	Resident ID	descent height (m)	descent duration (ms)	descent height from pelvis impact (m)	descent duration from pelvis impact (ms)	peak velocity	at 5cm height	at 7.5cm height	at 10cm height	at peak vertical velocity	at 5cm height	at 7.5cm height	at 10cm height	descent height (m)	descent duration (ms)	peak velocity	at peak vertical velocity
1	1	1.34	867	0.53	333	1.89	1.58	1.97	2.20	0.16	0.09	0.19	0.29	0.57	533	2.00	1.10
2	1	1.30	1900	0.51	333	2.95	1.81	2.30	2.48	1.70	0.67	0.97	1.17	0.53	1567	1.79	0.50
3	2	1.12	1167	0.37	200	2.33	1.60	1.87	2.13	2.48	1.33	1.75	2.17	0.56	967	1.79	0.94
4	3	1.26	833	0.36	133	3.31	1.81	2.12	2.42	2.84	1.92	2.08	2.24	0.59	700	1.04	0.72
5	4	1.32	1200	0.33	440	1.62	1.14	1.37	1.52	1.06	0.74	0.85	0.97	0.79	760	4.18	2.38
6	5	1.38	680	0.80	120	5.61	2.39	3.03	3.66	5.26	1.08	1.59	2.10	0.75	560	2.27	-0.14
7	6	0.96	1840	0.39	240	2.79	1.74	2.18	2.36	2.41	1.03	1.39	1.69	0.53	1600	1.04	0.48
8	7	1.12	1280	0.37	400	1.13	0.84	1.04	1.20	0.88	0.79	0.85	0.96	0.61	880	1.75	0.95
9	8	1.11	920	0.18	120	3.02	1.82	2.11	2.40	3.65	2.84	3.03	3.22	0.85	800	1.10	1.71
10	9	1.36	1040	0.52	200	3.72	2.06	2.61	2.89	4.03	1.48	1.82	2.10	0.53	840	1.77	0.98
11	10	1.17	1120	0.66	400	2.32	1.57	1.90	2.06	2.32	0.95	1.19	1.40	0.66	720	1.18	0.23
mean		1.22	1168	0.46	265	2.79	1.67	2.04	2.30	2.44	1.17	1.43	1.67	0.63	902	1.81	0.90
standard deviation		0.13	390	0.17	120	1.21	0.42	0.54	0.65	1.49	0.73	0.76	0.81	0.11	360	0.89	0.69
minimum		0.96	680	0.18	120	1.13	0.84	1.04	1.20	0.16	0.09	0.19	0.29	0.53	533	1.04	-0.14
maximum		1.38	1900	0.80	440	5.61	2.39	3.03	3.66	5.26	2.84	3.03	3.22	0.85	1600	4.18	2.38

On average, the head was found to reach peak velocity at a height of 20.83 cm higher than the head's minimum position, The lowest height at which the head attained peak velocity was 7.7 cm (Video ID = 1)

2.4.5. Segment angles

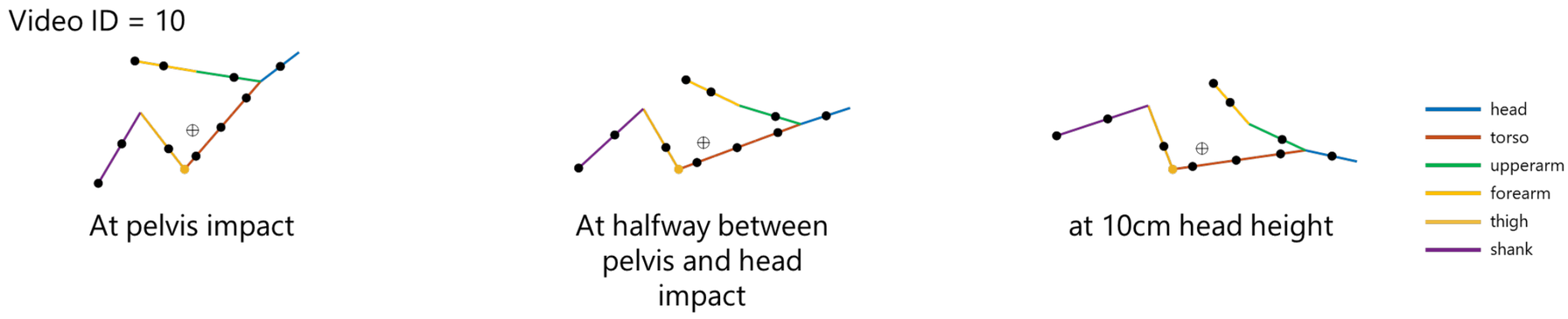

Figure 8. Supplementary segment angle stick figures
Figure provided to aid in interpreting the results shown in Table 7. These stick figures represent the segment angles formed by Resident 9 in Video 10 at three instants throughout the fall.

Table 7. Segment angle fall kinematics

Video number	Resident ID	at pelvis impact						halfway between pelvis and head impact						at 10cm height					
		head	torso	thigh	shank	upperarm	forearm	head	torso	thigh	shank	upperarm	forearm	head	torso	thigh	shank	upperarm	forearm
1	1	81.5	60.2	162.3	190.7	244.3	218.9	20.0	17.8	143.8	185.0	201.9	190.9	9.1	2.5	135.1	184.5	183.6	173.6
2	1	137.0	66.6	126.7	233.6	275.3	257.5	114.5	32.7	125.7	210.2	240.9	230.0	50.5	0.3	119.1	200.8	208.2	195.7
3	2	124.6	29.3	157.4	195.6	276.5	217.6	85.3	1.8	158.6	186.0	270.3	176.3	85.3	1.8	158.6	186.0	270.3	176.3
4	3	81.5	24.8	123.4	249.5	263.0	185.6	52.3	3.6	118.5	235.8	238.8	168.5	52.3	3.6	118.5	235.8	238.8	168.5
5	4	127.2	46.8	162.0	203.7	298.3	242.4	63.2	17.0	151.7	185.3	231.8	177.5	54.0	6.4	145.4	178.4	219.6	166.2
6	5	112.2	85.0	157.6	286.7	271.7	244.1	113.7	68.3	142.8	272.3	266.8	245.4	18.1	-6.6	146.1	187.5	189.8	167.9
7	6	126.5	56.2	117.7	249.7	298.3	182.9	96.9	13.3	100.9	206.7	261.2	134.2	81.2	5.1	97.9	198.4	250.9	122.1
8	7	108.3	52.9	173.9	193.4	304.3	240.1	76.0	12.0	166.8	200.8	233.8	174.6	54.9	5.0	163.4	204.2	219.5	159.3
9	8	68.2	11.9	138.3	250.4	228.3	191.3	35.3	1.4	138.2	251.4	206.7	182.9	51.6	5.7	137.0	252.0	216.1	186.6
10	9	44.1	55.7	121.5	244.9	168.8	167.7	22.6	25.2	114.7	229.3	159.1	148.5	-15.3	10.3	106.9	202.8	149.3	124.5
11	10	88.9	39.9	143.4	247.7	259.6	223.8	48.2	13.2	144.0	240.3	236.1	190.9	10.4	-5.8	142.3	239.3	208.1	174.0
mean		100.0	48.1	144.0	231.5	262.6	215.6	66.2	18.7	136.9	218.5	231.6	183.6	41.1	2.6	133.7	206.3	214.0	165.0
standard deviation		29.3	20.7	19.7	31.1	38.8	29.7	33.9	19.0	19.9	29.5	32.5	31.8	31.5	5.1	20.8	24.9	33.1	22.9
minimum		44.1	11.9	117.7	190.7	168.8	167.7	20.0	1.4	100.9	185.0	159.1	134.2	-15.3	-6.6	97.9	178.4	149.3	122.1
maximum		137.0	85.0	173.9	286.7	304.3	257.5	114.5	68.3	166.8	272.3	270.3	245.4	85.3	10.3	163.4	252.0	270.3	195.7

Figure 8 and Figure 7 are provided to aid in interpreting absolute segment angle values summarized in this table. All values are shown in degrees

At the instant of pelvis impact, the angles with respect to the horizontal averaged 99.98(SD=29.28) deg for the head, 48.10(20.66) for the torso, 144.03(19.67) for the thigh, 231.46(31.11) for the shank, 262.58(38.78) for the upper arm, and 215.62(29.71) for the forearm (Table 7). A comparison of angles across three instants (pelvis impact, midway between pelvis and head impact, and 10 cm above the ground shows how the head was often nearly upright until late in descent, and the thigh angle tended to decrease through descent (averaging 133.67 (SD=20.80) at the 10 cm head height), indicating raising of the legs after pelvis impact.

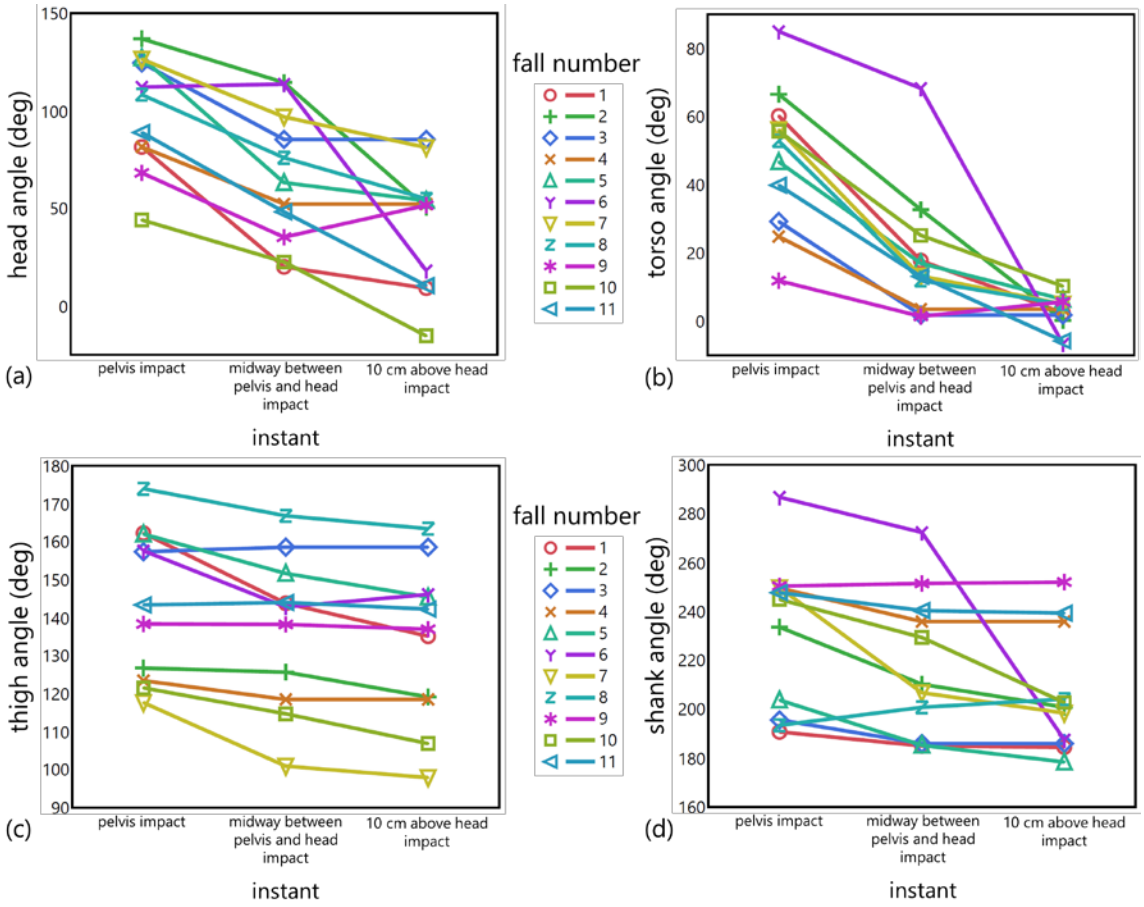

Figure 9. Summary plots of the body segment angles at three instants
Note that the straight lines connecting the data points are provided to enhance readability, but do not infer a linear trend between data points.

I summarized, in Table A2 and Table A3, the back curvature outcomes in terms of arc radii and angles at seven different instants ranging from 100 ms before pelvis impact to head impact. It was unclear from the results, if the back curvatures examined in the 11 falls could be categorized as either flat or curved as my results show a large

degree of variability in terms of back curvatures displayed throughout the fall. In terms of the back curvature features that were characterized by the six digitized back profile points (BP1 to BP6; Figure 3), arc 1, which covered the thoracic posterior torso region, was found to be more curved during the earlier parts of the fall compared to arc 2, which represented the lumbar posterior torso region, as reflected by a smaller average arc radius (measured at pelvis impact: 41.4 vs 64.0 cm, at midway between pelvis and head impact: 34.33 versus 282.1; and at head impact: 137.90 versus 266.21). Additionally, both arc 1 and arc 2 tended to show signs of 'flattening' as the fall progressed from the point of pelvis impact, as indicated by increasing average arc radius and arc angle values measured at pelvis impact, midway between pelvis and head impact, and at head impact. The range of arc 1 and arc 2 curvatures measured at pelvis impact was 14.9 cm to 151.3 cm, and 21.9 cm to 119.7 cm, respectively, and measured at head impact, the range exhibited was 7.33 to 600 cm and 46.68 to 1026.4 cm, for arc 1 and arc 2 respectively. Arc 1 was also found to be more curved during the earlier stage of the fall. These results show considerable variability in back curvature between falls and across different instances in each fall.

2.5. Discussion

Head impact is a common and often catastrophic consequence of falls in older adults. One-third of falls by older adults in LTC result in head impact (Schonnop et al., 2013), and falls are the underlying cause of 80% of traumatic brain injuries in older adults (Harvey & Close, 2012). The velocity and configuration of the head at impact are important determinants of injury risk, and essential initial conditions for biomechanical testing of protective headgear and flooring, which are promising strategies for reducing the risk of fall-related TBIs in high-risk populations or environments (Mackey et al., 2019; Post et al., 2013). In this study, I analyzed video footage of 11 real-life backward falls in older adults that involved head impact, to determine the time-varying positions and velocities of the body segments during the fall. I focused my analysis on determining the velocity of the head as it approached impact with the ground, and on describing the relative timing and configuration of the body when impact occurred to the pelvis, hands, shoulders and head.

My results show that backward falls in older adults involve complex dynamics that cause the downward velocity of the head to peak approximately mid-way between

pelvis and head impact, and slow before head impact. On average, the vertical velocity of the head peaked 138 ms before the perceived instant of head impact, with a magnitude of 2.79 m/s. However, when compared to its peak value, the vertical velocity was 18% slower (2.30 m/s) when the head was 10 cm above the ground, and 47% slower (1.67 m/s) when the head was 5 cm above the ground. The slowing in head velocity before impact may relate to the vertical forces generated by earlier impacts to the pelvis, torso, shoulders and upper limbs, or protective responses such as abdominal and neck muscle contraction (Choi et al., 2017; Kuo et al., 2020), and bracing of the upper limb with the ground (Chiu & Robinovitch, 1998; DeGoede, Ashton-Miller, & Schultz, 2003; Robinovitch & Chiu, 1998).

A study by Choi et al. reported peak velocities for the head and pelvis that were similar to mine, based on digitizing videos of eight backward falls in older adults that involved head impact (Choi et al., 2015). For example, peak head velocity in my study averaged 2.79 (SD=1.21) m/s) in the vertical direction and 2.44(1.49) m/s in the horizontal direction, while Choi et al. reported values of 2.91 (SD=0.86) and 2.64 (1.12) m/s, respectively. However, my results extend the findings of Choi et al. by showing that the velocity of the head at impact is nearly one-half the magnitude of the peak vertical velocity during descent. This observation has significant implications with regard to understanding TBI risk in falls, and in the design and evaluation of headgear or flooring to prevent fall-related TBIs.

A more recent study by Choi et al, 2017 (Choi et al., 2017) measured head impact velocities when young adults fell backward from standing onto a gym mat, while wearing a helmet. Impact velocities were measured at the instant the base of the helmet struck the mat. In trials when no attempt was made to slow head velocity, the impact velocity of the head averaged 3.23 m/s in the vertical direction and 2.74 m/s in the horizontal direction. The former value is 15% larger than my observed average value of peak vertical head velocity in falls by older adults (2.79 m/s), and 93% greater than the average value I observed when the heads was 5 cm above its maximum downward position (1.67 m/s). Choi et al. also conducted trials where participants were instructed to slow their head velocity before impact through activation of the neck extensor muscles (sternocleidomastoids). In this scenario, the head impact velocity averaged 1.73 m/s in the vertical direction and 1.50 m/s in the horizontal direction. Interestingly, the former

value is within 4% of the average value that I observed in older adults (1.67 m/s) at the 5 cm height.

Across the 11 falls, there were common features but considerable variation in the temporal sequence of impacts to body segments. In all falls, the pelvis impacted the ground before the head. The time interval separating these events averaged 265 ms, and ranged from 120 to 440 ms. Pelvis impact often caused a slowing of downward movement of the head, but never brought the head to zero velocity, and peak velocities of the head always exceeded those for the pelvis. Impact to the hand(s) occurred on average 38 ms before impact to the pelvis, which is similar to the near-simultaneous contact between the hands and pelvis observed in falls by young adults (Hsiao & Robinovitch, 1998). After pelvis impact, the upper-body descended in an inverted pendulum-like manner leading to head impact. Impact to the shoulders always occurred before the head, with an average time difference of 44 ms separating the events.

There was also considerable variability across the 11 falls in the configuration of the body segments at key instants. At the moment of pelvis impact, the angle of the head measured counterclockwise from the horizontal averaged 100 deg and ranged from 44 to 137 deg. The variability across falls in head orientation might reflect differences in neck strength and neuromuscular control (Anderson, Terzis, & Kryder, 1999; Kallman, Plato, & Tobin, 1990; Larsson, Grimby, & Karlsson, 1979). The angle of the torso from the horizontal averaged 48 deg, and ranged from 12 deg (nearly horizontal) to 85 deg (nearly vertical). The thigh angle averaged 144 deg and ranged from 118 deg (nearly vertical) to 174 deg (nearly horizontal). The relative angle between the torso and thigh averaged 96 deg, and the relative angle between the thigh and shank averaged 93 deg. As the fall progressed, the angle of the thigh with respect to the horizontal tended to decrease (by an average of 10.4 deg; range -1 to 27 deg), with clear evidence of leg raise between the instants of pelvis and head impact in 7 of the 11 videos (63%).

In an analysis of 215 backward falls in older adults (including 85 head impacts) Shishov & Robinovitch found that the occurrence of leg raise after pelvis impact reduced the odds for head impact 5-fold (Shishov & Robinovitch, 2018). The authors proposed that the underlying mechanisms may relate to conservation of angular momentum, with rotation of the lower limbs slowing downward rotation of the torso as the body pivots

about the pelvis. However, no study to my knowledge has assessed the effect of leg raise on head impact velocity.

We also recently showed how torque generation via contraction of flexor muscles at the hips and neck is essential to avoiding head impact in backward falls (Kuo et al., 2020). To my knowledge, previous studies have not examined how landing postures, or hip and neck torque generation during descent, affect head impact velocity in falls where head impact occurs. However, two previous studies report conflicting results on the effect of torso angle on the impact velocity of the pelvis in backward falls. Majumber et al., (Majumder, Roychowdhury, & Pal, 2009) conducted backward fall simulations at torso angles of 0, 15, 45, and 80 deg, and found that more upright torso configurations resulted in the higher peak force at the pelvis. However, (Sandler & Robinovitch, 2001) used one-, two-, and three-link inverted pendulum models of backwards falls to show how landing with an upright torso configuration reduced pelvis impact velocity through two mechanisms. First, when compared to landing with the trunk horizontal, landing with the torso upright reduced the change in potential energy during the fall. Second, landing with the torso upright allowed for greater hip rotation during descent that, when combined with hip extensor torques, allowed for greater joint energy absorption.

I observed considerable variation in the curvature of the torso between the instants of pelvis and head impact, reflecting that some falls involved a rolling contact spreading from the pelvis to the shoulders, while in others, contact occurred to the torso in a nearly flat configuration.

This study has several limitations. First, the small size of my dataset of 11 falls, along with the many factors that may affect head impact velocity in falls, prevents me from examining how factors such as leg raise, torso configuration at pelvis impact, and torso curvature after pelvis impact affected head impact velocities. However, my observations guide the development of physical reconstructions of falls with a falling dummy (Chapter 3) for systematically examining these factors. Second, variations across falls in video quality, camera orientation and accuracy in placement of the calibration board may have affected my results. However, the accuracy of my results is supported by my lab-based validation experiments, and the strong agreement between my results and those reported by (Choi et al., 2015) for peak vertical head velocity. Finally, I focused on analyzing backward falls from standing height involving head impact

with the ground, and the occurrence of impact to the pelvis and torso before head impact. While this represents a common scenario for head impact in falls by older adults, my results may not apply to falls from lower heights (e.g., falling off a chair), falls where the head strikes an object other than the ground (e.g., the wall or furniture), or falls involving mobility aids. Further work is required to analyze head impacts in these scenarios, and during forward and sideways falls. Finally, my analysis focused on describing the motion of the body in the perceived plane of the fall. Future work could investigate the feasibility of three-dimensional kinematic analysis of real-life falls, subject to the availability of two or more views of a given fall.

2.6. Conclusion

This study builds on previous work done to describe the kinematics of real-life backward falls involving head impact, as experienced by older adults in common areas of LTC facilities. My results show that such falls involve initial impact to the pelvis, with the torso oriented at 48 deg from the horizontal, followed by impact to the hands, torso and finally the head. The downward velocity of the head peaked between the instants of pelvis and head impact, and slowed by up to 48% before head impact, to a value that averaged 1.67 m/s. These results should inform the development of more externally valid approaches to biomechanical testing of TBI prevention strategies such as protective headgear and compliant flooring, and thereby contribute to the health and safety of older adults.

Chapter 3.

Development and application of a falling dummy to measure head accelerations during simulated backward falls

3.1. Introduction

Fall-related traumatic brain injury (TBI) is a significant cause of morbidity and death in older adults. People over age 75 have the highest rates of TBI-related emergency room visits, hospitalizations and deaths (Gardner et al., 2018). Nearly 80% of TBIs in this age group are caused by impact to the head during a fall. Indeed, TBI accounts for one-third of hospital admissions and more than 50% of deaths due to falls in older adults (Saari et al., 2007; Thomas, Stevens, Sarmiento, & Wald, 2008; Thompson, Mccormick, & Kagan, 2006).

Most older adult TBI patients report a history of head strike, typically from a fall from standing height or lower, and exhibit visible signs of head trauma (Hamden et al., 2014). The nature of the injury more often involves subdural hematoma than diffuse axonal injury (Gardner et al., 2018). However, in a study of 520 video-captured falls in long-term care, where 33% of falls were observed to involve the head impacting the ground or a nearby object, none resulted in diagnosed TBI (Yang et al., 2017). An improved understanding of the factors that separate injurious and non-injurious head strikes in falls should inform improvements in TBI prevention.

From a biomechanical perspective, the risk for TBI from a fall will depend on the magnitude and duration of translational and rotational accelerations of the head during the impact event. Animal studies (Gennarelli et al., 1981, 1972b, 1972a; Ommaya et al., 1967) and mechanical recreations of TBI events in humans hajiaghammemar, Nagata 2007 stuart 2011, Zhang 2004 (Caccese et al., 2016; Hajiaghamemar et al., 2015; Nagata & Ohno, 2007; Stuart Walsh, Rousseau, & Blaine Hoshizaki, 2011; L. Zhang et al., 2004) have shown that the occurrence and severity of TBI increases with the magnitude of head acceleration, and with increases in the duration of the acceleration impulse. However, linking head accelerations to the characteristics of falls in humans is

challenging, due to the obvious safety concerns involved in experiments with living humans, which have restricted human studies to the use of very low impact velocities (Ito et al., 1997) or landing surfaces that are highly padded (Choi et al., 2017, 2015). Existing knowledge is based largely on mechanical recreations (with anthropomorphic dummies of simplified physical systems) (Caccese et al., 2016; Doorly et al., 2005; Hajiaghamemar et al., 2015; Nagata & Ohno, 2007; Schulz et al., 2008; Seidi et al., 2015), and mathematical models (Doorly et al., 2005; Fréchède & McIntosh, 2009) of fall-related head impacts, which have examined how head accelerations depend on the mass, stiffness and impact velocity of the head and brain, the location of impact on the scalp, and the stiffness of the impact surface

However, previous studies involving fall recreations have been limited by lack of information on the kinematics of real-life falls in older adults to guide the physical or theoretical recreation of the impact event. For example, studies have used head impact velocity up to 7.70 m/s (J. Zhang et al., 2009), which far exceeds the mean impact velocity of the head of 2.79 m/s observed from my video analysis of real-life falls in older adults, as described in Chapter 2, and the mean impact velocity of 2.91 m/s reported by Choi et al. (Choi et al., 2015). Furthermore, anthropomorphic dummies may fall in a manner that poorly represents the typical sequence of impacts and landing configurations of real-life falls in older adults.

My goal in the current study was to examine, using a falling dummy, how the characteristics of backward falls affect the magnitude and duration of head accelerations during impact. I focused on backward falls, since clinical studies have shown that backward falls are the most common cause of head impact and TBI in older adults (Hwang et al., 2015; Pöyry et al., 2013; Schonnop et al., 2013). For older adults who have visited hospital emergency rooms after hitting their head in a fall, the likelihood for acute brain lesions from CT scanning was 4-fold higher for those who fell backward than forward (Hwang et al., 2015), and 2-fold higher for falls causing impact to the occipital (posterior) region of the skull, when compared to falls with an unknown impact location (Pöyry et al., 2013). For older adults in long-term care, forward falls create the greatest risk for head impact, but backward falls are nearly four times more common, and represent the most common scenario leading to head impact (Schonnop et al., 2013).

Furthermore, I focused on simulating the portion of the fall occurring between pelvis impact and head impact, based on my observation (presented in Chapter 2) that most backward falls in older adults leading to head impact involve impact to the pelvis before the head. Within this context, I systematically altered the characteristics of the dummy and environment, to address three research questions:

(1) How does head impact severity (as measured by the magnitude and duration of translational and rotational head acceleration at impact) depend on torso curvature during landing? As described in Chapter 2, I found that falls in older adults involve a wide range of torso curvature (secondary to spine flexion) between the instants of pelvis and head impact. Torso configurations ranged from a highly flexed condition that produced rolling contact of the torso against the ground, to a “flat back” condition where the torso impacted the ground near-simultaneous with the head. The rolling contact provided by a curved torso may more effectively distribute the impact energy of the fall and lower the impact velocity of the head. Based on this consideration, I hypothesized that head impact severity would be lower in falls with the dummy involving a curved torso than a flat torso configuration.

(2) How does head impact severity depend on lower limb dynamics after pelvis impact? I found that falls in older adults involved a considerable range of leg raise following pelvis impact. We previously reported that raising of the legs after pelvis impact reduced the risk for head impact in backward falls in older adults (Shishov & Robinovitch, 2018), possibly due to rotation of the lower limbs reducing the downward angular momentum of the torso. Accordingly, I hypothesized that falls with the dummy having fixed hips, thereby allowing leg raise, would result in lower magnitudes of head impact severity, when compared to falls with freely rotating hips (that allow for minimal leg raise).

(3) How does head impact severity depend on modifications to the stiffness of the ground, and how does the effect of surface stiffness on head impact severity depend on the potentially interacting effects of torso curvature, lower limb dynamics, and impact velocity? Compliant flooring is a promising approach for reducing the risk for TBI in high-risk environments such as long term care (Mackey et al., 2019), but such floors must be designed to be soft enough to substantially reduce impact severity during falls, while stiff enough to allow for rolling of equipment and wheelchairs. The reduction in impact

severity must be measured under conditions that realistically simulate falls in older adults. I used my falling dummy to evaluate the protective value of modifications in ground stiffness under different falling conditions. I hypothesized that the effect of reducing floor stiffness on head impact severity would depend on torso curvature, lower limb dynamics, and impact velocity.

3.2. Methods

3.2.1. Falling dummy

The falling dummy used in this study (Figure 10) consisted of a single torso segment, two legs and a Hybrid III head- and neckform (50th percentile; Humanetics ATD, USA). The torso was constructed of Unistrut, steel weight plates, and plywood rigidly fastened together, with foam rubber (1.3 cm-thick, 81 durometer) representing the peripheral soft tissues (Figure 11). The lower limbs were constructed of Unistrut and steel weight plates. The total mass of the dummy was 36.38 kg, and mass moment of inertia of the dummy about the sagittal axis with respect to its centre-of-mass was 4.4983 kgm^2. Further details on the inertial parameters of the dummy are described in Table C1 of 0.

Trials were conducted with two distinct torso profiles and two distinct hip stiffness conditions for the dummy Figure 10. The torso profiles (flat torso vs curved torso) varied in the geometry of the posterior margin of the torso. The curved torso (CT) mimicked and fell within the range of back curvature parameters exhibited by older adults during backward falls, as described in Chapter 2 (Table A2 and Table A3). The flat torso (FT) simulated a fall with near-simultaneous contact to the lumbar and thoracic regions of the torso just before head impact. The hip stiffness conditions (fixed versus freely rotating) allowed for different amounts of leg raise between the instants of pelvis and head impact. In the fixed hips (FH) condition, the lower limbs were rigidly fixed to the torso so the angle between the lower limbs and torso was maintained at 125^o throughout the fall. In the rotating hips (RH) condition, each of the two lower limbs were secured to the torso at the hip via low-friction piano hinges, which allowed them to freely rotate in flexion and extension.

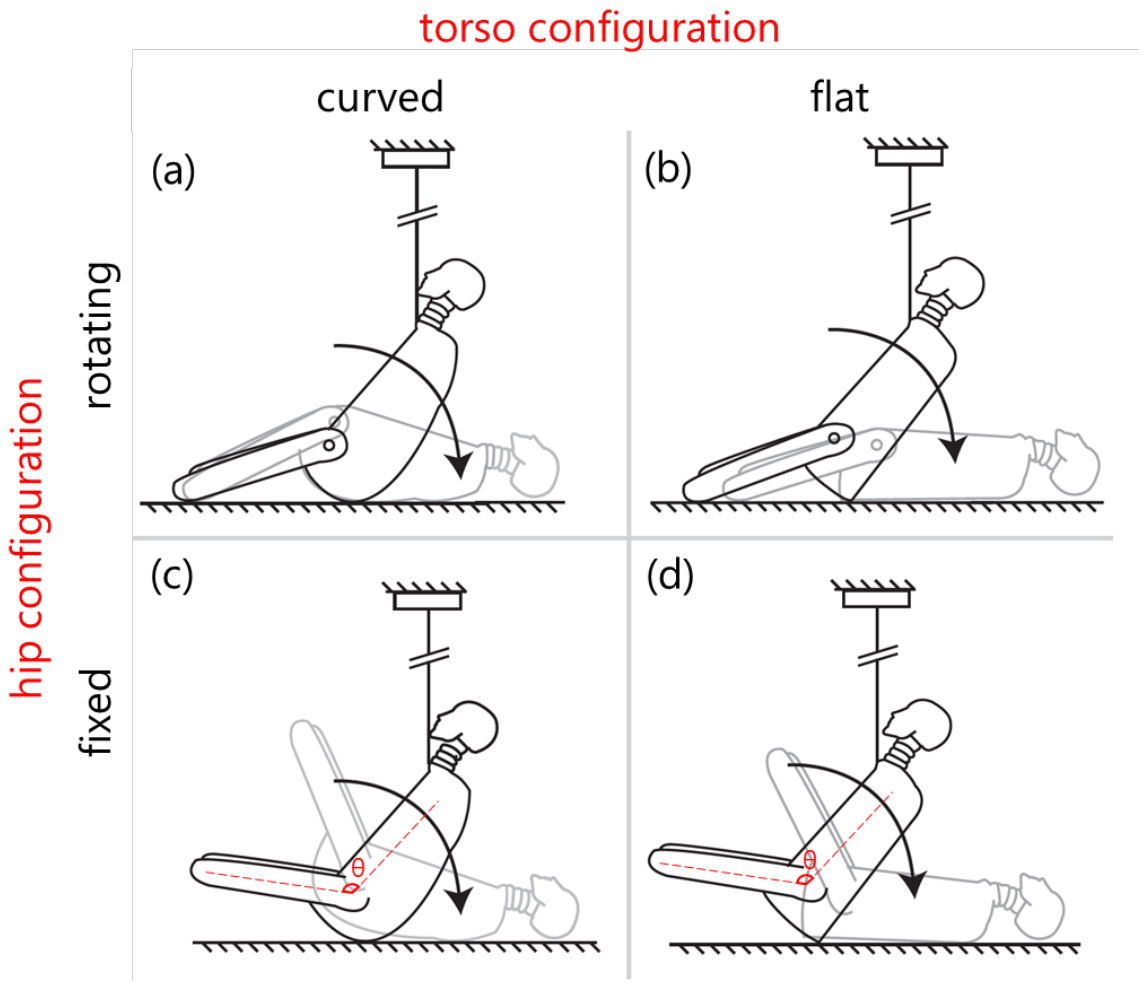

Figure 10. Schematics of the four dummy configurations used in fall simulations

The four configurations involved two torso curvatures (flat vs curved) and two hip stiffness conditions (rotating vs fixed). In the fixed hips condition, the relative angle between the torso and lower limbs (θ) was fixed at 125°. In all trials, the dummy was released from a seated position using an electromagnet and inextensible tether.

3.2.2. Flooring conditions

Tests were conducted with four different floor conditions: metal (aluminum 8080), plywood, high density polyethylene foam (HD80; of density 80 kg/m^3), and SmartCells compliant flooring (SATECH, Inc., Chehalis, WA, US). Each floor sample had a surface area of 30 cm x30 cm, centered at the approximate location of head impact, and a thickness of 2.54 cm. The surface of the floor sample was flush with the adjacent plywood platform supporting the pelvis and torso.

3.2.3. Experimental protocol

Before each trial, an inextensible overhead tether was used to secure the dummy in an inclined seated position, with the distal aspect of the torso (which represented the pelvis) contacting a large plywood platform. The tether was attached at one end to an overhead electromagnet and at the other end to an eye bolt fastened to the top (proximal aspect) of the torso. The height above the ground of the measured COG of the head was held constant at 73 cm for all trials. The electromagnet was then disengaged, causing the dummy to fall (rotate downward) under the force of gravity. A catch mechanism prevented the slackened tether from interfering with the dummy dynamics after fall initiation.

Three trials were conducted for each of the four dummy configurations (flat torso with fixed hips (FTFH), flat torso with rotating hips (FTRH), curved torso with fixed hips (CTFH), and curved torso with rotating hips (CTRH)) and for each of the four flooring conditions, for a total of 48 trials. All testing was conducted at 23^{o} C and 42% humidity. The time interval between trials was 90 seconds as per ASTM F1045.

Figure 11. Sequence of images showing a sample dummy fall simulation.
The figure shows the dummy in a curved torso with fixed hips configuration (CTFH) leading to head impact on a plywood impact surface.

3.2.4. Data collection

The head form was instrumented with an array of nine translational accelerometers (Model 7624C, Endevco, Meggitt, USA) mounted in a (3-2-2-2) configuration, which allowed for the measurement of the 3D translational and rotational acceleration of the head centre-of-gravity (CG) (Padgaonkar, Krieger, & King, 1975; Takhounts, Hasija, & Eppinger, 2009). A certified calibration of the head- and neckform was performed in 2016 by technicians from Humanetics. I further evaluated the accuracy of translational head CG acceleration measures through a set of drop tests onto a forceplate (model No. 4060H, Bertec, Columbus, OH; forceplate data acquisition rate =

1000 Hz) from five different heights (Figure 12). The measured mass of the instrumented head form (4.75 kg) was estimated with 0.21% error (true value = 4.76 kg), based on the best-fit line ($F_{max} = 4.75*a_{max}$; $R^2 = 0.99$) between peak resultant force from the force plate (F_{max}) and peak resultant acceleration from the Hybrid III sensors (a_{max}) (Potvin et al., 2019).

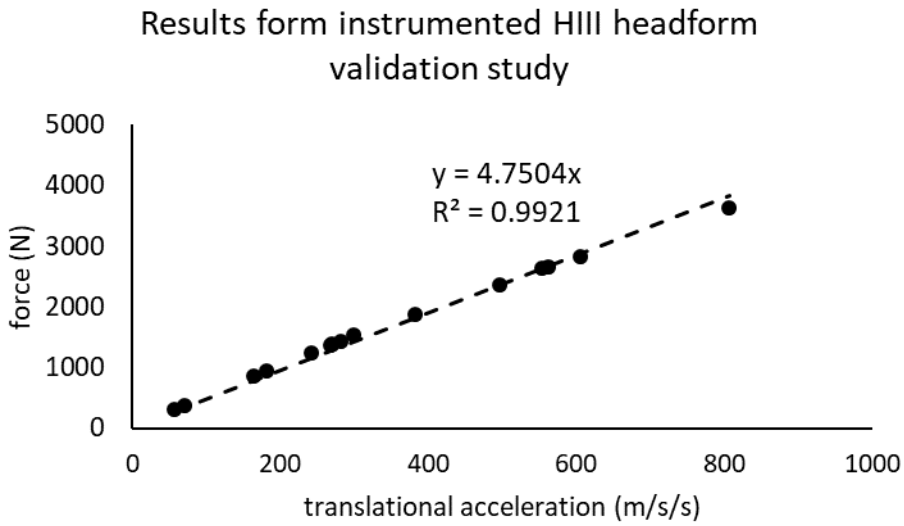

Figure 12. Hybrid III head form validation results
Measured peak force (from the forceplate) and measured peak translational head acceleration (from the headform accelerometers) from the headform validation experiment. The best-fit straight line through the data yielded a slope of 4.75 kg, which lies within 0.21% of the actual headform mass (4.76 kg).The Hybrid III head accelerometry was sampled at 20 kHz for a duration of six seconds spanning three seconds before and after a 1 g threshold trigger. The data were collected using a SLICE NANO (DTS, USA) with 16-bit resolution, and a successive approximation register (SAR)-type analog-to-digital convertor. Data acquisition, storage, processing and exporting was done using SLICEWare software on a Windows PC and then analyzed using MATLAB (Mathworks). As per (J211-1, 1995), the raw translational accelerometry data were filtered using a Channel Frequency Class 1000 (CFC1000) fourth order zero-phase digital filter (MATLAB filtfilt) with a cutoff frequency of 1650 Hz (Figure 13). The rotational acceleration data were solved for using the equations summarized in 0 as described by (Padgaonkar et al., 1975). For each trial, I determined peak magnitudes of translational and rotational head CG acceleration, along with time-to-peak (TTP) values, and durations of acceleration (Figure 13) based on the approaches described by (Post, Walsh, Hoshizaki, & Gilchrist, 2012).

I used Kinovea, an open-source digitization and video analysis software (Kinovea – 0.8.27, www.kinovea.org/), to capture the time-varying positions of markers placed on the head, torso, and legs of the dummy at 30Hz following the same method described in Chapter 2 - Digitization of time-varying positions methods section. Position data were low-pass filtered using a 4^{th} order recursive Butterworth filter with a cut-off frequency of 5 Hz, based on the rationale provided in Chapter 2 Section 2.2.4. The position data were then numerically differentiated to determine velocities. I report and focus on peak vertical velocities but, as with my analysis of real-life falls in Chapter 2, I compare their values to those measured at 5, 7.5, and 10 cm above the perceived instant of head impact in the Appendix (0).

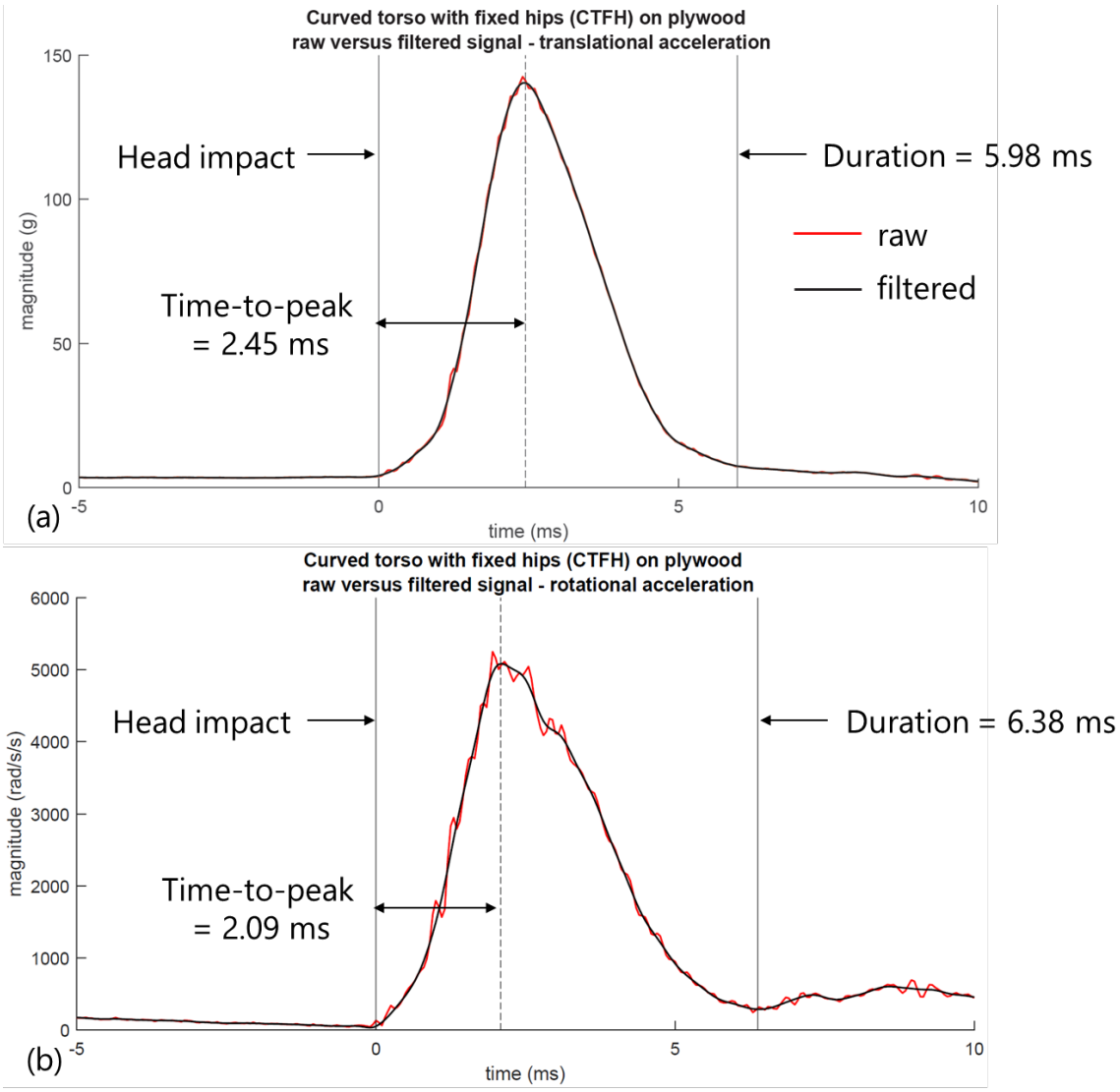

Figure 13. Example dummy head acceleration traces and effect of CFC1000 filtering

Traces from a typical trial of (a) translational acceleration and (b) rotational acceleration of the head CG data for an impact on plywood using the curved torso with fixed hips (CTFH) dummy configuration. Raw signals are shown in red and filtered signals are shown in black. The dashed vertical lines show the index at which the peak occurs, where the vertical solid lines show the signal onset and end points used to calculate time-to-peak (TTP) and duration.

3.2.5. Statistical analysis

I used three-way analyses of variance (ANOVA) and post hoc Tukey honestly significant difference (HSD) tests to examine the associations between my outcome variables (peak magnitudes and durations of head translational and rotational acceleration) and my explanatory variables (torso shape, hip stiffness and flooring

material). All tests were conducted with JMP (version 15, SAS Institute) using a significance level of $\alpha = 0.05$.

3.3. Results

3.3.1. Head impact velocity and fall descent duration

The impact velocity of the head (Figure 14 and Table 8) associated with torso configuration ($p<0.0001$) and hip stiffness ($p<0.0001$) but not with floor condition ($p=0.16$). When compared to the curved torso condition, the flat torso condition produced vertical impact velocities that averaged 25% higher (2.83 (SE=0.02) versus 2.19 (SE=0.03) m/s), and horizontal impact velocities that averaged 17% higher (1.41 (SE=0.02) versus 1.19 (SE=0.03) m/s). When compared to the fixed hip condition, the rotating hip condition produced vertical impact velocities that averaged 24% higher (2.82 (SE=0.02) versus 2.21 (SE=0.03) m/s), and horizontal impact velocities that averaged 46% higher (1.60 (SE=0.02) versus 1.00 (SE=0.03) m/s). There was a significant interaction between torso configuration and hip stiffness for vertical impact velocity ($p=0.0015$), but not horizontal impact velocity ($p=0.3282$).

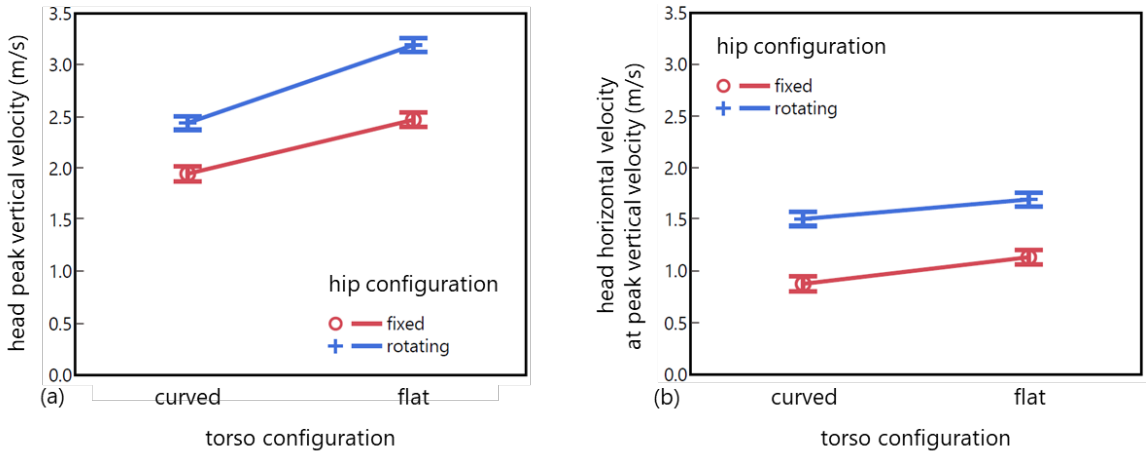

Figure 14. Dummy peak head velocities for all four configurations
Mean values of (a) the vertical and (b) the horizontal components of the impact velocity of the head for falls with the two torso configurations and two hip stiffness conditions. Error bars show ± one standard error. Note that the straight lines connecting the data points in these interaction plots are to enhance readability, and do not infer a linear trend between data points.

The descent duration (Table 1), defined as the interval between disengaging the electromagnet and the onset of head impact, associated with torso configuration

($p<0.0001$) and hip stiffness ($p<0.0001$) but not with floor condition ($p=0.5759$). Furthermore, there was a significant interaction between torso configuration and hip stiffness on fall duration ($p=0.0005$). The shortest average descent duration was observed in the FTRH condition (478 ms), and the longest (800 ms) was observed in the CTFH configuration.

3.3.2. Head accelerations during impact

Traces of head acceleration tended to be characterized by a single peak value, that was highly repeatable across trials (Figure 15). However, the flat torso, rotating hips condition produced greater variability, and the frequent existence of two peaks in both rotational and translational head accelerations, corresponding to shoulder impact and subsequent head impact. This two-peak behavior was not observed in the curved torso or fixed hips conditions.

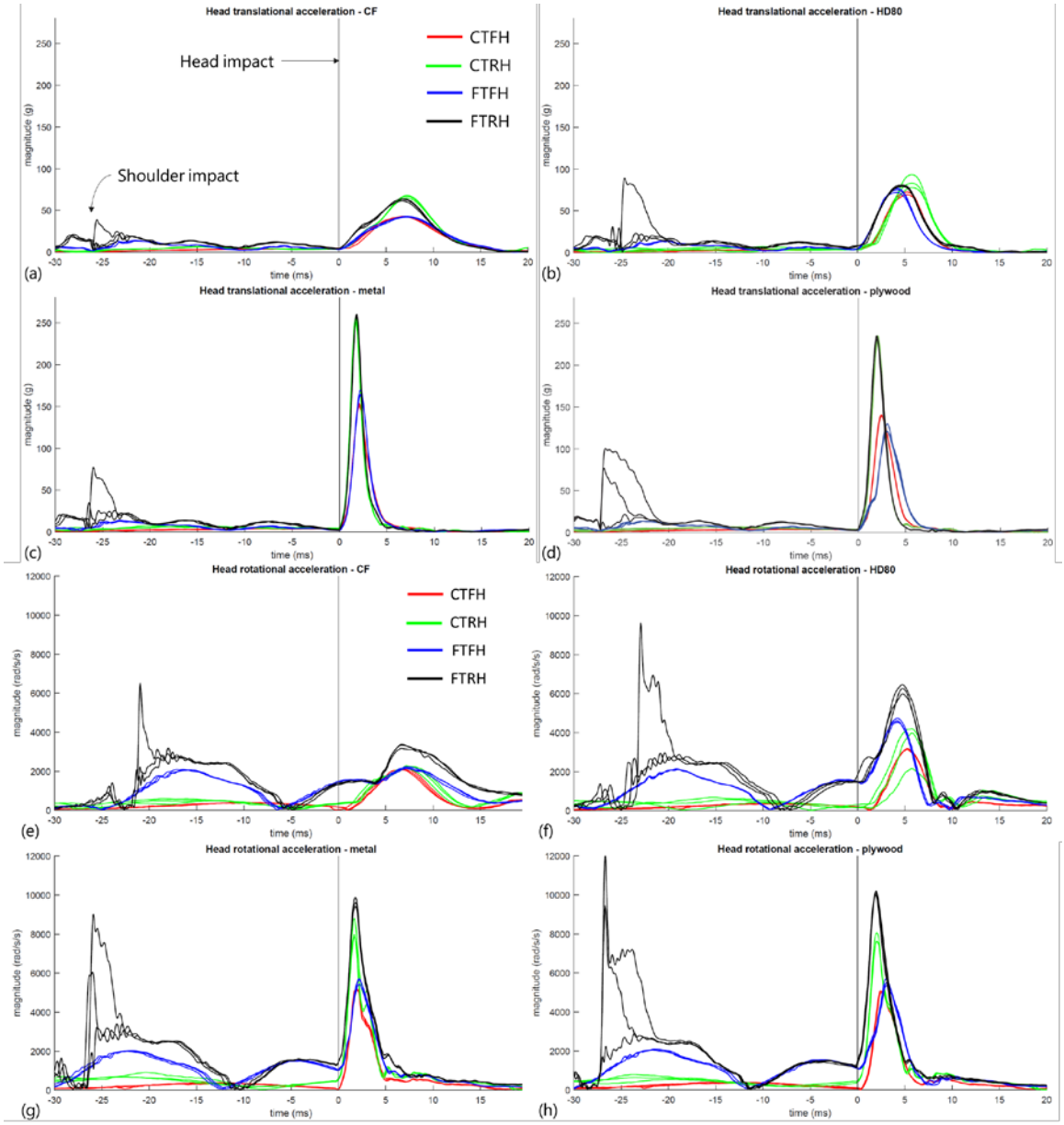

Figure 15. Acceleration loading curve plots for all test trials

Translational (a-d) and rotational (e-h) acceleration loading curve timeseries for all flooring conditions (CF, HD80, metal and plywood) using all four configurations of the dummy (CTFH, CTRH, FTFH, FTRH).The acceleration profiles show a 50 ms window, encompassing the instant of estimated shoulder impact (~-30 ms) and 20 ms after the onset of the head translational acceleration impulse (shown as the black vertical line at 0 ms) at head impact for each of the three trials collected per condition. The rotational acceleration profiles (e-h) were aligned based on the onset of head impact as detected using the translational acceleration profiles (a-d).

The peak magnitude of translational head acceleration (Figure 16 and Table 8) associated with hip stiffness ($p<0.0001$) and floor condition ($p<0.0001$) but not torso configuration ($p=0.8032$). When compared to the fixed hip condition, the rotating hip condition produced peak translational head accelerations that averaged 57% higher (158.7 versus 101.5 g; SE=0.6). There were significant differences between all four flooring conditions in peak translational head acceleration. When compared to the average value for metal flooring (207.2 g), the mean reduction in peak translational head acceleration was 12% for plywood, 63% for HD80, and 74% for compliant flooring. There was no interaction between torso configuration and hip stiffness ($p=0.8548$), but there were significant interactions for peak translational head acceleration between hip stiffness and flooring ($p<0.0001$) and torso configuration and flooring ($p<0.0001$). In other words, the reduction in peak translational head acceleration provided by compliant flooring depended on hip stiffness and torso configuration.

The peak magnitude of rotational head acceleration (Figure 16 and Table 8) associated with hip stiffness ($p<0.0001$), torso configuration ($p<0.0001$) and floor condition ($p<0.0001$). When compared to the fixed hip condition, the rotating hip condition produced peak rotational head accelerations that averaged 53% higher (6366 versus 4168 rad/s^2; SE=68.3). When compared to the curved torso condition, the flat torso condition produced peak rotational head accelerations that averaged 27% higher (5901 versus 4633 rad/s^2). There were no differences between plywood and metal, but when compared to metal (7151 rad/s^2), the mean reduction in peak rotational head acceleration was 39% for HD80, and 66% for compliant flooring. There were significant interactions for peak rotational head acceleration between torso configuration and flooring ($p<0.0001$), hip stiffness and flooring ($p<0.0001$) and torso configuration and hip stiffness ($p<0.0001$).

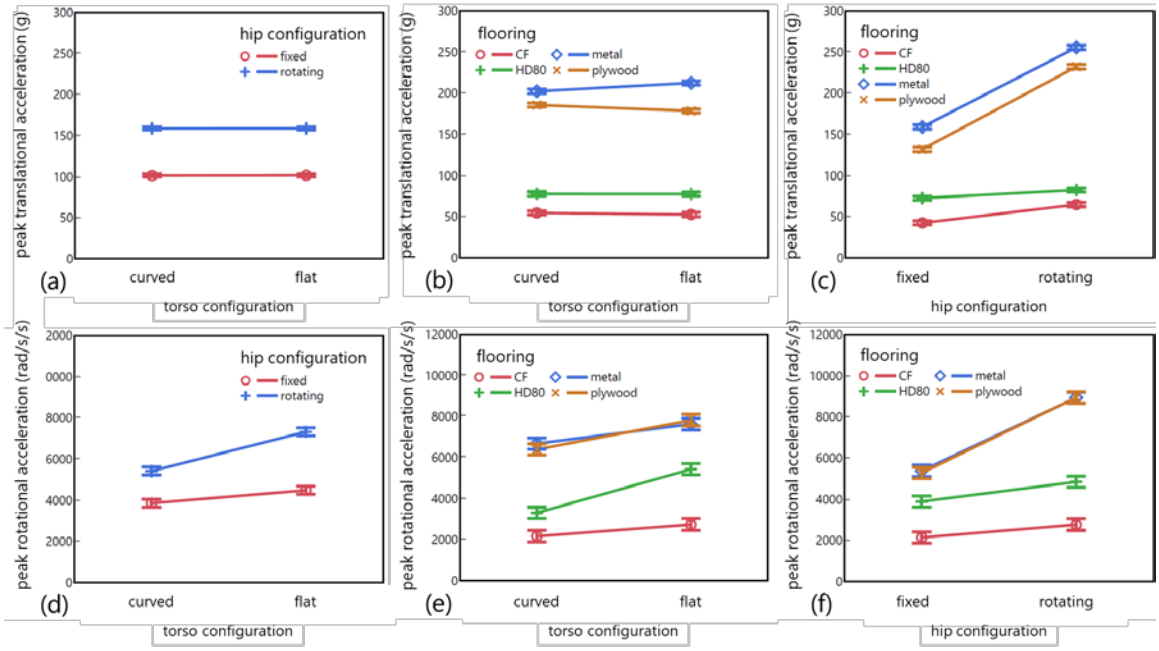

Figure 16. Summary of peak head acceleration outcomes
Mean values of peak translational and peak rotational head acceleration, for falls with the two torso configurations, two hip stiffness conditions, and four flooring conditions. Error bars show ± one standard error. Note that the straight lines connecting the data points in these interaction plots are to enhance readability, and do not infer a linear trend between data points.

The duration of the translational acceleration impulse (Table 8) associated with hip stiffness ($p<0.0001$; 10.14 versus 9.11 ms for fixed versus rotating hips; SE=0.07), torso configuration ($p=0.0032$; 9.77 versus 9.47 ms for flat versus curved torso configurations; SE=0.07) and flooring condition ($p<0.0001$; 5.02 ms for metal versus 17.18 ms for compliant flooring; SE = 0.09).

The duration of the rotational acceleration impulse (Table 8) associated with hip stiffness ($p<0.0001$; 8.26 versus 9.82 ms for fixed versus rotating hips; SE=0.14) and with flooring condition ($p<0.0001$; 5.13 ms for metal versus 15 ms for compliant flooring; SE = 0.8) but not with torso configuration ($p=0.8381$). There were significant interactions between flooring and torso configuration ($p<0.0001$) and flooring and hip stiffness ($p=0.0107$).

Table 8. Summary of head loading characteristics and descent kinematics

factors (n=3 trials per condition)			translational head acceleration, mean (SD)			rotational head acceleration, mean (SD)			descent velocity and duration, mean (SD)		
impact surface	torso shape	hip stiffness	peak magnitude (g)	time-to-peak (ms)	duration (ms)	peak magnitude (rad/s/s)	time-to-peak (ms)	duration (ms)	peak vertical velocity (m/s)	horizontal velocity at peak vertical velocity (m/s)	descent duration (ms)
CF	curved	fixed	42.56 (0.27)	6.84 (0.12)	17.22 (0.4)	2101.05 (45.55)	6.48 (0.11)	13.67 (0.19)	1.85 (0.06)	0.92 (0.09)	811 (19)
CF	curved	rotating	66.52 (1.63)	7.21 (0.15)	16.41 (0.39)	2231.27 (61.26)	8.55 (0.1)	15.33 (0.34)	2.26 (0.04)	1.32 (0.08)	491 (31)
CF	flat	fixed	42.27 (0.45)	7.19 (0.12)	18.25 (0.09)	2175.77 (42.24)	6.21 (0.05)	15.56 (0.48)	2.47 (0.06)	1.11 (0.05)	688 (38)
CF	flat	rotating	62.89 (1.3)	6.71 (0.08)	16.83 (0.22)	3293.81 (106.6)	7.01 (0.03)	18.77 (2.11)	3.24 (0.02)	1.68 (0.15)	466 (0)
HD80	curved	fixed	70.44 (1.83)	5.23 (0.16)	10.5 (0.23)	3153.75 (18.71)	4.89 (0.1)	8.73 (0.44)	2.02 (0.17)	0.82 (0.08)	783 (34)
HD80	curved	rotating	84.67 (7.83)	5.76 (0.31)	11.03 (0.62)	3442.92 (1121.87)	7.03 (0.2)	10.81 (1.3)	2.27 (0.05)	1.34 (0.05)	533 (27)
HD80	flat	fixed	74.73 (2.4)	4.2 (0.17)	10.19 (0.45)	4616.07 (107.42)	3.19 (0.16)	6.53 (0.18)	2.43 (0.07)	1.11 (0.09)	673 (27)
HD80	flat	rotating	80.06 (0.81)	4.73 (0.29)	9.59 (0.16)	6238.6 (237.84)	5.11 (0.26)	8.51 (0.24)	3.18 (0.03)	1.68 (0.03)	486 (29)
metal	curved	fixed	152.08 (1.75)	2.07 (0.04)	5.67 (0.16)	5141.31 (24.16)	1.59 (0.03)	4.65 (0.11)	1.88 (0.05)	0.92 (0.04)	822 (19)
metal	curved	rotating	252.16 (3.51)	1.7 (0.01)	4.28 (0.01)	8212.42 (508.56)	3.03 (0.03)	6.05 (0.06)	2.61 (0.04)	1.67 (0.16)	566 (0)
metal	flat	fixed	165.72 (3.51)	2.2 (0.03)	5.39 (0.13)	5606.26 (151.01)	1.18 (0.03)	4.34 (0.09)	2.49 (0.03)	1.15 (0.1)	700 (0)
metal	flat	rotating	258.75 (1.94)	1.79 (0.04)	4.73 (0.05)	9644.41 (229.18)	2.15 (0.07)	5.46 (0.64)	3.14 (0.02)	1.72 (0.09)	466 (0)
plywood	curved	fixed	139.8 (0.93)	2.45 (0.02)	5.98 (0.09)	5024.3 (52.44)	2.09 (0.02)	6.38 (0.05)	…	…	…
plywood	curved	rotating	231.13 (3.56)	2.03 (0.04)	4.66 (0.04)	7761.03 (260.48)	3.39 (0.05)	6.53 (0.05)	2.68 (0)	1.73 (0.06)	533 (47)
plywood	flat	fixed	123.71 (5.23)	3.03 (0.11)	7.89 (0.73)	5525.12 (172.72)	2.05 (0.11)	6.18 (0.16)	2.48 (0.09)	1.16 (0.03)	688 (19)
plywood	flat	rotating	233.02 (1.99)	1.97 (0.02)	5.29 (0.15)	10108.96 (90.63)	2.3 (0.03)	7.13 (0.56)	3.2 (0.07)	1.68 (0.07)	483 (19)

Ellipses (…) indicate missing data on peak head velocity and descent duration for the CTFH on plywood condition, due to equipment malfunction

3.4. Discussion

Falls with fixed versus rotating hips produced lower magnitudes of peak translational and rotational head acceleration ($p<0.0001$ for both accelerations). Specifically, rotating hips resulted in a 1.56-fold and 1.53-fold increase in peak translational and rotational accelerations at head impact, respectively. Both outcomes, however, are within range of brain injury according to suggested risk thresholds from the published literature. In a review of mechanisms of brain impact injuries (Post & Hoshizaki, 2012), Post reports that peak translational accelerations 81-82 g are on the lower end of risk for mTBI (Duma et al., 2005; Schnebel et al., 2007; L. Zhang et al., 2004). Where higher values in the range of 130 g could result in subdural hematoma (Willinger & Baumgartner, 2003). In terms of Rotational acceleration-based thresholds, primate reconstructions suggest that peak rotational head accelerations as low as 1800 rad/s^2 could result in mTBI, where magnitudes in the range of 16,000 rad/s/s could result in diffuse axonal injury (DAI) (Ommaya et al., 1967). A laboratory reconstruction study reported peak accelerations of 5900 rad/s^2 described a 50% risk for mTBI (L. Zhang et al., 2004), where others (Willinger & Baumgartner, 2003) have reported mTBIs at lower ranges (3000-4000 rad/s^2). My laboratory reconstruction revealed fall-related translational and rotational peak acceleration results ranging from a least squares means of 101.42 g and 4167.98 rad/s^2 for the fixed hips condition to 158.66 g and 6366.68 rad/s^2 for the rotating hips condition, suggesting that the backward falls with head impacts modeled by the dummy in the current study yield considerable risk of brain injury.

From a mechanics perspective, I propose that the fixed hips served to reduce the angular momentum of the torso and head segments leading up to head impact as the dummy pivoted about the pelvis site. This observation is supported by a previous study (Shishov & Robinovitch, 2018), who reported a 5-fold increased odds (odds ratio; OR = 4.9, $p<0.0001$) for head impact in backward falls without leg raise compared to backward falls involving leg raise ($p<0.0001$).

A different experimental study in the literature, (Nagata & Ohno, 2007) used a custom dummy fashioned after an older adult Japanese male, to simulate falls from standing height with different segment linkage properties by fixing or unfixing the lower limb joints (hips, knees and ankles). Their falling dynamics were characterized using

video analysis at a 30Hz capture rate, where average impact velocity was reported to be 5.14m/s. While the mentioned study does not take head accelerations into account, they report that the head impact velocity for the “unfixed hips” (similar to rotating hips (RH) in the present study), was lower than in other cases (5.14 m/s). My results show that the rotating hips condition was the most severe in terms of head acceleration and impact velocities. To account for the differences, I note that in the Nagata study, the ATD is released from a standing height, whereas my drop initiates from a posture representing a faller at the pelvis impact stage of a backward fall. It is likely the case that in the Nagata study, the torso remained relatively upright as the lower limbs rotated downwards independently of the torso during the initial stage of descent, and that the torso began the second stage of descent from a more upright position. Sandler & Robinovitch (Sandler & Robinovitch, 2001) showed that impact with the trunk in an upright posture reduced the impact severity of the fall as measured by vertical potential energy changes. Another important difference is that in their ‘fixed’ hips condition, the lower limbs were fully extended throughout the fall (forming a 180^{o} angle with the torso segment), which effectively means that as the ATD pendulums downwards, there is very little energy absorption before head impact, and functionally no instant of pelvis impact. The unfixed/rotating hips joint condition in the Nagata study resulted in the lowest descent durations when compared to other configurations. My results support this outcome.

A similar set of studies from the University of Maine (Hajiaghamemar et al., 2015; Seidi et al., 2015), used two different Hybrid III ATDs (one 50th percentile male and one 5th percentile female) to consider the recreation of five fall scenarios leading to head impact, including backward falls with and without hip flexion (accomplished by fixing/unfixing the hip joints). In a total of 67 backward fall trials, the group reports almost instantaneous head contact with the ground after pelvis impact for the no hip bending condition (25-45ms), where a descent duration range of 350-450ms was recorded for conditions where the hips were allowed to rotate.

The authors report an extremely short period of descent after pelvis impact for the fixed hips condition, similar to that of the (Nagata & Ohno, 2007) study, as the ATDs in both studies start from standing height with similar torso to lower limb relative angles of 180^{o}. under similar hip conditions (unfixed hips, or rotating hips in the current study), the time interval between pelvis impact and head impact for the ATD in the current study

is in close agreement ranging between 390 and 430 ms. In terms of acceleration measures, Hajiaghamemar (Hajiaghamemar et al., 2015a) reports average peak translational head acceleration values of 451 +/- 38 (range: 390-524) g and 295 +/- 89 (range: 198-447) g (41.8% difference) , and average peak rotational head acceleration values of 29.2 +/- 5.8 (range: 19.6-41.0) krad/s^2 and 19.3 +/- 9.6 (range: 10.7-38.2) krad/s^2 (40.8% difference) for the fixed and unfixed hip conditions respectively for trials conducted on the 50th percentile male ATD. Acceleration measures for the 5th percentile female ATD were 368 +/- 31 (range: 308-411) g and 289 +/- 47 (range: 157-361) g in terms of average peak translational acceleration for the unfixed and fixed hips respectively. Average peak rotational accelerations were reported to be 28.8 +/- 3.4 (range: 24.4-35.2) krad/s^2 and 23.6 +/- 4.5 (range: 13.5-33.8) krad/s^2 for the unfixed and fixed hips conditions. The impact durations reported were on the order of 3.0 +/- 0.4 (range: 2.6-4.0) ms and 3.4 +/- 0.4 (3.0-4.0) ms for the fixed hips and rotating hips conditions respectively, where the authors only accounted for the translational acceleration loading curve durations defined as the time difference between the leading and trailing pulse edges. By comparison, the acceleration outcomes from my study are closer to the acceleration measures attained in experiments with the 5th percentile female ATD from the (Hajiaghamemar et al., 2015) study. While the reported mean peak acceleration values are still considerably higher than in the current study, I note here that the average peak translational impact velocity magnitude ranges reported by (Hajiaghamemar et al., 2015) are 6.75 +/- 0.27 (range: 6.31-7.11) m/s and 4.85 +/- 1.33 (range: 3.29-6.80) m/s, for the fixed and unfixed hip conditions respectively, which are markedly larger averages than the more realistic translational head impact velocities experienced during backward falls in older adults, as noted by (Choi et al., 2015) and in Chapter 2 of my thesis.

Falls with a curved versus flat torso produced lower magnitudes of peak rotational head acceleration but had no effect on translational acceleration. The difference may relate to the effect of torso configuration on the rotational velocity of the head at impact. In particular, the curved torso achieves rolling contact with the ground, while the flat torso experiences a discreet impact just prior to head impact. The sudden halt in torso motion may have caused the head to rotate downward (due to its inertia) with a higher angular velocity in the flat than curved torso condition. This difference may also relate to the likelihood that, despite the flat torso producing higher peak vertical

velocities, these velocities occurred prior to head impact, at the instant of shoulder impact, so the actual impact velocity of the head was lower than the peak velocity in the flat torso trials. To support this proposition, I calculated the differences between the head vertical velocity of the dummy at a 10 cm height (representing impact velocity) and the peak vertical velocity to be 0.48m/s and 0.259 m/s for the flat and curved torsos respectively, where the head reaches a height of 10 cm 38.74 and 32.37 ms after peak velocity and 66.47 and 73.79 ms before head impact for the flat and curved torso respectively. To summarize this, in all dummy configurations, initial impacts to the torso and shoulders caused head velocity to peak during descent, and to be slowed leading to impact. This behavior mimics falling patterns observed in older adults. There are no studies to my knowledge that have assessed the differences in fall-injury severity outcomes between curved versus flat torsos. The closest area of exploration on this topic investigates the fall-risk association between degrees of kyphosis in older adults suffering from hyperkyphosis (McDaniels-Davidson et al., 2018) but not the injury severity risk association.

Floor type had a major effect on peak translational and rotational head accelerations. In terms of reduction in peak accelerations, the compliant flooring condition outperformed HD80 stiff foam and other flooring conditions in every trial. My results suggest that, on average, compliant flooring material can attenuate peak translational accelerations by up to 74.14% when compared to metal (the most severe impact surface), where trials on the HD80 and plywood conditions resulted in 62.6% and 12.19% attenuation respectively when compared to metal. In terms of attenuations in peak rotational accelerations, an LSMeans Tukey HSD test revealed no significant difference between metal and plywood flooring conditions, however compliant flooring and HD80 resulted in a 65.73% and 38.99% percent attenuation in peak accelerations. The influence of flooring on peak acceleration attenuation, in part, lends itself to the varying stiffness and energy absorption vs shunting properties associated with each floor type. A study by Laing (Laing & Robinovitch, 2009) examined the fall-related femoral-neck impact force attenuation properties of low stiffness floors and foams of soft and firm stiffnesses, when compared to a rigid floor. The authors found that their two compliant flooring conditions (SmartCell, similar to the CF used in the current study, and SoftTile floors) can attenuate impact force by up to 47%, however CF mean force attenuation was reported to be lowest (24.5%) when compared to the foam floors (76.6% and 52.4%

for firm and soft form respectively) used in the study. The tests involved three different impact velocities (2,3, and 4 m/s) and while compliant flooring showed an increase in force attenuation as impact velocity increased, an opposite trend emerged for the foam floors, due to the foam tiles bottoming out after repeated testing. Both foam floors used in the Laing study were softer and approximately 4.3 times thicker than the CF condition in both studies as well as the HD80 stiff foam condition used in the current study. Additionally, the rigid control floor thickness (2 mm) in the Laing study was approximately one order of magnitude thinner than the SmartCell CF condition, which may explain the difference in the order of rankings in terms of attenuation. The differences in percent attenuation between the two studies may also be explained due to the reference rigid flooring condition, where the Laing study used a rigid commercial rubber material (Noraplan Classic, Nora Systems Inc., Lawrence, MA, USA) compared to the more rigid metal flooring used in this study.

A more recent 2011 study on the influence of flooring systems on simulated fall-related head impact dynamics (Wright & Laing, 2011) at three different velocities (1.5, 2.5, and 3.5 m/s), concluded that all impact variables, namely peak impact force, peak translational acceleration, and Head Injury Criteria (HIC), were associated with flooring type. The authors found that impact severity on compliant flooring, by these measures, was reduced by 25-85% ($p<0.001$) compared to common flooring systems (carpets and rubber). In terms of translational accelerations specifically, the authors reported that peak values were attenuated by at least 25% and up to 70%, across all three impact velocities, for impacts onto compliant flooring compared to the commercial carpet flooring. Reported peak acceleration values ranged from 54 to 262g for impacts onto common floors, and from 27 to 157g on the compliant floors, these attenuations fall within the range reported in the current study.

The peak accelerations during falls on softer floors (HD80 and compliant flooring) depended on torso curvature and hip stiffness. My results suggest that fall dynamics may not change the relative ranking between products but will affect whether specific floor designs reduce peak accelerations below defined threshold values for concussion. Current standards for sports turf classify products based on their ability to reduce peak accelerations below specific threshold value(s). For example, the ASTM F1292 standard (ASTM F1292-18, 2004) specifies that surfacing materials for use within the zone of playground equipment must satisfy a pass/fail performance criteria, where peak

translational acceleration shall not exceed 200 g, when subject to a drop tower test that simulates the impact of a child's head with the surface. Our results show that the ability of a given product to pass such a test will depend strongly on the design of the test system. However, if the criteria are instead based on a percent from baseline, the differences we observed across our four test systems were not large. Despite the significant interaction between flooring type and hip stiffness for peak rotational acceleration, I found that compliant flooring reduced peak head accelerations for all four hip and torso configurations of the dummy. The consistency suggests that compliant flooring should provide protection for the range of backward falling condition observed in older adults.

The design of the ATD used in this study has several important limitations in terms of the simplified postural geometry, and the extent to which it is able to realistically simulate the natural flexibility of the human body. While the Hybrid III dummy neck has been criticized in the past for its lack of Biofidelity in terms of ROM and directional stiffness and more biofidelic options have since been developed (Nelson & Cripton, 2010), the 50th percentile hybrid III head and neck complex is the most widely- accepted and used surrogate in the impact literature. Results from (Mertz, 1985), comparing the Hybrid III head to cadaver data support the claim that the Hybrid III is humanlike for frontal impacts and viable for surrogate comparisons with post-mortem human subject data. Furthermore, a study by (Caccese et al., 2016), using a Hybrid III head and neck assembly, examined the influence of neck stiffness on acceleration outcomes for rear and frontal impacts, and found the effect of neck stiffness to be less than 10% for rear and frontal impacts in terms of both translational and rotational accelerations. The standard Hybrid III neck was designed to provide biofidelic flexion and extension response under high-speed rear-end and frontal impacts (Foster et al., 1977), and was thus deemed sufficient for my design and testing purposes. That notwithstanding, my results indicate the important role of the neck in coupling head and torso dynamics during falls, and the need for future research to confirm my results for different neck rotational stiffness characteristics.

My tests with the dummy simulated only the portion of a backward fall occurring between the instant of pelvis impact, and the instant of head impact, which is based on my observation (described in Chapter 2) that, in 97% of backward falls causing head impact in older adults, the pelvis strikes the ground before the torso or head.

Experiments with the dummy simulated extremes in hip stiffness approaching zero stiffness (for rotating hips) or infinite stiffness (for fixed hips) throughout the fall. In reality, hip stiffness will tend to fall between these extremes and vary during landing (e.g. leg raise may occur early or late during impact). Additional work is required to more fully characterize the effects of different hip stiffness profiles. However, my results provide encouraging agreement to measures of biofidelity, that have been reported in other ATD studies and more realistic fall-related impact velocities were attained by comparison, tending towards those results reported by previous kinematic studies in older adult falls with head impact (Choi et al., 2015).

I focused on using the dummy to explore how torso configuration and hip stiffness affect head impact severity in backward falls. The dummy provides a means for systematically exploring, in future studies, how additional characteristics of falls, such as the impact velocity of the body at pelvis impact, the occurrence of upper limb impact, and the direction of the fall can affect head impact severity. The results of this study also provide a valuable benchmark for the performance of Smartcells CF, a type of compliant flooring that is widely studied for fall injury prevention (Mackey et al., 2019; Wright & Laing, 2011), compared to other more rigid surfaces

Chapter 4.

Conclusion

4.1. Thesis synthesis

Falls are the most common cause of injuries amongst Canadians over age 65, and traumatic brain injuries (TBIs) are the number one cause of fall-related deaths in the older adult population. Backward falls represent the most common scenario leading to head impact, and for severe TBI from falls in older adults. The goal of this thesis was to improve our understanding of the biomechanics of head impact in falls in older adults. I pursued this goal by analyzing the kinematics of backward falls involving head impact in older adults living in long term care (Chapter 2). I then developed a falling dummy that reconstructed backward falls, and used the dummy to systematically evaluate how head accelerations were affected by the mechanics of the fall (torso curvature and hip stiffness), and variations in floor stiffness (Chapter 3).

Novel outcomes from this thesis include more accurate estimates of head impact velocities experienced by older adults during backward falls. While previous studies had reported only peak head velocities during falls, my results described in Chapter 2 show that the head tends to slow down considerably leading to head impact, reaching velocities as low as 0.84 m/s. I report the first measures of the time-varying angles of the body segments during real-life falls, and applied novel approaches for determining the curvature of the back throughout the fall, by modelling the posterior margin using two arcs, and for estimating the inertial properties of body segments based on anthropometric regression data. These data provide valuable novel benchmarks for mechanical testing systems, mathematical models of falls, and the development of fall detection algorithms based on wearable sensors or video. Chapter 3 of my thesis described the development of an anthropomorphic falling dummy, used to simulate and systematically study the previously unexplored influence of the effect of torso curvature, hip stiffness, and flooring stiffness on head impact severity in backward falls. Results from the falling dummy experiments also provide valuable performance outcomes for common flooring conditions including Smartcells, a type of compliant flooring that is promoted for fall injury prevention. My data supports the hypothesis that the ability of a

given product to pass mechanical testing standard specifications relies strongly on the design of the test system.

I found that, in real-life backward falls in older adults causing head impact, the velocity of the head peaked after pelvis impact and slowed before impact of the head. Specifically, the vertical velocity of the head peaked, with a mean value of 2.79 m/s, when the head was, on average, 20.83 cm above its minimum height during impact, and at minimum 7.7 cm above its minimum height. The corresponding horizontal velocity averaged 2.44 m/s. When the head was 10 cm above its minimum height, the vertical velocity had slowed 18% to average 2.30 m/s, and the horizontal velocity slowed 32% to average 1.67 m/s. When the head was 5 cm above its minimum height, the vertical velocity had slowed 40% to average 1.67 m/s (range: 0.84 -2.39), and the horizontal velocity had slowed 50% to average 1.17 m/s (range: 0.09 -2.84).

My observed values of head impact velocities in falls are well below the range used in standards for measuring the biomechanical performance of helmets or sport surfaces. For example, (ASTM F1447-18, 2018) specifies that bicycle helmets be evaluated in vertical drop tests from a height of 1.2 to 2 m, resulting in head form impact velocities between 4.8 and 6.2 m/s. Canadian standards specify impact velocities of 4.7-5.7 m/s for bicycle helmets (CSA D113.2-M89, 2009), and 4.5 - 5.2 m/s for hockey helmets (CSA Z262.1-15, 2015). At present, no standards exist for fall-related head injury prevention technologies. My results suggest that current standards involve impact velocities that are at least 2.7-fold higher than those generated by falls, and may poorly reflect the value of products in the context of falls in older adults.

I observed considerable variation in the impact configuration of the body in real-life backward falls. At the instant of pelvis impact, the angle of the head, measured counterclockwise from the horizontal, averaged 100 deg and ranged from 44 to 137 deg. The variability across falls in head orientation might reflect differences in neck strength and neuromuscular control (Anderson et al., 1999; Kallman et al., 1990; Larsson et al., 1979). The angle of the torso from the horizontal averaged 48 deg and ranged from 12 deg (nearly horizontal) to 85 deg (nearly vertical). The thigh angle averaged 144 deg and ranged from 118 deg (nearly vertical) to 174 deg (nearly horizontal). As the fall progressed, the angle of the thigh with respect to the horizontal tended to decrease (by an average of 10.4 deg; range -1 to 27 deg), reflecting leg raise between the instants of

pelvis and head impact. Previously, we found that the odds for head impact in backward falls were 5-fold lower in falls with (versus without) leg raise after pelvis impact (Shishov & Robinovitch, 2018). The underlying mechanism, which we proposed related to angular momentum considerations, may also serve to reduce head impact severity.

Furthermore, I found there was considerable variation in torso curvature between the instants of pelvis and head impact. In the early portion of the fall, the thoracic region of the spine tended to have greater curvature than the lumbar region. However, both thoracic and lumbar regions tended to flatten as the fall progressed. Head impact severity may be reduced by the rolling contact and distribution of impact energy provided by a curved torso.

While my sample of 11 real-life falls was too small to examine how head impact velocity associated with the mechanics of falls, my experiments with the falling dummy allowed me to reconstruct the portion of the fall between pelvis and head impact, and systematically examine how hip stiffness (and thus leg raise) and torso curvature affected both impact velocities and the magnitude and duration of translational and head accelerations at impact.

My falling dummy recreated key aspects of real-life backward falls. First, the mass and moment of inertia properties of the dummy were similar to a 5th percentile older woman in long term care (within 2.2% with respect to full body mass, and within the measured range of full body mass moment of inertia). Second, the shape of the dummy in the “curved torso” configuration was within the observed range exhibited by older adults. Third, the dummy produced head impact velocities that matched the observed range of velocities in real-life falls, with a vertical head velocity at 5 cm above the ground which averaged 1.66 and 1.61 m/s for the CTRH and FTFH conditions (within 4% of average older adult values). Fourth, as observed in real-life falls in older adults, the vertical head velocity of the dummy decreased as the head approached the ground, due to torso and shoulder impact. Finally, in terms of leg raise, the dummy in the “fixed hips” configuration had a lower limb angle of 125 degrees (with respect to the horizontal at the instant before head impact), while the average older adult exhibited an angle of 133 degrees (6.2% difference).

Results from my experiments with the falling dummy suggest that backward falls create head accelerations that exceed proposed thresholds for TBI for some but not all conditions. Translational head accelerations averaged 101.5 g in the fixed hip condition and 158.7 g in the freely rotating hip condition. The former is just beyond while the latter is well above proposed concussion thresholds (of 60-100 g (Post & Hoshizaki, 2012)). The underlying mechanism may relate to angular momentum, with rotation of the lower limbs (in the fixed hip condition) causing a reduction in the angular momentum of the torso and head, as the dummy pivoted about the pelvis leading to head impact.

Rotational head accelerations were 27% lower in falls with curved versus flat torso configurations. The difference may relate to the effect of torso configuration on the rotational velocity of the head at impact. In particular, the curved torso achieves rolling contact with the ground, while the flat torso experiences a discreet impact just prior to head impact. The sudden halt in torso motion may have caused the head to rotate downward (due to its inertia) with a higher angular velocity in the flat than curved torso condition.

Floor type had a major effect on head accelerations. A type of compliant flooring (CF) marketed for fall impact protection (25 mm thick Smartcells) attenuated peak translational acceleration by up to 74.14% when compared to metal. However, the reduction in head acceleration provided by CF depended on the mechanics of the fall. My results show that the mechanics of the fall influenced both the percent attenuation (reduction from baseline), and the ability of specific products to common pass/fail criteria for peak translational or rotational acceleration.

My results show that body segment movements during falls are diverse, and relatively subtle changes in the dynamics of falls can have large effects on head impact severity. This makes it challenging to recommend a specific falling scenario to use as the basis for mechanical test systems. The challenge of evaluating the protective benefit of specific products (compliant flooring and protective head gear) is further confounded by variations in human susceptibility to brain injury, and lack of agreement on threshold values of head acceleration that are likely to cause injury. Pass/ fail criteria must seek to balance the sometimes competing needs to prevent injury in the average person, versus an at-risk demographic. Overly strict performance criteria may result in over-engineered products that target users refuse to wear (e.g., excessively padded headgear that is

aesthetically unappealing) or technologies that create mobility limitations (e.g., excessively compliant flooring that effectively attenuates impact acceleration, by limits or challenges ambulation and wheelchair mobility). In terms of recommending a specific test setup based on the falling dummy, a reasonable approach may be to use the flat torso, rotating hips configuration, which provided the highest magnitudes of average head acceleration, and therefore reconstructs an externally valid but high severity falling scenario.

4.2. Future directions

Future research should examine through a larger dataset how hip stiffness and torso curvature associate with head impact velocity in real-life falls. The current sample of 11 fall prevented meaningful exploration of these trends. Furthermore, future experiments with the falling dummy can provide additional insights on how fall dynamics affect head impact severity. For example, studies could examine a wider range of values for hip stiffness and torso curvature, and include systematic manipulation of body size, fall height, neck stiffness, and pelvis impact velocity. Joint torques at the neck, and hip, could be designed to better simulate human behavior in falls. Future iterations of the dummy could examine the effects of upper limb bracing, and head impact severity in sideways and forward landing configurations. Mathematical models could provide a valuable complement to physical models in estimating brain strains through finite element modeling, and in exploring through link-segment models how the mechanics of falls affect head impact severity. To prevent fall-related TBIs in older adults, efforts are required to develop consensus on priorities for knowledge generation and standards development amongst industry, researchers, health providers, older adults and their families.

References

Anderson, J. L., Terzis, G., & Kryder, A. (1999). Increase in the degree of coexpression of mysosin heavy chain isoforms in skeletal muscle fibers of the very old. *Muscle and Nerve*, *22*, 449–454.

ASTM F1045-07. (2007). *Standard Performance Specification for Ice Hockey Helmets*. https://doi.org/10.1520/F1045-07.2

ASTM F1292-18. (2004). *Standard specification for impact attenuation of surfacing materials within the use zone of playground equipment* (No. F1292-18). West Conshohocken, PA, US.

ASTM F1446-15. (2011). Standard Test Methods for Equipment and Procedures Used in Evaluating the Performance Characteristics of Protective Headgear. In *ASTM Standards*. West Conshohocken, PA, US.

ASTM F1447-18. (2018). *Standard Specification for Helmets Used in Recreational Bicycling or Roller Skating*. Retrieved from https://www.astm.org/Standards/F1447.htm

ASTM F2223-19a. (2019). *Standard Guide for ASTM Standards on Playground Surfacing*. Retrieved from https://www.astm.org/Standards/F2223.htm

Balsalobre-Fernández, C., Tejero-González, C. M., Campo-Vecino, J. Del, & Bavaresco, N. (2014). The concurrent validity and reliability of a low-cost, high-speed camera-based method for measuring the flight time of vertical jumps. *Journal of Strength and Conditioning Research*, *28*(2), 528–533. https://doi.org/10.1519/JSC.0b013e318299a52e

Bergen, G., Stevens, M. R., & Burns, E. R. (2016). Falls and Fall Injuries Among Adults Aged ≥65 Years — United States, 2014. *MMWR. Morbidity and Mortality Weekly Report*, *65*(37), 993–998. Retrieved from https://www.cdc.gov/mmwr/volumes/65/wr/mm6537a2.htm#:~:text=Falls are the leading cause,65 years (older adults).&text=In 2014%2C 28.7%25 of older,an estimated 29.0 million falls.

Berthonnaud, E., Dimnet, J., Roussouly, P., & Labelle, H. (2005). Analysis of the Sagittal Balance of the Spine and Pelvis Using. *Journal Of Spinal Disorders And Techniques*, *18*(1), 40–47.

Billette, J.-M., & Janz, T. (2011). *Injuries in canada: Insights from the canadian community healthy survey*. Ottawa, ON, CA: Statistics Canada.

Blake, A. J., Morgan, K., Bendall, M. J., Dallosso, H., Ebrahim, S. B. J., Arie, T. H. D., … Bassey, E. J. (1988). FALLS BY ELDERLY PEOPLE AT HOME: PREVALENCE AND ASSOCIATED FACTORS. *Age and Ageing*, *17*(6), 365–372. https://doi.org/10.1093/ageing/17.6.365

Caccese, V., Ferguson, J., Lloyd, J., Edgecomb, M., Seidi, M., & Hajiaghamemar, M. (2016). Response of an Impact Test Apparatus for Fall Protective Headgear Testing Using a Hybrid-III Head/Neck Assembly. *Experimental Techniques*, *40*(1), 413–427. https://doi.org/10.1111/ext.12079

Campbell, A. J., Reinken, J., Allan, B. C., & Martinez, G. S. (1981). FALLS IN OLD AGE: A STUDY OF FREQUENCY AND RELATED CLINICAL FACTORS. *Age and Ageing*, *10*(4), 264–270. https://doi.org/10.1093/ageing/10.4.264

Campolettano, E. T., Gellner, R. A., & Rowson, S. (2018). Relationship between impact velocity and resulting head accelerations during head impacts in youth football. *Proceedings of the International Research Council on Biomechanics of Injury Conference*, 326–333. https://doi.org/10.1016/j.physbeh.2017.03.040

CDC. (2012). How many people have TBI? Retrieved June 29, 2020, from Centers for Disease Control and Prevention website: https://www.cdc.gov/TraumaticBrainInjury/data/index.html

Chiu, J., & Robinovitch, S. N. (1998). Prediction of upper extremity impact forces during falls on the outstretched hand. *Journal of Biomechanics*, *31*(12), 1169–1176. https://doi.org/10.1016/S0021-9290(98)00137-7

Choi, W. J., Robinovitch, S. N., Ross, S. A., Phan, J., & Cipriani, D. (2017). *Effect of neck flexor muscle activation on impact velocity of the head during backward falls in young adults*. https://doi.org/10.1016/j.clinbiomech.2017.08.007

Choi, W. J., Wakeling, J. M., & Robinovitch, S. N. (2015). Kinematic analysis of video-captured falls experienced by older adults in long-term care. *Journal of Biomechanics*, *48*, 911–920. https://doi.org/10.1016/j.jbiomech.2015.02.025

Cholewick, J., Crisco, J. J., Oxland, T. R., Yamamoto, I., & Panjabi, M. M. (1996). Effects of posture and structure on three-dimensional coupled rotations in the lumbar spine. *SPINE*, *21*(21), 2421–2428. Retrieved from file:///C:/Users/karam/OneDrive/Desktop/Cholewicki 1996_Effects of posture and structure on three-dimensional coupled rotations in the lumbar spine.pdf

CIHI. (2010). *Health Care in Canada*. Retrieved from https://secure.cihi.ca/free_products/HCIC_2010_Web_e.pdf

CIHI. (2011). *Health Care in Canada*. Ottawa, ON, CA.

Connor, T. A., Meng, S., Zouzias, D., Burek, R., Cernicchi, A., De Bruyne, G., … Ivans, J. (2016). Current standards for sports and automotive helmets: a review. In *Ref. Ares 3151745*. Retrieved from http://www.heads-itn.eu/pdfs/Helmets_Standard_Evaluation.pdf

CSA D113.2-M89. (2009). *Cycling Helmets*. Ottawa, ON, CA.

CSA EXP08. (2017). Hip Protectors. In *CSA standards*. Retrieved from https://webstore.ansi.org/standards/csa/csaexp082017

CSA Z262.1-15. (2015). *Ice Hockey Helmets*. Toronto, ON, CA.

CSA Z325:20. (2020). Hip protectors. *CSA Standards*. Retrieved from https://www.techstreet.com/standards/csa-z325-20?product_id=2102870

CSA Z611-02. (2012). Riot helmets and faceshield protection. *CSA Standards*, (reaffirmed). Retrieved from https://www.scc.ca/en/standardsdb/standards/18340

DeGoede, K. M., Ashton-Miller, J. A., & Schultz, A. B. (2003). Fall-related upper body injuries in the older adult: a review of the biomechanical issues. *Journal of Biomechanics*, *36*(7), 1043–1053. https://doi.org/10.1016/S0021-9290(03)00034-4

Denny-Brown, D., & Russell, W. R. (1941). Experimental cerebral concussion. *Brain*, *64*(2), 93–164.

Doorly, M. C., Phillips, J. P., & Gilchrist, M. D. (2005). Reconstructing Real Life Accidents Towards Establishing Criteria for Traumatic Head Impact Injuries. In M. D. Gilchrist (Ed.), *IUTAM Symposium on Impact Biomechanics: From Fundamental Insights to Applications* (pp. 81–90). Dordrecht: Springer Netherlands.

Du Bois, J. L., Lieven, N. A. J., Adhikari, · S, & Adhikari, S. (2009). Error Analysis in Trifilar Inertia Measurements. *Experimental Mechanics*, *49*, 533–540. https://doi.org/10.1007/s11340-008-9142-4

Duma, S. M., Manoogian, S. J., Bussone, W. R., Brolinson, P. G., Goforth, M. W., Donnenwerth, J. J., … Crisco, J. J. (2005). Analysis of real-time head accelerations in collegiate football players. *Clinical Journal of Sport Medicine*, *15*(1), 3–8. https://doi.org/10.1097/00042752-200501000-00002

El-Raheem, R. M. A., Kamel, R. M., & Ali, M. F. (2015). Reliability of Using Kinovea Program in Measuring Dominant Wrist Joint Range of Motion. *Trends in Applied Sciences Research*, *10*(4), 224–230. https://doi.org/10.3923/tasr.2015.224.230

Ewing, C. L., Thomas, D. J., Patrick, L. M., Beeler, G. W., & Smith, M. J. (1969, February 1). *Living Human Dynamic Response to —G $_x$ Impact Acceleration II— Accelerations Measured on the Head and Neck*. https://doi.org/10.4271/690817

Exton-Smith, A. N. (1977). Functional consequences of ageing: clinical manifestations. *Care of the Elderly: Meeting the Challenge of Dependency*, *41*.

Fanta, O., Kubový, P., Lopot, F., Pánková, B., & Jelen, K. (n.d.). Kinematic Analysis of Backward Falls of Pedestrian and Figurine in Relation to Head Injury. *VOLUME 5 TRANSACTION ON TRANSPORT SCIENCES NUMBER*, *4*, 2012. https://doi.org/10.2478/v10158-012-0020-5

Filer, W., & Harris, M. (2015). Falls and Traumatic Brain Injury Among Older Adults. *North Carolina Medical Journal*, *76*(2), 111–114. https://doi.org/DOI: https://doi.org/10.18043/ncm.76.2.111

Foster, J., Kortege, J., & Wolanin, M. (1977). Hybrid III - A Biomechanically-Based Crash Test Dummy. *SAE Paper*.

Fréchède, B., & McIntosh, A. S. (2009). Numerical reconstruction of real-life concussive football impacts. *Medicine and Science in Sports and Exercise*, *41*(2), 390–398. https://doi.org/10.1249/MSS.0b013e318186b1c5

Fu, W. W., Fu, T. S., Jing, R., Mcfaull, S. R., & Cusimano, M. D. (2017). Predictors of falls and mortality among elderly adults with traumatic brain injury : A nationwide , population-based study. *PLoS ONE*, 1–15. https://doi.org/https://doi.org/10.1371/journal.pone.0175868

Gardner, R. C., Byers, A. L., Barnes, D. E., Li, Y., Boscardin, J., & Yaffe, K. (2018). Mild TBI and risk of Parkinson disease: A Chronic Effects of Neurotrauma Consortium Study. *Neurology*, *90*(20), E1771–E1779. https://doi.org/10.1212/WNL.0000000000005522

Gennarelli, T. A., Adamns, J. H., & I., Gr. D. (1981). Acceleration induced head injury in the monkey: Neuropathology. *Experimental and Clinical Neuropathology*, *7*, 26–28.

Gennarelli, T. A., Thibault, L. E., & Ommaya, A. K. (1972a). Comparison of translational and rotational head motions in experimental cerebral concussion. *Stapp Car Crash Conference Fifteenth Proceedings*, 797–803. New York, NY, USA: SAE.

Gennarelli, T. A., Thibault, L. E., & Ommaya, A. K. (1972b). Pathophysiologic Responses to Rotational and Translational Accelerations of the Head. *SAE Technical Paper 720970*. https://doi.org/https://doi.org/10.4271/720970

Genta, G., & Delprete, C. (1994). Some Considerations on the Experimental Determination of Moments of Inertia. *Meccanica*, *29*, 25–41. Retrieved from https://link.springer.com/content/pdf/10.1007/BF01007497.pdf

Greenwald, R. M., Gwin, J. T., Chu, J. J., & Crisco, J. J. (2008). *Head Impact Severity Measures for Evaluating Mild Traumatic Brain Injury Risk Exposure*. *62*(4), 789–798. https://doi.org/10.1227/01.neu.0000318162.67472.ad

Gurdjian, E., Lissner, H., Evans, F., Patrick, L., & Hardy, W. (1961). Intracranial pressure and acceleration accompanying head impacts in human cadavers. *Surgery, Gynecology & Obstetrics*, *113*, 185–190.

Gurdjian, E. S., Webster, J. E., & Lissner, H. R. (1955). Observations on the Mechanism of Brain Concussion, Contusion, and Laceration. *Surgery, Gynecology & Obstetrics*, *101*(6), 680–690. Retrieved from https://pubmed.ncbi.nlm.nih.gov/13274275/

Hajiaghamemar, M., Seidi, M., Ferguson, J. R., & Caccese, V. (2015). Measurement of Head Impact Due to Standing Fall in Adults Using Anthropomorphic Test Dummies. *Annals of Biomedical Engineering*, *43*(9), 2143–2152. https://doi.org/10.1007/s10439-015-1255-1

Hamden, K., Agresti, D., Jeanmonod, R., Woods, D., Reiter, M., & Jeanmonod, D. (2014). Characteristics of elderly fall patients with baseline mental status: high-risk features for intracranial injury. *The American Journal of Emergency Medicine*, *32*(8), 890–894. https://doi.org/10.1016/j.ajem.2014.04.051

Hardy, W. N., Khalil, T. B., & King, A. I. (1994). Literature review of head injury biomechanics. *International Journal of Impact Engineering*, *15*(4), 561–586. https://doi.org/https://doi.org/10.1016/0734-743X(94)80034-7

Hardy, W. N., Mason, M. J., Foster, C. D., Shah, C. S., Kopacz, J. M., Yang, K. H., … Tashman, S. (2007). A study of the response of the human cadaver head to impact. *Stapp Car Crash Journal*, *51*, 17–80. Retrieved from http://www.ncbi.nlm.nih.gov/pubmed/18278591

Harrison, D. D., Harrison, D. E., Janik, T. J., Cailliet, R., Ferrantelli, J. R., Haas, J. W., & Holland, B. (2004). Modeling of the sagittal cervical spine as a method to discriminate hypolordosis: Results of elliptical and circular modeling in 72 asymptomatic subjects, 52 acute neck pain subjects, and 70 chronic neck pain subjects. *Spine*, *29*(22), 2485–2492. https://doi.org/10.1097/01.brs.0000144449.90741.7c

Harvey, L. A., & Close, J. C. T. (2012). Traumatic brain injury in older adults: characteristics, causes and consequences. *Injury*, *43*, 1821–1826. https://doi.org/10.1016/j.injury.2012.07.188

Hoang, K.-L. H., & Mombaur, K. (2015). Adjustments to de Leva-anthropometric regression data for the changes in body proportions in elderly humans. *Journal of Biomechanics*, *48*, 3732–3736. https://doi.org/10.1016/j.jbiomech.2015.08.018

Hodgson, V. R., Thomas, L. M., Gurdjian, E. S., Fernando, O. U., Greenberg, S. W., & Chason, J. L. (1969, February 1). *Advances in Understanding of Experimental Concussion Mechanisms*. https://doi.org/10.4271/690796

Holbourn, A. H. S. (1943). MECHANICS OF HEAD INJURIES. *The Lancet*, *242*(6267), 438–441. https://doi.org/10.1016/S0140-6736(00)87453-X

Holliday, P. J., Fernie, G. R., Gryfe, C. I., & Griggs, G. T. (1990). Video recording of spontaneous falls of the elderly. *ASTM Special Technical Publication*, (1103), 7–16. https://doi.org/10.1520/stp15497s

Hoshizaki, T. B., & Brien, S. E. (2004). The science and design of head protection in sport. *Neurosurgery*, *55*(4), 956–967. https://doi.org/10.1227/01.NEU.0000137275.50246.0B

Hsiao, E. T., & Robinovitch, S. N. (1998). Common protective movements govern unexpected falls from standing height. In *Journal of Biomechanics* (Vol. 31). Retrieved from https://pdf.sciencedirectassets.com/271132/1-s2.0-S0021929000X03867/1-s2.0-S0021929097001140/main.pdf?X-Amz-Security-Token=IQoJb3JpZ2luX2VjECIaCXVzLWVhc3QtMSJIMEYCIQCasRXnGNlHfjYGTKTHvrpNhjIZtbx8GJ8ZSIexRolcNAIhAMURxsEQZYCmEcl9w7KuDNPD4ChqOOzByXgReoEIEWzE

Hukkelhoven, C. W., Steyerberg, E. W., Rampen, A. J., & Farace, E. (2003). Patient age and outcome following severe traumatic brain injury: an analysis of 5600 patients. *Journal of Neurosurgery*, *99*, 666–673. https://doi.org/10.3171/jns.2003.99.4.0666

Hwang, H.-F., Cheng, C.-H., Chien, D.-K., Yu, W.-Y., & Lin, M.-R. (2015). Risk Factors for Traumatic Brain Injuries During Falls in Older Persons. *Journal of Head Trauma Rehabilitation*, *30*(6), E9–E17. https://doi.org/10.1097/HTR.0000000000000093

ISO 8894-2. (2006). Motorcycles — Test and analysis procedures for research evaluation of rider crash protective devices fitted to motorcycles. *International Standards Organization*, *2006*, 13.

Ito, Y., Corna, S., von Brevern, M., Bronstein, A., & Gresty, M. (1997). The functional effectiveness of neck muscle reflexes for head-righting in response to sudden fall. *Experimental Brain Research*, *117*(2), 266–272. https://doi.org/10.1007/s002210050221

Ivancic, P. C. (2014). Biomechanics of Thoracolumbar Burst and Chance-Type Fractures during Fall from Height. *Global Spine Journal*, *4*(3), 161–168. https://doi.org/10.1055/s-0034-1381729

J211-1, S. (1995). *Instrumentation for Impact Test, Part 1, Electronic Instrumentation*.

Janik, T. J., Harrison, D. D., Cailliet, R., Troyanovich, S. J., & Harrison, D. E. (1998). Can the sagittal lumbar curvature be closely approximated by an ellipse? *Journal of Orthopaedic Research*, *16*(6), 766–770. https://doi.org/10.1002/jor.1100160620

Jensen, R., & Fletcher, P. (1994). Distribution of mass to the segments of elderly males and females. *Journal of Biomechanics*, *27*, 89–96. Retrieved from file:///C:/Users/karam/OneDrive/Desktop/Anthropometry/Jensen 1994_Distribution of mass to the segments of elderly males and females.pdf

Jensen, R. K., & Fletcher, P. (1993). Body Segment Moments of Inertia of the Elderly. *Journal of Applied Biomechanics*, *9*(4), 287–305. https://doi.org/10.1123/jab.9.4.287

Kalache, Alexandre. Ku, D., Kannus, P., Palvanen, M., Niemi, S., Parkkari, J., Jaglal, S. B., … Chambers, R. (2007). WHO Global Report on Falls Prevention in Older Age. In *World Health Organisation* (Vol. 5). https://doi.org/10.1016/S0003-9993(98)90059-4

Kallman, D. A., Plato, C. C., & Tobin, J. D. (1990). The role of muscle loss in the age-related decline of grip strength: cross-sectional and longitudinal perspectives. *Journal of Gerontology*, *45*.

Kannus, P., Parkkari, J., & Poutala, J. (1999). Comparison of force attenuation properties of four different hip protectors under simulated falling conditions in the elderly: An in vitro biomechanical study. *Bone*, *25*(2), 229–235. https://doi.org/10.1016/S8756-3282(99)00154-4

Kim, K. J., & Ashton-Miller, J. A. (2009). Segmental dynamics of forward fall arrests: A system identification approach. *Clinical Biomechanics*, *24*(4), 348–354. https://doi.org/10.1016/j.clinbiomech.2009.01.007

King, A. I., Yang, K. H., Zhang, L., & Hardy, W. (2003). Is head injury caused by linear or angular acceleration? *Proceedings of the International Research Conference on the Biomechanics of Impacts (IRCOBI)*, (September), 1–12.

Kloepper, R., & Okuma, M. (2010). Experimental identification of rigid body inertia properties using single-rotor unbalance excitation. *Proceedings of the Institution of Mechanical Engineers, Part K: Journal of Multi-Body Dynamics*, *223*(4), 293–308. https://doi.org/10.1243/14644193JMBD200

Kuo, C., Shishov, N., Elabd, K., Komisar, V., Chong, H., Phu, T., … Robinovitch, S. (2020). Estimating Trunk and Neck Stabilization for Avoiding Head Impact during Real-World Falls in Older Adults. *42nd Annual International Conference of the IEEE Engineering in Medicine and Biology Society*. Montreal.

Laing, A. C., & Robinovitch, S. N. (2009). Low stiffness floors can attenuate fall-related femoral impact forces by up to 50% without substantially impairing balance in older women. *Accident Analysis and Prevention*, *41*, 642–650. https://doi.org/10.1016/j.aap.2009.03.001

Larsson, L., Grimby, G., & Karlsson, J. (1979). Muscle strength and speed of movement in relation to age and muscle morphology. *Journal of Applied Physiology*, *46*, 451–456.

Le Huec, J. C., Demezon, H., & Aunoble, S. (2014). Sagittal parameters of global cervical balance using EOS imaging: normative values from a prospective cohort of asymptomatic volunteers. *European Spine Journal*, *24*(1), 63–71. https://doi.org/10.1007/s00586-014-3632-0

Lemoine, D. S., Tate, B. J., Lacombe, J. A., & Hood, T. C. (2017). A Retrospective Cohort Study of Traumatic Brain Injury and Usage of Protective Headgear During Equestrian Activities. *Journal of Trauma Nursing : The Official Journal of the Society of Trauma Nurses*, *24*(4), 251–257. https://doi.org/10.1097/JTN.0000000000000300

Lord, S. R., Webster, I. W., Sambrook, P. N., Gilbert, C., Kelly, P. J., Nguyen, T., & Eisman, J. A. (1994). Postural stability, falls and fractures in the elderly: results from the Dubbo Osteoporosis Epidemiology Study. *Medical Journal of Australia*, *160*(11), 684–691. https://doi.org/10.5694/j.1326-5377.1994.tb125905.x

Luukinen, H., Koski, K., Hiltunen, L., & Kivelä, S.-L. (1994). Incidence rate of falls in an aged population in Northern Finland. *Journal of Clinical Epidemiology*, *47*(8), 843–850. https://doi.org/10.1016/0895-4356(94)90187-2

Mackey, D. C., Lachance, C. C., Wang, P. T., Feldman, F., Laing, A. C., Leung, P. M., … Robinovitch, S. N. (2019). The Flooring for Injury Prevention (FLIP) Study of compliant flooring for the prevention of fall-related injuries in long-term care: A randomized trial. *PLOS Medicine*, *16*(6), e1002843. https://doi.org/10.1371/journal.pmed.1002843

Majumder, S., Roychowdhury, A., & Pal, S. (2009). Effects of body configuration on pelvic injury in backward fall simulation using 3D finite element models of pelvis-femur-soft tissue complex. *Journal of Biomechanics*, *42*(10), 1475–1482. https://doi.org/10.1016/j.jbiomech.2009.03.044

Mattey, R. A. (1974). *Bifilar pendulum technique for determining mass properties of discos packages*. Retrieved from https://www.physlab.org/wp-content/uploads/2017/05/Bifilar-pendulum_old.pdf

McDaniels-Davidson, C., Davis, A., Wing, D., Macera, C., Lindsay, S. P., Schousboe, J. T., … Kado, D. M. (2018). Kyphosis and incident falls among community-dwelling older adults. *Osteoporosis International*, *29*(1), 163–169. https://doi.org/10.1007/s00198-017-4253-3

McIntosh, A., McCrory, P., & Finch, C. F. (2004). Performance enhanced headgear: a scientific approach to the development of protective headgear. *British Journal of Sports Medicine*, *38*(1), 46–49. https://doi.org/10.1136/bjsm.2002.003103

Mertz, H. J. (1985). Biofidelity of the Hybrid III head. *SAE Technical Papers*, *8512*. https://doi.org/10.4271/851245

Music, J., Kamnik, R., & Munih, M. (2008). *Model based inertial sensing of human body motion kinematics in sit-to-stand movement*. https://doi.org/10.1016/j.simpat.2008.05.005

Nagata, H., & Ohno, H. (2007). Analysis of backward falls caused by accelerated floor movements using a dummy. *Industrial Health*, *45*(3), 462–466. https://doi.org/10.2486/indhealth.45.462

Nelson, T. S., & Cripton, P. A. (2010). A new biofidelic sagittal plane surrogate neck for head-first impacts. *Traffic Injury Prevention*, *11*(3), 309–319. https://doi.org/DOI:10.1080/15389581003614870

Nguyen, T. C., & Reynolds, K. J. (2014). The effect of variability in body segment parameters on joint moment using Monte Carlo simulations. *Gait and Posture*, *39*(1), 346–353. https://doi.org/10.1016/j.gaitpost.2013.08.002

O'loughlin, J. L., Robitaille, Y., Boivin, J. F., & Suissa, S. (1993). Incidence of and risk factors for falls and injurious falls among the community-dwelling elderly. *American Journal of Epidemiology*, *137*(3), 342–354. https://doi.org/10.1093/oxfordjournals.aje.a116681

O'Riordain, K., Thomas, P. M., Phillips, J. P., & Gilchrist, M. D. (2003). Reconstruction of real world head injury accidents resulting from falls using multibody dynamics. *Clinical Biomechanics*, *18*, 590–600. https://doi.org/10.1016/S0268-0033(03)00111-6

Oeur, R. A., Gilchrist, M. D., & Hoshizaki, T. B. (2018). Interaction of impact parameters for simulated falls in sport using three different sized Hybrid III headforms Interaction of impact parameters for simulated falls in sport using three different sized Hybrid III headforms. *International Journal of Crashworthiness*, *24*(3), 326–335. https://doi.org/10.1080/13588265.2018.1441617

Oeur, R. A., Gilchrist, M. D., & Hoshizaki, T. B. (2019). Parametric study of impact parameters on peak head acceleration and strain for collision impacts in sport. *International Journal of Crashworthiness*, 1–10. https://doi.org/10.1080/13588265.2019.1634336

Ommaya, A. K., Hirsch, A. E., Yarnell, P., & Harris, E. H. (1967). Scaling of experimental data on cerebral concussion in sub-human primates to concussion threshold for man. *11th Stapp Car Crash Conference*. Anaheim, FL, USA.

Ono, K., Kikuchi, A., Nakamura, M., Kobayashi, H., & Nakamura, N. (1980). Human Head Tolerance to Sagittal Impact—Reliable Estimation Deduced from Experimental Head Injury Using Subhuman Primates and Human Cadaver Skulls. *SAE Transactions*, Vol. 89, pp. 3837–3866. https://doi.org/10.2307/44632635

Padgaonkar, A. J., Krieger, K. W., & King, A. I. (1975). Measurement of angular acceleration of a rigid body using linear accelerometers. *Journal of Applied Mechanics, Transactions ASME*, *42*(3), 552–556. https://doi.org/10.1115/1.3423640

Pavol, M. J., Owings, T. M., & Grabiner, M. D. (2002). Body segment inertial parameter estimation for the general population of older adults. *Journal of Biomechanics*, *35*(5), 707–712. https://doi.org/10.1016/S0021-9290(01)00250-0

Pellman, E. J., Viano, D. C., Tucker, A. M., Casson, I. R., & Waeckerle, J. F. (2003). CLINICAL STUDIES CONCUSSION IN PROFESSIONAL FOOTBALL: RECONSTRUCTION OF GAME IMPACTS AND INJURIES. *Neurosurgery*, *53*, 799–814. https://doi.org/10.1227/01.NEU.0000083559.68424.3F

Pincemaille, Y., Trosseille, X., Mack, P., Tarrière, C., Breton, F., & Renault, B. (1989, October 1). *Some New Data Related to Human Tolerance Obtained from Volunteer Boxers*. https://doi.org/10.4271/892435

Plagenhoef, S. O. (1983). Anatomical Data for Analyzing Human Motion. *Research Quarterly for Exercise and Sport*, *54*(2), 169–178. Retrieved from https://eric.ed.gov/?id=EJ282116

Post, A., & Hoshizaki, T. B. (2012). Mechanisms of brain impact injuries and their prediction: A review. *Trauma*, *14*(4), 327–349. https://doi.org/10.1177/1460408612446573

Post, A., Koncan, D., Kendall, M., Cournoyer, J., Michio Clark, J., Kosziwka, G., … Blaine Hoshizaki, T. (2018). Analysis of speed accuracy using video analysis software. *Sports Engineering*, *21*(3), 235–241. https://doi.org/10.1007/s12283-018-0263-4

Post, A., Oeur, A., Hoshizaki, B., & Gilchrist, M. D. (2013). Examination of the relationship between peak linear and angular accelerations to brain deformation metrics in hockey helmet impacts. *Computer Methods in Biomechanics and Biomedical Engineering*, *16*(5), 511–519. https://doi.org/10.1080/10255842.2011.627559

Post, A., Walsh, E. S., Hoshizaki, T. B., & Gilchrist, M. D. (2012). Analysis of loading curve characteristics on the production of brain deformation metrics. *Proceedings of the Institution of Mechanical Engineers, Part P: Journal of Sports Engineering and Technology*, *226*(3–4), 200–207. https://doi.org/10.1177/1754337112449420

Potvin, B. M., Aguiar, O. M. G., Komisar, V., Sidhu, A., Elabd, K., & Robinovitch, S. N. (2019). A comparison of the magnitude and duration of linear and rotational head accelerations generated during hand-, elbow-and shoulder-to-head checks delivered by hockey players. *Journal of Biomechanics*, *91*, 43–50. https://doi.org/10.1016/j.jbiomech.2019.05.002

Pöyry, T., Luoto, T. M., Kataja, A., Brander, A., Tenovuo, O., Iverson, G. L., & Öhman, J. (2013). Acute assessment of brain injuries in ground-level falls. *The Journal of Head Trauma Rehabilitation*, *28*(2), 89–97. https://doi.org/10.1097/HTR.0b013e318250eadd

Prudham, D., & Evans, J. G. (1981). Factors Associated with Falls in the Elderly: A Community Study. *Age and Ageing*, *10*(3), 141–146. https://doi.org/10.1093/ageing/10.3.141

Puig-Diví, A., Escalona-Marfil, C. I., Maria Padullé s-Riu, J., Busquets, A., Padullé s-Chando, X., & Marcos-Ruiz, D. (2019). *Validity and reliability of the Kinovea program in obtaining angles and distances using coordinates in 4 perspectives*. https://doi.org/10.1371/journal.pone.0216448

Ringegni, P. ., Actis, M. ., & Patanella, A. . (2000). An experimental technique for determining mass inertial properties of irregular shape bodies and mechanical assemblies. *Measurement*, *29*(2001), 63–75. Retrieved from https://pdf.sciencedirectassets.com/271454/1-s2.0-S0263224100X00541/1-s2.0-S0263224100000282/main.pdf?X-Amz-Security-Token=AgoJb3JpZ2luX2VjEKP%2F%2F%2F%2F%2F%2F%2F%2F%2F%2FwEaCXVzLWVhc3QtMSJIMEYCIQC4mjxV99rB3m1KIBf%2BQTHkQY%2FuPB3h4Us5dElXysE5DAIhANy2QyDR

Robinovitch, S. N., & Chiu, J. (1998). Surface stiffness affects impact force during a fall on the outstretched hand. *Journal of Orthopaedic Research*, *16*(3), 309–313. https://doi.org/10.1002/jor.1100160306

Robinovitch, S. N., Feldman, F., Yang, Y., Schonnop, R., Leung, P. M., Sarraf, T., … Loughi, M. (2013). Video capture of the circumstances of falls in elderly people residing in long-term care: An observational study. *The Lancet*, *381*(9860), 47–54. https://doi.org/10.1016/S0140-6736(12)61263-X

Roussouly, P., & Pinheiro-Franco, J. L. (2011). Sagittal parameters of the spine: biomechanical approach. *European Spine Journal : Official Publication of the European Spine Society, the European Spinal Deformity Society, and the European Section of the Cervical Spine Research Society*, *20 Suppl 5*, 578–585. https://doi.org/10.1007/s00586-011-1924-1

Rubenstein, L. Z. (2006). Falls in older people: Epidemiology, risk factors and strategies for prevention. *Age and Ageing*, *35*(SUPPL.2). https://doi.org/10.1093/ageing/afl084

Rubenstein, L. Z., Robbins, A. S., Schulman, B. L., Rosado, J., Osterweil, D., & Josephson, K. R. (1988). Falls and Instability in the Elderly. *Journal of the American Geriatrics Society*, *36*(3), 266–278. https://doi.org/10.1111/j.1532-5415.1988.tb01811.x

Saari, P., Heikkinen, E., Sakari-Rantala, R., & Rantanen, T. (2007). Fall-related injuries among initially 75-and 80-year old people during a 10-year follow-up. *Archives of Gerontology and Geriatrics*, *45*, 207–215. https://doi.org/10.1016/j.archger.2006.10.012

Sandler, R., & Robinovitch, S. (2001). An analysis of the effect of lower extremity strength on impact severity during a backward fall. *Journal of Biomechanical Engineering*, *123*(6), 590–598. https://doi.org/10.1115/1.1408940

Schedlinski, C., & Link, M. (2001). A SURVEY OF CURRENT INERTIA PARAMETER IDENTIFICATION METHODS. In *Mechanical Systems and Signal Processing* (Vol. 15).

Schnebel, B., Gwin, J. T., Anderson, S., & Gatlin, R. (2007). In vivo study of head impacts in football: A comparison of National Collegiate Athletic Association Division I versus high school impacts. *Neurosurgery*, *60*(3), 490–495. https://doi.org/10.1227/01.NEU.0000249286.92255.7F

Schonnop, R., Yang, Y., Feldman, F., Robinson, E., Loughin, M., & Robinovitch, S. N. (2013). Prevalence of and factors associated with head impact during falls in older adults in long-term care. *Cmaj*, *185*(17), 803–810. https://doi.org/10.1503/cmaj.130498

Schulz, B. W., Lee, W. E., Lloyd, J. D., Lee Iii, W. E., & Lloyd, J. D. (2008). Estimation, simulation, and experimentation of a fall from bed. *Journal of Rehabilitation Research and Development*, *45*(8), 1227–1236. https://doi.org/10.1682/JRRD.2007.06.0092

Seidi, M., Hajiaghamemar, M., & Caccese, V. (2015). Evaluation of effective mass during head impact due to standing falls. *International Journal of Crashworthiness*, *20*(2), 134–141. https://doi.org/10.1080/13588265.2014.983261

Sen, D. T., & Vinh, T. C. (2016). Determination of Added Mass and Inertia Moment of Marine Ships Moving in 6 Degrees of Freedom. *International Journal of Transportation Engineering and Technology*, *2*(1), 8–14. https://doi.org/10.11648/j.ijtet.20160201.12

Shan, G., & Bohn, C. (2003). Anthropometrical Data and Coefficients of Regression Related to Gender and Race. *Applied Ergonomics*, *34*(4). https://doi.org/10.1016/S0003-6870(03)00040-1

Shishov, N., & Robinovitch, S. N. (2018). an Analysis of the Association Between Leg Raise and Head Impact During. *Canadian Society of Biomechanics*, *215*, 215.

Southerland, L. T., Stephen, J. A., Robinson, S., Falk, J., Phieffer, L., Rosenthal, J., & Caterino, J. (2016). Head Trauma From Falling Increases Subsequent Emergency Department Visits More Than Other Fall-Related Injuries in Older Adults. *Journal of the American Geriatrics Society*, *64*(4), 870–874. https://doi.org/10.1111/jgs.14041

Stinchcombe, A., Kuran, N., & Powell, S. (2014). Seniors' Falls in Canada. In *Chronic Diseases and Injuries in Canada* (Vol. 34).

Stuart Walsh, E., Rousseau, P., & Blaine Hoshizaki, T. (2011). The influence of impact location and angle on the dynamic impact response of a Hybrid III headform. *International Sports Engineering Association 2011*, *13*, 135–143. https://doi.org/10.1007/s12283-011-0060-9

Takhounts, E. G., Hasija, V., & Eppinger, R. H. (2009). Analysis of 3D Rigid Body Motion Using the Nine Accelerometer Array and the Randomly Distributed In-Plane Accelerometer Systems. *Esv 2009*, *09–0402*, 59–76.

Taylor, C. A., Bell, J. M., Breiding, M. J., & Xu, L. (2017). Traumatic Brain Injury-Related Emergency Department Visits, Hospitalizations, and Deaths - United States, 2007 and 2013. *Morbidity and Mortality Weekly Report. Surveillance Summaries (Washington, D.C. : 2002)*, *66*(9), 1–16. https://doi.org/10.15585/mmwr.ss6609a1

Teasdale, G., Maas, A., Lecky, F., Manley, G., Stocchetti, N., & Murray, G. (2014). The Glasgow Coma Scale at 40 years: Standing the test of time. *The Lancet Neurology*, *13*(8), 844–854. https://doi.org/10.1016/S1474-4422(14)70120-6

Thomas, K. E., Stevens, J. A., Sarmiento, K., & Wald, M. M. (2008). *Fall-related traumatic brain injury deaths and hospitalizations among older adults-United States, 2005 ☆*. https://doi.org/10.1016/j.jsr.2008.05.001

Thompson, H. J., Mccormick, W. C., & Kagan, S. H. (2006). Traumatic Brain Injury in Older Adults: Epidemiology, Outcomes, and Future Implications. *J Am Geriatr Soc*, *54*, 1590–1595. https://doi.org/10.1111/j.1532-5415.2006.00894.x

Unterharnscheidt, F. J. (1971, February 1). *Translational versus Rotational Acceleration-Animal Experiments with Measured Input*. https://doi.org/10.4271/710880

Utomo, W. K., Gabbe, B. J., Simpson, P. M., & Cameron, P. A. (2009). Predictors of in-hospital mortality and 6-month functional outcomes in older adults after moderate to severe traumatic brain injury. *Injury*, *40*(9), 973–977. https://doi.org/10.1016/j.injury.2009.05.034

van Schooten, K. S., Yang, Y., Feldman, F., Leung, M., McKay, H., Sims-Gould, J., & Robinovitch, S. N. (2018). The Association Between Fall Frequency, Injury Risk, and Characteristics of Falls in Older Residents of Long-Term Care: Do Recurrent Fallers Fall More Safely? *The Journals of Gerontology: Series A*, *73*(6), 786–791. https://doi.org/10.1093/gerona/glx196

Viano, D. C., King, A. I., Melvin, J. W., & Weber, K. (1989). Injury biomechanics research: An essential element in the prevention of trauma. *Journal of Biomechanics*, *22*(5), 403–417. https://doi.org/10.1016/0021-9290(89)90201-7

Voinea, G. D., Butnariu, S., & Mogan, G. (2017). Measurement and geometric modelling of human spine posture for medical rehabilitation purposes using a wearable monitoring system based on inertial sensors. *Sensors (Switzerland)*, *17*(1). https://doi.org/10.3390/s17010003

Vrtovec, T., Pernuš, F., & Likar, B. (2009). A review of methods for quantitative evaluation of spinal curvature. *European Spine Journal*, *18*(5), 593–607. https://doi.org/10.1007/s00586-009-0913-0

Wach, W., & Unarski, J. (2014). Fall from height in a stairwell - mechanics and simulation analysis. *Forensic Science International*, *244*, 136–151. https://doi.org/10.1016/j.forsciint.2014.08.018

Watson, W. L., & Mitchell, R. (2011). Conflicting trends in fall-related injury hospitalisations among older people: variations by injury type. *Osteoporosis International*, *22*(10), 2623–2631. https://doi.org/10.1007/s00198-010-1511-z

Willinger, R., & Baumgartner, D. (2003). Human head tolerance limits to specific injury mechanisms. *International Journal of Crashworthiness*, *8*(6), 605–617. https://doi.org/10.1533/ijcr.2003.0264

World Health Organization. (2014). *Injuries and violence: the facts 2014*. Retrieved from www.who.int/healthinfo/global_burden_disease/projections/en/

Wright, A. D., & Laing, A. C. (2011). The influence of headform orientation and flooring systems on impact dynamics during simulated fall-related head impacts. *Medical Engineering and Physics*. https://doi.org/10.1016/j.medengphy.2011.11.012

Wu, J.-S., & Hsieh, M. (2001). An experimental method for determining the frequency-dependent added mass and added mass moment of inertia for a floating body in heave and pitch motions. *Ocean Engineering*, *28*, 417–438. Retrieved from www.nm.ncku.edu.tw

Wu, L. C., Kuo, C., Loza, J., Kurt, M., Laksari, K., Yanez, L. Z., … Camarillo, D. B. (2017). Detection of American Football Head Impacts Using Biomechanical Features and Support Vector Machine Classification. *Nature Scientific Reports*. https://doi.org/10.1038/s41598-017-17864-3

Yang, Y., MacKey, D. C., Liu-Ambrose, T., Leung, P.-M. M., Feldman, F., & Robinovitch, S. N. (2017). Clinical Risk Factors for Head Impact during Falls in Older Adults: A Prospective Cohort Study in Long-Term Care. *Journal of Head Trauma Rehabilitation*, *32*(3), 168–177. https://doi.org/10.1097/HTR.0000000000000257

Yang, Y., Schonnop, R., Feldman, F., & Robinovitch, S. N. (2013). Development and validation of a questionnaire for analyzing real-life falls in long-term care captured on video. *BMC Geriatrics*, *13*(1), 1–11. https://doi.org/10.1186/1471-2318-13-40

Zatsiorsky, V. M., International Federation of Sports Medicine., & IOC Medical Commission. (2000). *Biomechanics in sport : performance enhancement and injury prevention*. Blackwell Science.

Zhang, J., Yoganandan, N., & Pintar, F. A. (2009). Dynamic biomechanics of the human head in lateral impacts. *53rd AAAM Annual Conference Annals of Advances in Automotive Medicine* , 249–256. Retrieved from https://www.ncbi.nlm.nih.gov/pmc/articles/PMC3256796/pdf/file40_final.pdf

Zhang, L., Yang, K. H., & King, A. I. (2004). A Proposed Injury Threshold for Mild Traumatic Brain Injury. *Journal of Biomechanical Engineering*, *126*(2), 226–236. https://doi.org/10.1115/1.1691446

Zhi-Chao, H., Lu, Y.-N., Yao-Xin, L., & Dan, L. (2008). A new trifilar pendulum approach to identify all inertia parameters of a rigid body or assembly. *Mechanism and Machine Theory*, *44*, 1270–1280. https://doi.org/10.1016/j.mechmachtheory.2008.07.004

Appendix A.

Back curvature analysis of real-life falls

LTC residents exhibited a range of time-varying torso postures and back curvatures between the instants of pelvis impact and head impact. The curvature of the spine is a key determinant of body posture and torso shape and an important geometrical parameter that is recognized to have considerable influence on mechanical response in both static and dynamic loading scenarios (Cholewick, Crisco, Oxland, Yamamoto, & Panjabi, 1996; Janik, Harrison, Cailliet, Troyanovich, & Harrison, 1998).

Most previous studies on torso and back sagittal shape have been limited to reporting lordotic and kyphotic curvatures by means of trunk inclinations measured via radiographs or rasterstereography under static posture conditions, which do not accurately describe the marginal features of the spine (Berthonnaud, Dimnet, Roussouly, & Labelle, 2005; Vrtovec, Pernuš, & Likar, 2009). Other works presenting geometric models of spinal lordoses or kyphoses have used complex-coefficient higher-order polynomials, but such parameters are difficult to interpret.

I identified studies in the literature that have attempted to model the sagittal spine curvature using circle/ellipse-based approaches (Harrison et al., 2004). Roussouly & Pinheiro-Franco (Roussouly & Pinheiro-Franco, 2011) describes a widely used biomechanical approach (Le Huec, Demezon, & Aunoble, 2014) for determining the global shape of the thoracic and lumbar spine regions using tangent arcs of two circles. A study by Janik et al., (Janik et al., 1998), concluded that the sagittal lumbar curvature can be closely approximated to a least-squares error of 1.2 mm using variations of ellipse-quadrants. When modeling the sagittal cervical spine shape using ellipses, a least-squares error model by Harrison et al., (Harrison et al., 2004) concluded that a circle arc was the one best-fit geometric shape, a result of observing ellipse major- and minor- axis length ratios approach unity. All mentioned studies report global angle and radius of curvature values, as well as major- and minor-axis length ratios in the case of ellipses, as the geometric outcomes of their models. A study by Voinea et al., (Voinea, Butnariu, & Mogan, 2017) presents a similar arc-based mathematical model for representing spine curvature using wearable inertial sensors. The authors determined

that the minimal number of points needed to accurately identify spine posture using circular arcs is five.

I characterized each resident's back curvature throughout the fall by using the six digitized markers (BP1 – BP6; Figure 3) between T1 and L5 to create two arcs. Arc 1 approximated the upper torso region (thoracic; T1 to T12), and arc 2 approximated the lower torso region (lumbar; L1 to L5). Since the unique solution to any one arc requires three points, my method utilized five of the six digitized back profile markers to derive the characteristics (radii and arc angles) of the two arcs, such that each arc shared a common endpoint. Furthermore, I compared the goodness of fit (via displacement error to the sixth, unused or bypassed marker) provided by four combinations as shown in Figure A1. Fit 1: where the 2nd back profile marker (BP2) was bypassed; similarly, Fit 2: where the 3rd back profile marker (BP3) was bypassed, Fit 3: BP4 bypassed; and Fit 4: BP5 bypassed (Figure A1). I provide the results of my displacement error analysis in Table A1, and the back curvature results in Table A2 and Table A3.

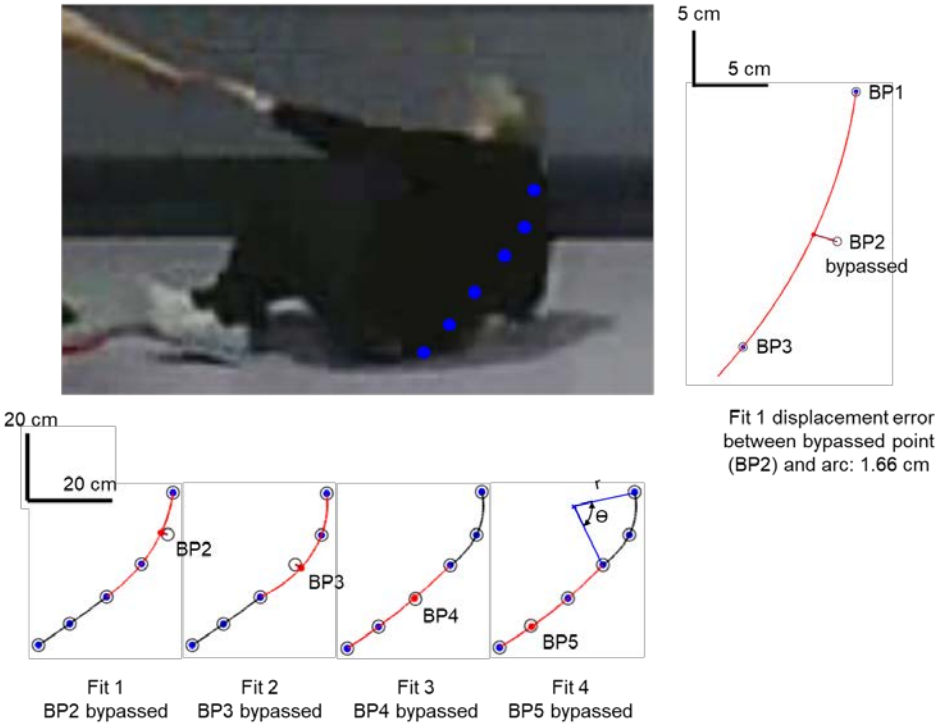

Figure A1. The four different back curvature fit combinations.
Example resultant family for four different back profile curvature fits using a pair of arcs (bottom left). Example displacement error illustration for the Fit 1at the instant of pelvis impact (top right).

Table A1. Back curvature displacement error analysis results

Video ID	Resident ID	Fit 1 - BP2 bypassed				Fit 2 - BP3 bypassed				Fit 3 - BP4 bypassed				Fit 4 - BP5 bypassed			
		average across all frames (cm)	pelvis impact (cm)	between pelvis and head impact (cm)	head impact (cm)	average across all frames (cm)	pelvis impact (cm)	between pelvis and head impact (cm)	head impact (cm)	average across all frames (cm)	pelvis impact (cm)	between pelvis and head impact (cm)	head impact (cm)	average across all frames (cm)	pelvis impact (cm)	between pelvis and head impact (cm)	head impact (cm)
1	1	0.29	0.20	0.28	0.12	0.20	0.30	0.20	0.31	2.57	9.26	8.09	0.02	3.18	0.15	0.13	9.04
2	1	0.14	0.01	1.68	0.30	0.66	0.14	0.01	1.57	0.19	1.03	0.71	0.18	0.15	0.72	0.64	0.16
3	2	1.34	0.26	4.14	3.54	2.65	2.95	0.35	9.05	0.48	1.72	2.43	0.59	0.40	1.61	2.02	0.43
4	3	0.17	0.01	0.23	0.11	0.12	0.17	0.01	0.23	0.12	0.17	0.01	0.23	0.12	0.17	0.01	0.22
5	4	0.28	1.65	0.27	0.01	0.64	0.31	1.76	0.33	0.20	0.81	0.66	0.25	0.21	0.88	0.64	0.26
6	5	0.33	0.53	0.51	0.34	0.46	0.35	0.57	0.54	0.25	0.48	0.99	0.02	0.25	0.46	1.04	0.02
7	6	0.21	7.26	0.58	0.15	2.66	1.54	0.37	7.70	0.08	0.09	0.28	0.35	0.09	0.10	0.28	0.36
8	7	0.22	0.88	1.08	0.10	0.69	0.24	0.89	1.14	0.09	0.47	0.09	0.04	0.10	0.47	0.11	0.05
9	8	0.15	0.75	0.27	0.04	0.35	0.18	0.90	0.32	0.13	0.01	0.38	0.22	0.13	0.01	0.38	0.22
10	9	0.38	1.66	1.98	1.66	1.76	0.40	1.69	2.02	0.23	0.32	0.38	0.01	0.20	0.28	0.35	0.01
11	10	0.16	0.22	0.23	0.35	0.27	0.17	0.23	0.24	0.17	0.33	0.35	0.47	0.17	0.34	0.35	0.46
mean		0.33	1.22	1.02	0.61	0.95	0.61	0.63	2.13	0.41	1.34	1.31	0.22	0.45	0.47	0.54	1.02
standard deviation		0.34	2.09	1.20	1.08	0.95	0.87	0.62	3.16	0.73	2.67	2.34	0.19	0.91	0.46	0.57	2.66
minimum		0.14	0.01	0.23	0.01	0.12	0.14	0.01	0.23	0.08	0.01	0.01	0.01	0.09	0.01	0.01	0.01
maximum		1.34	7.26	4.14	3.54	2.66	2.95	1.76	9.05	2.57	9.26	8.09	0.59	3.18	1.61	2.02	9.04

BP = back profile marker (e.g. BP2 = back profile marker 2). For each back curvature fit (Fit 1-4), the error was estimated as the displacement between the bypassed marker and the closest point on the arc formed by the three adjacent markers. For example, considering Fit 1 with BP2 bypassed for video ID 10; arc 1 was formed using BP1, BP3, and BP4, and at the instant of pelvis impact, the displacement measured between BP2 and arc 1 was 1.66 cm. This example is also illustrated in Figure A1.

The outcome of my displacement error analysis to find the best fit is summarized in Table A1. Despite Fit 1 slightly outperforming all other configurations when averaging across all frames (average displacement of 1.19 mm smaller than the next best fit), I found that Fit 4 was at least two-fold more accurate than the next best fit at two critical instants; with the smallest average error of 4.71 and 5.41 mm at the instant of pelvis impact and the instant midway between pelvis and head impact respectively.

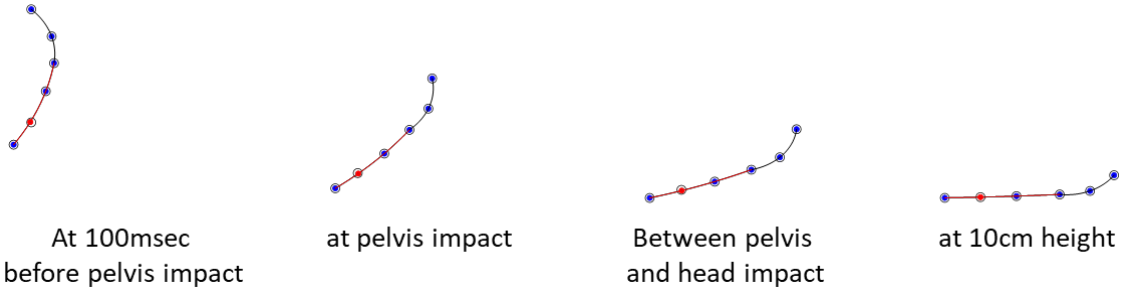

Figure A2. Back profile at four different instants.
Arc 1, shown in black represents the thoracic posterior region of the back curvature, and Arc 2, shown in red, represents the lumbar posterior region of the back curvature. Using back curvature Fit 4 to measure the time-varying back curvature of each resident throughout each fall, I summarized, in Table A2 and Table A3, the back curvature outcomes in terms of arc radii and angles at seven different instants ranging from 100 ms before pelvis impact to head impact. It was unclear from the results, if the back curvatures examined in the 11 falls could be categorized as either flat or curved as my results show a large degree of variability in terms of back curvatures displayed throughout the fall. Notably, the arc 1 radius was, on average, always smaller than the arc 2 radius.(Measured at pelvis impact: 41.4 vs 64.0 cm, at midway between pelvis and head impact: 34.33 versus 282.1; and at head impact: 137.90 versus 266.21), indicating that the thoracic region was consistently more curved than the lumbar region. Additionally, both arc 1 and arc 2 tended to show signs of ‘flattening’ as the fall progressed from the point of pelvis impact, as indicated by increasing average arc radius and arc angle values measured at pelvis impact, midway between pelvis and head impact, and at head impact. The range of arc 1 and arc 2 curvatures measured at pelvis impact was 14.9 cm to 151.3 cm, and 21.9 cm to 119.7 cm, respectively, and measured at head impact, the range exhibited was 7.33 to 600 cm and 46.68 to 1026.4 cm, for arc 1 and arc 2 respectively.

Table A2. Thoracic back curvature characteristics summary for arc 1.

		arc 1														
		radius (cm)							angle (degrees)							
Video number	Resident ID	100 ms before pelvis impact	pelvis impact	100 ms after pelvis impact	between pelvis and head impact	10cm higher	100 ms before head impact	head impact	100 ms before pelvis impact	pelvis impact	100 ms after pelvis impact	between pelvis and head impact	10cm higher	100 ms before head impact	head impact
1	1	35.32	21.06	17.19	23.29	152.62	152.62	294.49	31.49	50.36	68.33	34.82	4.63	4.63	2.35
2	1	130.12	151.31	29.22	19.08	128.05	27.40	133.12	8.89	7.54	36.89	53.15	5.16	28.69	4.81
3	2	25.67	45.93	17.46	17.46	17.46	17.46	7.33	24.09	12.93	35.56	35.56	35.56	35.56	75.50
4	3	51.42	30.44	39.63	28.85	28.85	30.44	39.63	19.69	29.37	21.23	28.71	28.71	29.37	21.23
5	4	21.10	18.00	30.94	58.21	95.68	95.68	198.41	47.59	56.77	34.37	17.57	10.32	10.32	4.31
6	5	42.53	29.32	25.20	27.61	49.53	33.64	49.53	22.07	33.29	39.29	38.98	21.76	31.30	21.76
7	6	20.44	62.12	59.77	44.18	46.57	44.18	46.40	35.74	13.46	14.28	17.73	16.07	17.73	16.11
8	7	19.69	14.89	11.50	14.46	27.49	27.49	52.96	38.48	53.64	62.98	50.28	25.69	25.69	13.13
9	8	18.33	21.21	76.13	43.17	28.30	21.21	76.13	48.73	41.13	12.20	21.10	31.56	41.13	12.20
10	9	25.95	22.80	17.37	19.05	18.92	21.45	18.92	53.74	59.19	73.60	71.87	62.08	64.67	62.08
11	10	22.42	38.35	68.46	82.31	600.00	82.31	600.00	47.14	25.95	15.37	12.80	1.59	12.80	1.59
mean		37.54	41.40	35.72	34.33	108.50	50.35	137.90	34.33	34.88	37.64	34.78	22.10	27.45	21.37
standard deviation		32.48	39.02	22.53	20.95	169.42	42.50	176.02	14.38	18.71	22.03	18.07	17.65	16.69	24.67
minimum		18.33	14.89	11.50	14.46	17.46	17.46	7.33	8.89	7.54	12.20	12.80	1.59	4.63	1.59
maximum		130.12	151.31	76.13	82.31	600.00	152.62	600.00	53.74	59.19	73.60	71.87	62.08	64.67	75.50

back curvature radii and angles were measured using the Fit 4 arcs configuration as shown in Figure A1.

Table A3. Lumbar back curvature characteristics summary for arc 2.

		arc 2														
		radius (cm)							angle (degrees)							
Video number	Resident ID	100 ms before pelvis impact	pelvis impact	100 ms after pelvis impact	between pelvis and head impact	10cm higher	100 ms before head impact	head impact	100 ms before pelvis impact	pelvis impact	100 ms after pelvis impact	between pelvis and head impact	10cm higher	100 ms before head impact	head impact
1	1	1130.42	56.86	48.36	158.06	168.25	168.25	397.62	1.58	27.75	33.03	9.56	8.25	8.25	3.38
2	1	73.55	68.91	409.32	128.60	56.84	43.98	108.79	22.79	24.88	3.65	10.89	17.54	26.16	9.10
3	2	136.51	21.92	23.51	23.51	23.51	23.51	79.45	9.07	63.27	76.47	76.47	76.47	76.47	22.76
4	3	65.99	57.92	306.84	95.93	95.93	57.92	306.84	18.83	20.53	4.06	12.83	12.83	20.53	4.06
5	4	50.60	75.23	126.58	89.90	79.89	79.89	213.29	33.55	23.74	14.82	22.19	25.80	25.80	8.99
6	5	660.48	111.93	82.61	86.49	294.29	133.41	294.29	2.04	13.72	21.14	20.88	4.79	11.69	4.79
7	6	102.83	38.79	92.54	2105.80	211.86	2105.80	187.76	14.98	35.75	13.04	0.59	5.79	0.59	6.32
8	7	28.69	24.51	35.30	36.34	36.23	36.23	67.95	49.58	51.01	36.61	36.66	38.30	38.30	20.55
9	8	96.55	62.31	199.25	128.21	81.44	62.31	199.25	18.29	27.88	9.48	14.69	22.39	27.88	9.48
10	9	83.76	119.72	525.85	212.90	1026.37	128.75	1026.37	24.98	16.47	4.02	9.51	2.10	15.27	2.10
11	10	115.48	66.24	40.60	37.17	46.68	37.17	46.68	15.30	23.98	38.74	42.58	33.20	42.58	33.20
mean		231.35	64.03	171.89	282.08	192.84	261.57	266.21	19.18	29.91	23.19	23.35	22.50	26.69	11.34
standard deviation		346.03	31.01	170.33	607.49	288.73	613.46	275.35	13.85	14.94	22.00	21.49	21.49	20.69	9.88
minimum		28.69	21.92	23.51	23.51	23.51	23.51	46.68	1.58	13.72	3.65	0.59	2.10	0.59	2.10
maximum		1130.42	119.72	525.85	2105.80	1026.37	2105.80	1026.37	49.58	63.27	76.47	76.47	76.47	76.47	33.20

back curvature radii and angles were measured using the Fit 4 arcs configuration as shown in Figure A1.

Appendix B.

Inertial modeling of real-life falls

A fundamental property which determines the character and outcome of any dynamic event governed by Newtonian mechanics is the inertia of the system in motion. Mass is one such example of a physical quantity that describes the body's resistance to changes in translational acceleration. Analogously, mass moment of inertia describes the body's resistance to angular or rotational acceleration as a function of the distribution of mass of the system about a point of rotation.

Body segment inertia parameters (BSIPs) are highly variable based on the individual, and the variation can in-part be explained and accounted for by differences in age (R. Jensen & Fletcher, 1994; Pavol, Owings, & Grabiner, 2002), sex (Plagenhoef, 1983; Zatsiorsky, International Federation of Sports Medicine., & IOC Medical Commission., 2000), race and ethnicity (Shan & Bohn, 2003), and morphology (R. K. Jensen & Fletcher, 1993). In the current study, I characterized the role of inertial parameters (moment of inertia (MOI) and center of mass positions (COM)) in falls using a six-segment model including the head, torso, upper arm, forearm, thigh, and shank (Figure B1).

Medical datasheets collected at the time of admission into the LTC facility, as well as fall incident reports populated at the time of the fall, included each resident's standing height, full body mass and sex. I used these details to derive, based on scaling constants from literature (Hoang & Mombaur, 2015), the length, mass, longitudinal distance of the COM with respect to the proximal joint, and radius of gyration for each segment (Figure B1). To simplify the model, I constrained motion to the sagittal plane, and assumed symmetry of limb movements. Segment angles (as described in Section 2.3.5) were used to orient the segments with respect to one another. The hands and feet were treated as point masses affixed to the distal endpoints of the forearm and shank respectively.

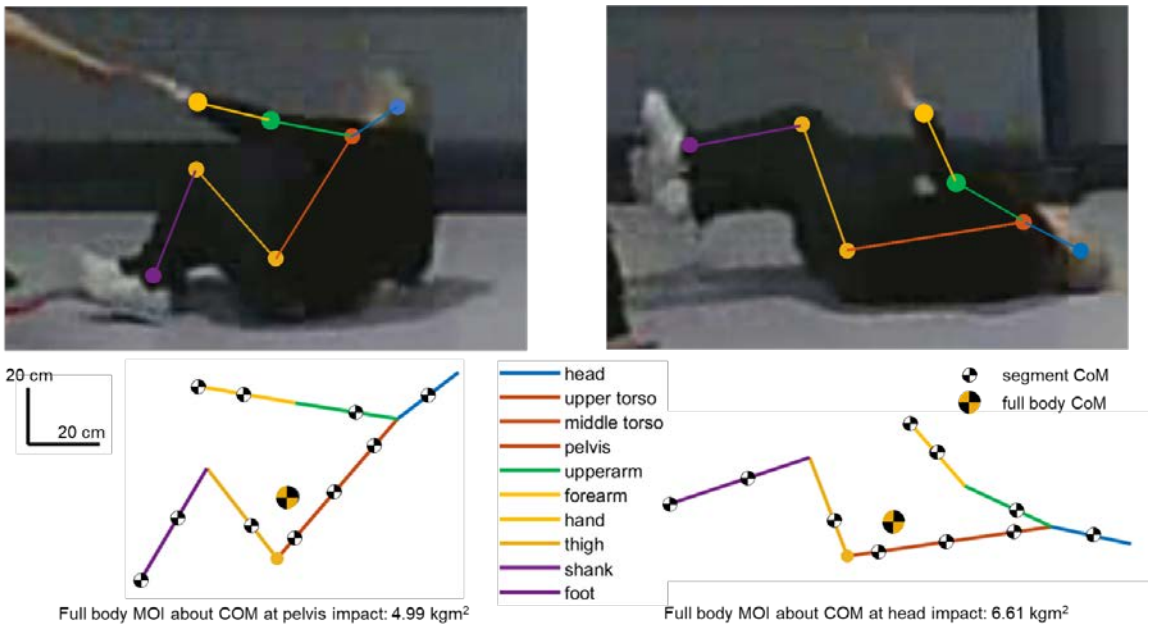

Figure B1. Six-segment inertial model for a sample fall
This model was generated using demographic-adjusted anthropometry data provided by Hoang & Mombaur (Hoang and Mombaur, 2015), which was used to calculate body segment inertia parameters including segment lengths, COM positions, and full body and segment mass moments of inertia (MOI).

At the instant of pelvis impact, the full body MOI calculated about the COM averaged 5.33(SD=2.04) kgm^2 (Table B1). Upper and lower body MOI calculated about the pelvis averaged 5.40(SD=1.89), and 1.87(SD=0.67) kgm^2 respectively. At the instant halfway between pelvis and head impact, the full body MOI calculated about the COM averaged 6.03(2.01) kgm^2, where upper and lower body MOI about the pelvis averaged 5.56(1.95), and 1.91(0.56) kgm^2. At the instant of head impact, full body MOI about the COM averaged 6.59(1.98) kgm^2, where upper and lower body MOI about the pelvis averaged 5.57(1.94), and 2.12(0.55) kgm^2.

Table B1. Summary of segment inertia model results

						at pelvis impact						between pelvis and head impact						at head impact					
									sagittal						sagittal						sagittal		
Video ID	Resident ID	Sex	Age	Body mass (kg)	Standing height (cm)	full body COM height (cm)	upper body COM height (cm)	lower limbs COM height (cm)	full body MOI about COM (kgm2)	upper body MOI about pelvis (kgm2)	lower limbs MOI about pelvis (kgm2)	full body COM height (cm)	upper body COM height (cm)	lower limbs COM height (cm)	full body MOI about COM (kgm2)	upper body MOI about pelvis (kgm2)	lower limbs MOI about pelvis (kgm2)	full body COM height (cm)	upper body COM height (cm)	lower limbs COM height (cm)	full body MOI about COM (kgm2)	upper body MOI about pelvis (kgm2)	lower limbs MOI about pelvis (kgm2)
1	1	F	68	46.5	162	17.30	34.51	4.55	4.76	4.01	2.42	9.94	12.26	11.03	5.72	4.41	2.22	5.67	-0.52	14.65	5.47	4.41	1.90
2	1	F	68	46.5	162	19.22	32.59	12.73	3.22	4.12	1.34	13.95	21.02	12.22	4.27	4.14	1.60	3.88	-4.40	14.99	5.21	4.38	1.69
3	2	F	78	59	156	9.45	15.54	6.91	6.95	5.13	2.85	2.30	-0.11	6.19	7.66	5.51	2.76	0.14	-7.56	8.94	7.72	5.58	2.74
4	3	M	83	89.7	161	10.27	14.27	12.28	7.34	8.22	1.96	3.98	0.70	14.51	8.34	8.39	2.19	2.31	-3.66	15.59	8.65	8.34	2.36
5	4	F	89	47.9	152	12.90	26.52	2.71	5.03	4.00	2.08	8.12	10.84	8.16	5.37	3.97	2.08	3.81	-4.57	14.20	5.36	3.95	1.99
6	5	F	59	59	164	17.86	40.20	-0.14	4.24	5.57	1.22	17.82	37.60	4.32	4.31	5.61	1.19	1.93	-4.79	10.16	7.98	5.71	2.89
7	6	F	90	48.4	153	18.16	31.94	9.48	2.80	4.06	0.84	9.81	8.64	15.10	3.70	4.13	1.17	6.67	-1.54	17.95	4.04	4.12	1.36
8	7	F	89	46.7	152	13.52	30.04	0.22	5.23	4.11	2.19	3.80	7.54	1.67	5.45	3.82	2.03	-0.42	-2.16	1.71	5.41	3.74	2.00
9	8	M	83	97.8	168	5.42	6.81	8.36	9.93	9.12	2.82	1.64	0.06	8.52	10.43	9.55	2.75	0.59	-1.86	8.06	10.76	9.60	2.91
10	9	F	93	65.6	165	21.49	38.47	9.81	4.99	7.11	1.49	14.30	21.09	12.38	5.98	7.02	1.64	11.18	10.02	16.28	6.61	6.93	2.07
11	10	F	86	53.3	152	11.35	20.51	6.12	4.17	3.99	1.39	4.65	7.61	4.64	5.12	4.55	1.42	-0.80	-5.08	5.16	5.24	4.55	1.41
mean			80.5	60.0	158.8	14.27	26.49	6.64	5.33	5.40	1.87	8.21	11.57	8.98	6.03	5.56	1.91	3.18	-2.38	11.61	6.59	5.57	2.12
standard deviation			11.0	17.9	6.0	4.92	10.81	4.44	2.04	1.89	0.67	5.44	11.34	4.44	2.01	1.95	0.56	3.61	4.57	5.16	1.98	1.94	0.55
minimum			59	46.5	152	5.42	6.81	-0.14	2.80	3.99	0.84	1.64	-0.11	1.67	3.70	3.82	1.17	-0.80	-7.56	1.71	4.04	3.74	1.36
maximum			93	97.8	168	21.49	40.20	12.73	9.93	9.12	2.85	17.82	37.60	15.10	10.43	9.55	2.76	11.18	10.02	17.95	10.76	9.60	2.91

COM heights are measured with respect to the pelvis joint center of rotation marke

Appendix C.

Experimental determination of dummy inertia values

When considering the kinematics and dynamics of a rigid body, the body's response to external excitation is governed by three inertial parameters: mass, center of mass location and mass moment of inertia (MMOI). While the determination of an object's mass and center of mass position is relatively trivial by means of static weighting, determining the mass moment of inertia requires dynamic testing. It is possible to describe the mass distribution profile or moment of inertia characteristics of a rigid body using analytical methods by first determining the mass distribution of each component separately using material datasheets or advanced imaging techniques (Sen & Vinh, 2016). However, these parameters are commonly identified experimentally as there is typically little to no accurate models of a given structure's geometry and density distribution, especially for cases where the structure is made up of multiple complex parts (Kloepper & Okuma, 2010; Mattey, 1974; Ringegni, Actis, & Patanella, 2000; J.-S. Wu & Hsieh, 2001).

Once the object mass and center of mass coordinates are known, the MMOI can be determined using multifilar gravitational pendulum-type methods based on small angular motions. This is done by solving, from measured oscillations, the equation of motion of a single-degree-of-freedom oscillator (Equation 1.) where the test specimen oscillates, due to a restorative gravitational force, about the axis of rotation after being manually displaced by a small angle theta <10 degrees (Du Bois, Lieven, Adhikari, & Adhikari, 2009). A study surveying different inertia estimation approaches (Genta & Delprete, 1994), parses the methods into two general categories: oscillatory and acceleratory. They conclude that there are less unwanted effects of damping in the oscillatory methods. Furthermore, In terms of accuracy, error analysis studies have shown that deviations of less than +/-1% can be achieved from theoretical values when using oscillatory approaches (Du Bois et al., 2009; Schedlinski & Link, 2001).

$$I = \frac{M*T^2*R^2}{4*\pi^2*L^2} \qquad \text{Equation 1.}$$

I: $mass\ moment\ of\ inertia\ (kg*m^2)$

M: $total\ mass\ of\ the\ loaded\ trifilar\ pendulum\ system\ (kg)$

T: $trifilar\ pendulum\ period\ of\ oscillation\ (s)$

R: $effective\ radius, from\ the\ center\ to\ the\ attachement\ point\ (m)$

L: $effective\ suspension\ cable\ length\ (m); where\ L = L_o + \Delta L;$

L_o: $unloaded\ cable\ length;\ \Delta L = change\ in\ suspension\ cable\ length\ due\ to\ loading$

For the fully-assembled dummy as well as for each constitutive article (Hybrid III head, neck, head and neck complex, torso, and lower limbs), I determined the segment length, segment mass, coordinates of the sagittal/lateral axis passing through the COM and the sagittal/lateral mass moment of inertia (Iyy). This was done using conventional biomechanics lab-based instruments such as motion capture and a forceplate.

The mass and center of mass axis location values were determined by statically weighing each target body using a six degree of freedom 50 cm x 50 cm AMTI forceplate (Model No. 2535-08). As the Target body is rigid in each case, I used the forceplate point of force and couple application equations (Equation 2a and Equation 2b) to identify the center of pressure (COP) of the body on the surface of the forceplate, which coincides with the COM coordinates. The COM location was tagged on the lateral side of each segment and subsequently used for aligning the body on a custom trifilar pendulum (Figure C1) for determining MMOI values.

$$x_p = \frac{-t*F_x - M_y}{Fz} \qquad \text{Equation 2a.}$$

$$y_p = \frac{-t*F_y - M_x}{Fz} \qquad \text{Equation 2b.}$$

x_p: $point\ of\ force\ application\ (x-coordinate)\ in\ (m)$

y_p: $point\ of\ force\ application\ (y-coordinate)$ in (m)

t: $forceplate\ thickness\ (m)$

$F_x, F_y, F_z, M_x, M_y, M_z$: $6\ DOF\ forces\ (N)\ and\ moments\ (N*m)$

I constructed a trifilar pendulum which was comprised of a 1.9 cm-thick 8.5 kg plywood plate carved to be 50 cm in radius. An equilateral triangular Unistrut frame was

mounted to a reinforced ceiling beam at two vertices, and a makeshift adjustable vertical support pillar was used to level and support the third cantilevered vertex. The pendulum test plate was suspended (parallel with the ground and at an elevation of 20 cm) from the upper frame using three congruent inextensible mesh cables (length = 254 cm each) that have been threaded and clipped through the test plate at three equidistant locations along the circumference of the plate, such that they were all parallel with one another and orthogonal to the surface of the test plate (Figure C1)

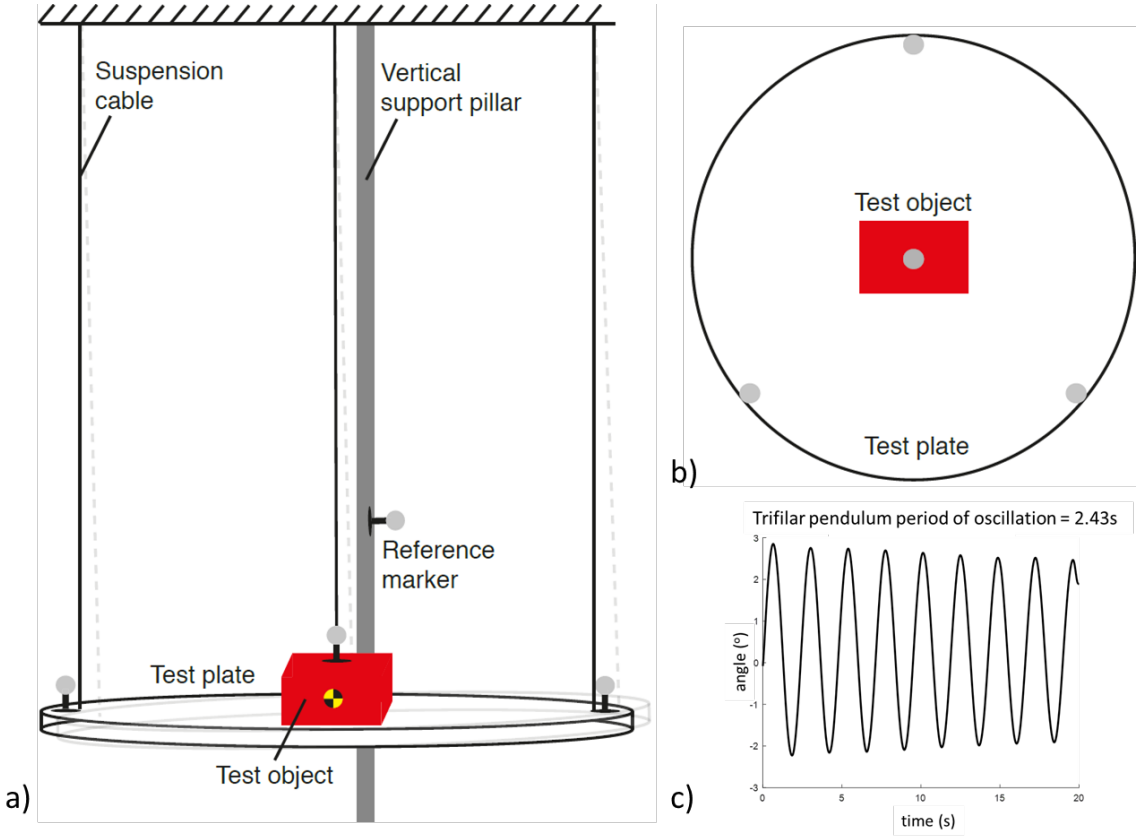

Figure C1. Sketch of the custom-built trifilar pendulum.
The test object (shown in red) is placed at the center of the trifilar pendulum where the COM of the test body is aligned with the axis of rotation of the trifilar pendulum system, a) shows a frontal view of the setup, and b) shows a top-down view. Also shown is a sample period measurement for the trifilar pendulum c). The measured period, along with known pendulum geometry values are plugged-in to Equation 1. to determine the mass moment of inertia of the system.With the aid of real-time trajectory tracking using motion capture (600 Hz; Qualisys MIQUS), the test object (the dummy, or a component of the dummy) is then mounted onto the pendulum such that the lateral or y-axis (and thus the inertial frame) of the object coincides with the center of the test plate (axis of rotation). And the period of oscillation

of the pendulum system is timed and measured using the motion capture system Figure C2.

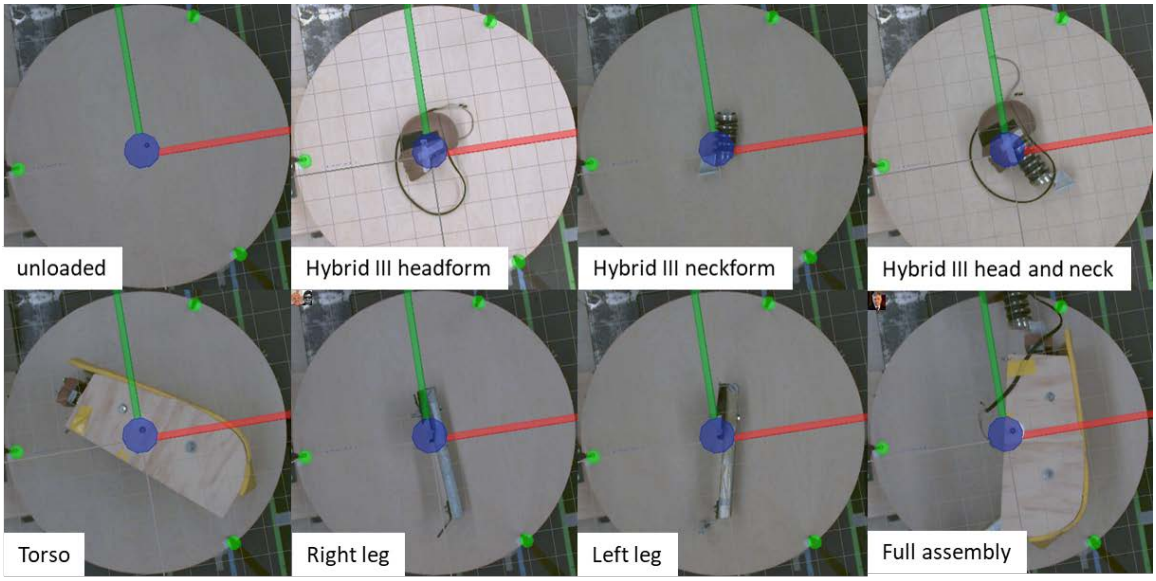

Figure C2. Top-down view of the trifilar pendulum experimental setup.
Motion capture footage was overlaid to illustrate the positioning of the objects at the center of the pendulum and the orientation of the axes using the marker trajectory tracking. Each component's MMOI was determined by subtracting the MMOI of the loaded system via the parallel axis theorem.

To calibrate the trifilar pendulum, a ten-trial protocol was first conducted to determine the mass moment of inertia of the unloaded test plate (MMOI = 10121 (SD=53.34) kgcm^2). This value was compared to the theoretical MMOI of a solid uniform plate of radius 50 cm and mass 8.5 kg resulting in a percent error value of 4.84%. To determine the MMOI of a target object (e.g. the Hyrbid III dummy head), the MMOI of the test plate is subtracted from the full system MMOI based on the parallel axis theorem. This approach was verified by measuring the MMOI of two weighted 4.54 kg steel plates that were placed adjacent to one another on the test plate such that the COM coincided with the axis of rotation of the pendulum. This yielded a percent error of 1.54% compared to theoretical values. The accuracy of my measured MMOI calculations was further improved by accounting for cable extensions using a static reference marker which measured deltas in suspension cable lengths between loaded and unloaded conditions for each target body, and by discarding trials where the mean angle of oscillation exceeded 10 degrees, as is recommended by Du Bois et al., (Du Bois et al., 2009). The period of oscillation for each object was averaged over five different 20-

second trials and Table C1. summarizes the measured segment inertia parameters for each of the dummy components as well as the fully assembled dummy.

Table C1. Summary of the measured dummy segment inertia parameters

Test object	longitudinal length (cm)	COM position (cm)	mass (kg)	sagittal radius of gyration about COM (cm)	sagittal mass moment of inertia about COM (kgcm2)
Hybrid III head and neck form	35.54	21.30	6.55	9.17	550.80
Hybrid III head form	22.99	12.47	4.76	6.28	187.77
Hybrid III neck form	16.82	9.90	1.90	6.13	71.32
Torso	72.72	31.43	21.06	15.87	5304.71
Left leg	52.90	31.18	4.44	13.79	843.85
Right leg	53.06	29.87	4.20	13.59	775.34
fully assembled dummy	-	37.27	36.38	35.16	44983.34

By comparison, full body mass for a 5th percentile older adult female LTC resident was determined to be 37.2 kg (difference of 0.82 kg or 2.23% compared to the fully assembled dummy mass). The fully assembled dummy MOI values were also found to be within range of, albeit smaller than, MOI vaules observed during real-life falls in older adults, as summarized in Table B1.

From the database of 2776 total fall videos experienced by 795 residents, which was utilized to select the 11 fall videos analyzed in Chapter 2 (Figure 2), height and weight data existed for 469 residents (248 female). The height and weight data corresponding to a 5th percentile female from that population of older adult residents in the two LTC facilities (Delta View in Delta, BC, and New Vista in Burnaby, BC) was 142 cm and 37.2 kg (difference of 0.82 kg or 2.23% compared to the full dummy assembly summarized in Table C1).

Appendix D.

Calculation of dummy head center of gravity accelerations

The Hyrbid III head accelerometry was sampled at 20 kHz for a duration of six seconds spanning three seconds before and after a 1 g threshold trigger. The data were collected using a three Bridge SLICE NANO stacked simultaneous data acquisition system (DAS) with nine total channels and a 16-bit (resolution) successive approximation register (SAR)-type analog-to-digital convertor (ADC) per channel. The DAS was powered using a Diversified Technical Systems (DTS) SLICE USB interface device connected to a wall electrical outlet. Data acquisition, storage, processing and exporting was done using SLICEWare software on a Windows PC and then analyzed using MATLAB (Mathworks). As per (J211-1, 1995), the raw linear accelerometry data were filtered using a Channel Frequency Class 1000 (CFC1000) fourth order zero-phase digital filter (MATLAB filtfilt) with a cutoff frequency of 1650Hz.

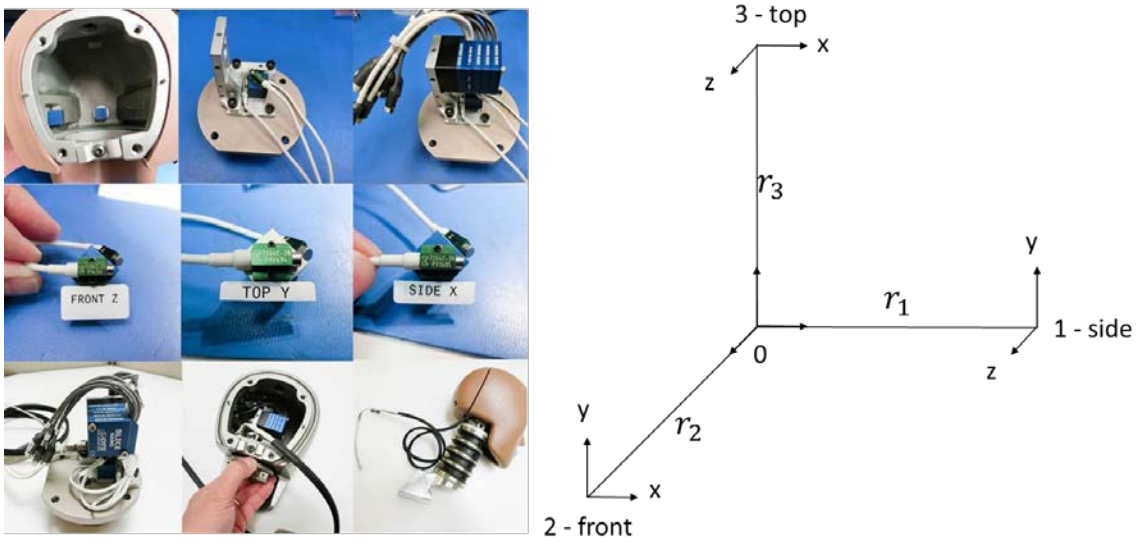

Figure D1. Accelerometer array placement in the head form.
Placement of the SLICE DAS in the head form (left) and figure showing the orientation of the sidearm accelerometer channels in the 3-2-2-2 accelerometer configuration (right).

The translational acceleration data were determined by calculating the three-dimensional resultant acceleration of the three linear accelerometers placed at the head CG, shown as the three orthogonal vectors situated at the origin in Figure D1. The rotational acceleration data were solved for using equations derived from a method described by (Padgaonkar et al., 1975).

$$\dot{\omega}_x = \frac{A_{z1} - A_{z0}}{2 * r_1} - \frac{A_{y3} - A_{yo}}{2 * r_3} \qquad \textit{Equation 3a}$$

$$\dot{\omega}_y = \frac{A_{x3} - A_{x0}}{2 * r_3} - \frac{A_{z2} - A_{zo}}{2 * r_2} \qquad \textit{Equation 3b}$$

$$\dot{\omega}_z = \frac{A_{y2} - A_{y0}}{2 * r_2} - \frac{A_{x3} - A_{xo}}{2 * r_1} \qquad \textit{Equation 3c}$$

$\dot{\omega}_x, \dot{\omega}_y, \dot{\omega}_z$: $rigid\ body\ rotational\ acceleration\ \left(\frac{rad}{s^2}\right)$
A_{x1}, A_{y1}, A_{z1}: $linear\ acceleration\ from\ channel\ 1\ sidearm\ sensors\ (g)$
r_1, r_2, r_3: $distance\ between\ center\ of\ gravity\ and\ sidearm\ sensors\ (m)$

Appendix E.

Dummy head velocity comparisons

I observed in Chapter 2 that the peak head velocity experienced by older adults during backward falls involving head impact was not representative of the velocity of the head at impact. Possible reasons for this apparent slowing down of the head leading up to impact may relate to 1) the opposing vertical forces generated by the successive earlier impacts to other body sites, such as pelvis, torso, shoulders and upper limbs, or 2) protective responses such as neck muscle contraction (Choi et al., 2017; Kuo et al., 2020), and bracing of the upper limb with the ground (Chiu & Robinovitch, 1998; DeGoede et al., 2003; Robinovitch & Chiu, 1998).

For these reasons, I treated head velocities at specific heights (5, 7.5, and 10 cm) above the position of the head at impact, as representative of the impact velocity of the head just before it contacts the ground. This process is illustrated diagrammatically in Figure 6 of Chapter 2. And more details are provided in Section 2.3.2.

Using the same approach detailed in Section 2.3.2., on the dummy fall trials, I have included results, shown in Figure E1, that provide a basis for comparison between peak vertical velocities (shown on the horizontal axis) to vertical velocities measured at heights 5, 7.5, and 10cm of the head above the ground. This plot shown how (a) vertical velocities decreased as the head approached the ground due to torso/shoulder impact, and (b) how the velocities at various heights above the ground scaled with peak velocity. This trend mimics head velocity behaviour observed by the backward falls in older adults analyzed in Chapter 2 of this thesis.

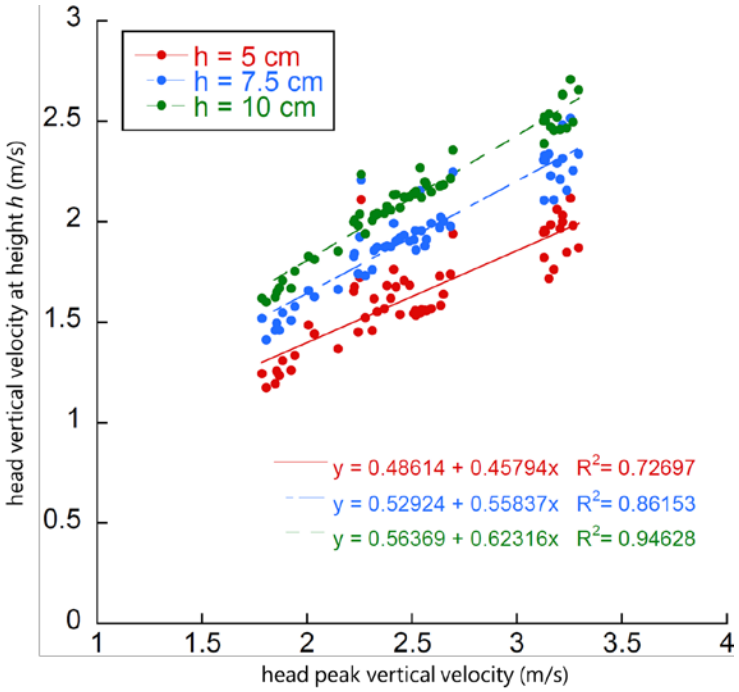

Figure E1. Comparison between dummy impact velocity estimates.